UC San Diego

UC San Diego Electronic Theses and Dissertations

Title

Cell type differences in intrinsic membrane properties regulate responsiveness and energy consumption

Permalink

https://escholarship.org/uc/item/7sb155sv

Author

Otte, Stephani L.

Publication Date

2011

Peer reviewed|Thesis/dissertation

eScholarship.org Powered by the California Digital Library
University of California

UNIVERSITY OF CALIFORNIA, SAN DIEGO

Cell Type Differences in Intrinsic Membrane Properties Regulate Responsiveness and Energy Consumption

A dissertation submitted in partial satisfaction of the

requirements for the degree of Doctor of Philosophy

in

Neurosciences

by

Stephani L Otte

Committee in Charge:

Professor Edward Callaway, Chair
Professor William Kristan, Co-Chair
Professor John Reynolds
Professor Massimo Scanziani
Professor Terry Sejnowski

2011

©

Stephani L. Otte, 2011

All rights reserved.

The Dissertation of Stephani L. Otte is approved, and it is acceptable in quality and form for publication on microfilm:

Co-Chair

Chair

University of California, San Diego

2011

DEDICATION

To my best friend and partner, Brian:
I dedicate this dissertation to you.
You were my everything through this process.
I could not have done this without you.

To my parents, Don and Joni Otte:
Thank you for your unwavering love and support.
You have both grounded me and given me courage to explore this world.

TABLE OF CONTENTS

Signature Page iii

Dedication iv

Table of Contents v

List of Abbreviations vii

List of Figures viii

Acknowledgements x

Vita, Publications, and Conference Abstracts xi

Abstract xiii

Chapter I. Introduction 1
- Background 5
  - Correlations of gamma oscillations to information processing 6
  - Generation and modulation of gamma activity 9
  - Possible functions of gamma-frequency activity 13
  - Gamma oscillations and energy consumption 17

Chapter II. Cell-type specific control of neuronal responsiveness by gamma-band oscillatory inhibition 19
- Summary. 20
- Introduction. 21
- Results 23
- Discussion 36
- Methods 41
  - In vitro slice experiments 41
  - Dynamic Clamp 44
  - Analysis 44
  - Model 45
- Acknowledgements 46
- Publication Acknowledgments 46

Chapter III. Neuronal Biophysics modulates the ability of gamma-frequency input to control spike timing 47
- Summary. 48
- Introduction. 49
- Results. 51

Discussion 60
Methods 64
In vitro slice experiments 64
Dynamic Clamp 67
Analysis 68
Model 69
Acknowledgements 69
Publication Acknowledgements 69

Chapter IV. Metabolic Cost as a Unifying Principle Governing Neuronal biophysics… 70
Summary. 71
Introduction/Results. 71
Discussion 88
Materials and Methods. 91
Model 91
Dynamic Clamp 91
Supplemental Material. 92
Model 92
Slice Preparation 94
Recordings 94
Dynamic Clamp 95
Acknowledgements 96
Publication Acknowledgements 96

References 98

LIST OF ABBREVIATIONS

AC	alternating current
ADHD	attention deficit hyperactivity disorder
AMPA	α-amino-3-hydroxyl-5-methyl-4-isoxazole-propionate
ATP	adenosine triphosphate
DC	direct current
EEG	electroencephalograph
GABA	gamma-aminobutyric acid
Hz	hertz
K+	potassium ion
Kv	voltage-gated potassium channel
LFP	local field potential
MEG	magnetoencephalograph
Na+	sodium ion
NMDA	N-methyl-D-aspartate
PSP	post-synaptic potential

LIST OF FIGURES

Figure 2.1 Six electrically and morphologically distinct types of neurons in the mouse somatosensory cortex. 24

Figure 2.2 Gamma oscillation stimulation protocol and analysis. 26

Figure 2.3 Systematic, cell type specific differences in responsiveness to gamma-band oscillatory synchronized inhibition. 28

Figure 2.4 Neuron's relative synchrony dependence depends on passive membrane filtering properties. 20

Figure 2.5 Neuron's dynamic range depends on afterhyperpolarizaaiton amplitude and duration 33

Figure 2.6 The relative synchrony dependence of neurons changes with background conductance input. 34

Figure 3.1 Electrically and morphologically distinct neuronal types in the mouse somatosensory cortex 53

Figure 3.2 Stimulation protocol and analysis. 54

Figure 3.3 Representative responses of different neuronal types to gamma-band synchronized inhibition 56

Figure 3.4 Systematic, cell type specific differences in average phase of firing, entrainment, and precession 57

Figure 3.5 Interactions between intrinsic properties determine cell-type differences in average phase, precession and entrainment 59

Figure 4.1 State of the sodium and potassium channels during action potential generation 72

Figure 4.2 Membrane dynamics during action potential generation 73

Figure 4.3 Model: Effects of changing the kinetics of the spike generating conductances on spike rate and spike cost 77

Figure 4.4 Model: Effects of changing the densities of the spike generating conductances on spike rate and spike cost 79

Figure 4.5 Effects of changing the kinetics and densities of dynamic clamp generated sodium conductance on spike rate and spike cost. 82

Figure 4.6 Survey of the literature: Spike generating conductances in neurons 85

ACKNOWLEDGMENTS

I would like to thank the members of my dissertation committee: William Kristan, John Reynolds, Massimo Scanziani, and Terry Sejnowski. Their guidance has been invaluable.

I would also like to thank the members of the Callaway lab for their friendship and collaboration. I especially would like to thank Andrea Hasenstaub for training and mentoring me, and collaborating on the work presented in this dissertation.

Finally, I would like to thank my advisor, Ed Callaway, for his optimistic, patient, and thoughtful guidance. His view of science and his approach to life should be emulated.

Chapter 2, in full, is a reprint of the material as it appears in J Neuroscience 2010; Otte S, Hasenstaub A, Callaway EM. J Neuroscience 30:2150-2159. The dissertation author was co-primary authors of this material. Secondary author is thesis advisor.

Chapter 3, in part, is currently being prepared for submission for publication of the material. Otte SL, Hasenstaub AR, Callaway EM. The dissertation author is co-primary author of this material. Secondary author is thesis advisor.

Chapter 4, in full, is a reprint of the material as it appear in PNAS 2010; Hasenstaub A, Otte S, Callaway E, and Sejnowski T. PNAS 2010 : 0914886107v1-200914886. The dissertation author and thesis advisor were contributing investigators and authors of this material. The primary author is Andrea Hasenstaub, the secondary author is Terry Sejnowski, thesis committee member.

VITA

1997-2001 University of Illinois – Urbana-Champaign
B.S. in Cellular and Structural Biology
B.S. in Psychology
Minor Chemistry

2001-2005 Abbott Laboratories
Neuropharmacologist

2005-2011 University of California, San Diego
Ph.D. in Neurosciences

PUBLICATIONS

Otte S, Andrea Hasenstaub, Callaway E. Cell-type differences in gamma frequency entrainment and precession. In preparation.

Otte S*, Hasenstaub A*, Callaway E. Cell type-specific control of neuronal responsiveness by gamma-band oscillatory inhibition. J. Neurosci, 30(6):2150-9. 2010. (*Equal contributors)

Hasenstaub A, Otte S, Callaway E, Sejnowski Metabolic constraints of the biophysics of action potential generation. T. PNAS

Bitner RS, Nikkel AL, Markosyan S, Otte S, Puttfarcken P, Gopalakrishnan. Selective alpha7 nicotinic acetylcholine receptor activation regulates glycogen synthase Kinase3beta and decreases tau phosphorylation in vivo. M Brain Res 1265:65-74. 2009.

Hancock AA, Bitner RS, Krueger KM, Otte S, Nikkel AL, Fey TA, Bush EN, Dickinson RW, Shapiro R, Knourek-Segel V, Droz BA, Brune ME, Jacobson PB, Cowart MD, Esbenshade TA. Distinctions and contradistinctions between antiobesity histamine H(3) receptor (H (3)R) antagonists compared to cognition-enhancing H (3) receptor antagonists.

Bitner RS, Nikkel AL, Otte S, Martino B, Barlow EH, Bhatia P, Stewart AO, Brioni JD, Decker MW, Moreland RB. Dopamine D4 receptor signaling in the rat paraventricular hypothalamic nucleus: Evidence of natural coupling involving immediate early gene induction and mitogen activated protein kinase phosphorylation. Neuropharmacology 50:521-531. 2006.

Grossman AW, Churchill JD, McKinney BC, Kodish IM, Otte SL, Greenough WT.Experience effects on brain development: possible contributions psychopathology. *J Child Psychol Psychiatry.* 44(1):33-63. 2003.

CONFERENCE ABSTRACTS

S. Otte*, A. Hasenstaub *, E. Callaway. Neuronal biophysics modulate the ability of gamma oscillations to control response timing. *Cold Spring Harbor Neural Circuits* 2010. **Selected for talk.**

A. Hasenstaub*, S. Otte*, E. Callaway. Neuronal biophysics modulate the ability of gamma oscillations to control response timing. *Cosyne* 2010. **Selected for talk.**

S.L. Otte*, A.R. Hasenstaub*, E.M. Callaway. Intrinsic properties control gamma frequency input integration. *Society for Neuroscience* Abstracts. 2009.

E.M. Callaway, S.L. Otte, A.R. Hasenstaub. Intrinsic properties, gamma oscillations, and control of response timing. *Society for Neuroscience* Abstracts. 2009.

S.L. Otte*, A.R. Hasenstaub*, T.J. Sejnowski, E.M. Callaway. Intrinsic membrane properties control gamma-frequency input integration. *Cosyne.* 2009.

A.R. Hasenstaub*, S.L. Otte*, E.M. Callaway, T.J. Sejnowski. The Energetic Cost of Action Potential Generation. *Cosyne*. 2008. **Selected for talk.**

A.R. Hasenstaub, S.L. Otte, E.M. Callway, T.J. Sejnowski.The Energetic Cost of Fast Spiking *Nature/IPSEN Genes, Circuits, and Behavior*. 2008.

K.B. Gallagher, S.L. Otte, M.W. Decker, A.L. Nikkel, R.S. Bitner, L.E. Rueter, A.M. Basso. Prolonged Physical State Deterioration, Circadian Activity Disturbances, and Decreased Neurogenesis in Mice Exposed to Chronic Unpredictable Mild Stress (CMS). *Society for Neuroscience* Abstracts. 2005.

A.A. Hancock, R.S. Bitner, S.L. Otte, A.L. Nikkel, K.M. Kruegger, E.N. Bush, P.B. Jacobson, K.E. Browman, G.B. Fox, T.A. Esbenshade, M.D. Differentiation of Histamine H_3 Receptor (H_3R) Antagonist with Cognition-Enhancing or Antiobesity Effects. *Society for Neuroscience* Abstracts. 2005.

S. L. Otte, A.L. Nikkel, M. Nakane, L. Miller, M.W. Decker, J.D. Brioni, R.B. Moreland, R.S. Bitner. In Vitro and In Vivo Functional D4 Receptor Expression: Immunodetection of c-Fos and pERK following PD168077. *Society for Neuroscience* Abstracts. 2003.

I.M. Kodish, S.L. Otte, G. Yuan, K. Nguyen, E. Schuit, N.A. Uranova; A. Y. Klintsova, J.E. Black, W.T. Greenough. Reduced Basilar Dendritic Length and Total Spine Number on Layer III Pyramidal Neurons in Schizophrenic Prefrontal Cortex. *Society for Neuroscience* Abstracts. 2001.

I.M. Kodish, S.L. Otte; L. Prendergast, N.A. Uranova; A. Y. Klintsova, W.T. Greenough, J.E. Black. Decreased Dendritic Length in Bitufted and Stellate Interneurons in Prefrontal Cortex of Schizophrenic Brain. *Society for Neuroscience* Abstracts. 2000.

ABSTRACT OF THE DISSERTATION

Cell Type Differences in Intrinsic Membrane Properties Regulate

Responsiveness and Energy Consumption

by

Stephani L. Otte

Doctor of Philosophy in Neurosciences

University of California, San Diego, 2011

Professor Edward Callaway, Chair
Professor William Kristan, Co-Chair

Information processing in the brain depends upon the interactions of diverse signaling units, neurons, which vary in their circuit positions, biophysical and biochemical properties, and electrophysiological phenotypes. These distinguishing properties enable neurons to serve different computational and functional roles. For instance, the fast-spiking inhibitory subclasss, which synchronizes its firing at fast frequencies and makes divergent and convergent contacts onto the persimomatic

compartments of its targets, is hypothesized to play an important role in regulating the timing and probability of spike output and thus the flow of information through the brain (**reviewed in Chapter 1**). However, the functional consequences of synchronized inhibition will depend on the integrative properties and circuit locations of the recipient neurons.

Using a combination of in-vitro whole cell electrophysiology, modeling, and model-neuron hybrids (dynamic clamp), we determined how fast synchronized inhibition interacts with integrative properties of a variety of neuronal types to regulate the rate (**Chapter 2**) and timing (**Chapter 3**) of spike generation. We find that a neuron's intrinsic physiology substantially affects the ability of fast synchronized inhibition to control neuronal responsiveness. In addition, we demonstrate how the relevant physiology can be flexibly altered by contextual and neuromodulatory factors. The results of these experiments suggest that synchronized fast-spiking activity can differentially affect various circuit elements and each element's responsiveness can be adjusted on a range of time scales to suit the cortex's changing computational requirements.

Because the brain is one of the most energetically expensive organs in the body with action potential generation accounting for significant portion of the energy usage, we hypothesized that differences in neuronal properties may also serve to minimize energy consumption subject to functional constraints. Again using electrophysiology, modeling, and dynamic clamp, we compared the energy needed to produce action potentials singly and in trains for a wide range of channel densities and kinetic parameters, and examined which combinations of parameters maximized spiking

function while minimizing energetic cost **(Chapter 4)**. We found evidence supporting our hypothesis in a wide range of neurons from several species. We conclude that neuronal biophysics are tuned to perform cost-effective functions.

.

CHAPTER I

INTRODUCTION

Our experience and reaction to the world depends on the relay and transformation of sensory information through a complex and dynamic neural system. The system does more than passively integrate sensory information, creating an internal world model; it actively engages with a dynamic environment, selectively processing relevant information and suppressing the irrelevant. This gives us the ability to adapt to an ever changing environment and generate actions that are optimally adapted to a particular situation. To understand this dynamic and selective processing of information, we need to investigate the nature of effective neuronal communication.

Neurons communicate via the transmission of action potentials to their anatomical connections. However, only a small subset of the inputs is effective at generating a post-synaptic spike. The mechanisms responsible for regulating the effectiveness of neuronal communication are likely to underlie our ability to efficiently interact with our world. For example, even though we are bombarded by sensory inputs we can restrict processing to a single item and select an appropriate behavioral response. At the neuron level, this involves the selective communication between sensory neurons processing the attended stimuli and ultimately motor neurons instructing behavioral output. The relevant stimulus and the appropriate behavioral response are constantly changing; thus, the brain needs to be able to flexibly route information depending upon the contextual demands.

It has been hypothesized that neuroelectric oscillations, rhythmic shifts in excitability due to synchronous neuronal activity, act as dynamic mechanism to regulate the effectiveness of neuronal communication (Fries, 2005; Womelsdorf and

Fries, 2006). Synchronous neuronal activity can be detected by electrodes placed along the scalp (electroencephalographic [EEG] and magnetoencephalographic [MEG]), inside the brain (intracortical EEG and LFP), and on a neuron (whole-cell electrophysiology); creating a bridge to study neuronal synchronization across biological scales. Behavior and cognition can be linked to coordinated neuronal activity. Using these methods, coordinated activity in the gamma-frequency range (30-80 Hz) has received significant attention for several reasons. First, gamma activity has been correlated to numerous cognitive functions involved in information processing such as selective attention, memory maintenance, and sensory motor integration [reviewed in (Herrmann and Demiralp, 2005; Womelsdorf and Fries, 2006; Jensen et al., 2007)]. Second, disruptions in gamma activity are associated with disorders exhibiting information processing deficits, including schizophrenia, autism, and attention deficit hyperactivity disorder [reviewed in (Herrmann and Demiralp, 2005; Basar and Guntekin, 2008)]. Third, the fast frequency oscillations have been found to be modulated by both intrinsic (anticipation, experience, contextual influence, and action goals) (Scholvinck et al.; Riehle et al., 1997; von Stein et al., 2000; Engel et al., 2001; Engel and Singer, 2001; Fries et al., 2001; Womelsdorf and Fries, 2007) and extrinsic factors (saliency and familiarly of objects) (Busch et al., 2004; Schadow et al., 2007a; Schadow et al., 2007b) allowing for top-down and bottom-up control respectively. Finally, the fast oscillations are generated locally by the coordinated activity of interneurons which target the soma of principle neurons, an ideal location for gating the timing and probability of spike output. Thus, this locally

generated, actively modulated signal is hypothesized to be a fundamental mechanism for dynamically regulating information processing.

Information can be carried by action potentials based on several different coding schemes. On one end of the spectrum, action potentials may contain information based solely on the firing rate (the average number of spikes per unit of time). For instance the strength at which an innervated muscle is flexed depends solely on a rate code. At the other end of the spectrum, action potentials may contain information based on their precise timing relative to an external stimuli or the activity of other neurons.

Taking an agnostic approach to how information is actually encoded, the goal of this dissertation was to determine whether fast-frequency oscillations can affect the spike output of cortical neurons. Given that neurons are not homogenous entities, but differ considerably in their biochemical, electrical, synaptic, and functional properties, the approach was to determine how fast oscillatory activity interacts with the biophysical properties of neurons to regulate spike output. The results of these experiments suggest that a neuron's intrinsic physiology substantially affects the ability of gamma-synchronized inhibitory inputs to control response rate (**Chapter 2**) and response timing (**Chapter 3**), suggesting that fast-oscillatory activity can differentially affect different cortical circuit elements. In addition, the relevant physiology is not fixed, but flexibly altered by contextual and neuromodulatory factors, suggesting the gamma-frequency oscillations can be dynamically shaped to suit the cortex's changing computational requirements.

Background

Since the discovery of the electroencephalogram (EEG) over 80 years ago, oscillatory patterns in neuroelectric activity could be observed (Berger, 1929). The first detected and most prominent oscillations in spontaneous EEG were between 8-12 Hz and coined the alpha rhythm. The next detected frequency range between 12-30Hz was given the name beta. Faster oscillations in the human EEG between 30-80 Hz, termed gamma, could only be identified later because the amplitude of the oscillations decreases with increasing frequencies. Today oscillatory activity has been detected in frequencies ranges spanning over three orders of magnitude: from slow oscillations in the delta (0.5-3 Hz) to ultrafast (90-200 Hz) ranges.

Neuronal oscillations are the result of coordinated neuronal activity. In more detail, when a neuron fires an action potential in a regular manner, rhythmic fluctuations in the membrane potential can be detected in its post-synaptic targets by placing a microelectrode on the cell body of the recipient neuron. When several neurons fire action potentials both regularly and synchronously, the fluctuations are amplified creating rhythmic oscillations in excitability over a larger population of cells which can be detected by electrodes placed on the scalp (EEG and MEG) and inside the brain (intracortical EEG and LFP). The properties of the neuronal oscillations are the result of the physical architecture of the neuronal network and the speed of neuronal communication due to axon conduction and synaptic delays [reviewed in (Buzsaki and Draguhn, 2004)]. Thus, higher frequency oscillations (beta and gamma) are typically confined to a small neuronal space (Gray et al., 1989; Womelsdorf et al.,

2007), whereas large networks can be recruited during slow oscillations (von Stein et al., 2000).

Because the voltage signal from correlated neuronal activity can be detected across biological scales, researchers have been using these electrophysiological and other innovative techniques to investigate the cause and effect of synchronized neuronal activity. The different temporal and spatial frequencies of the oscillations may be functionally relevant as different brain states and neuronal networks are associated with particular oscillatory bands. The fast frequency oscillations in the gamma-frequency range have received a lot of attention—as well as skeptism—because of their association with active cognitive processes and the regulation of information processing. Here, I discuss gamma activity's correlation to active cognition; the generation and modulation of gamma activity at the network, cellular and molecular levels; the theories on gamma activity's role in information processing; and the energy expenditure due to high frequency activity.

Correlation of gamma oscillations to information processing

Gamma-frequency activity has been correlated to physiological and cognitive processes that are known to impact information processing. For instance, the level of arousal determines the body's receptivity to sensory stimuli and preparedness for action. Increasing arousal levels—up to a point—enhances the ability to effectively respond to the environment. Activation of the mesencephalic reticular formation, one of the primary systems involved in the biological mechanisms of arousal, has been shown to facilitate gamma-frequency oscillatory activity (Munk et al., 1996). In

addition, microelectrode recordings of neuronal activity have demonstrated that fast synchronization of neuronal discharges is prevalent during periods of vigilance and arousal (Steriade et al., 1996).

Information processing is also dependent upon top-down mechanisms—processes that are based upon expectations, intrinsic goals, and motivational states. These top-down processes act to intrinsically regulate the processing of sensory information. For instance, selective attention is the cognitive process of selectively concentrating on one aspect on the environment while ignoring other aspects. A stereotypical example of selective attention is the "cocktail party effect"—the ability to focus one's listening attention on a single talker among a cacophony of conversations and background noise. The effects of selective attention on neuronal synchronization has been assessed by presenting identical sensory stimulation across conditions where covert attention is directed to different aspects of the sensory input. In these tasks, gamma-frequency neuronal synchronization has been found to be upregulated or downregulated in brain regions (Tiitinen et al., 1993; Tallon-Baudry et al., 1997; Gruber et al., 1999; Muller et al., 2000; Ray et al., 2008) and individual neurons (Fries et al., 2001a; Womelsdorf et al., 2006) processing relevant and distracting sensory information, respectively. Other top-down mechanism such as anticipation (Fujioka et al., 2009; Schadow et al., 2009a) and working memory maintenance [reviewed in (Jensen et al., 2007)] have also been associated with enhanced gamma-frequency activity.

The selective processing of information will also be driven by sensory inputs that demand attention due to their novelty or salience. Researchers investigating the

effect of visual stimulus properties on fast neuronal synchronization have found that increasing the size of the stimulus (Busch et al., 2004), increasing stimulus contrast (Busch et al., 2004), and presenting objects centrally compared to laterally (Schadow et al., 2007b), all enhance gamma-frequency activity. In the auditory domain, more gamma activity is evoked with higher compared to lower intensity sounds (Schadow et al., 2007a); and the frequency of the sinusoidal tone modulates the strength of the evoked gamma response (Lenz et al., 2008).

The above examples demonstrate that gamma-band activity is associated with active information processing and modulated by both top-down (the brain's integration of past experiences and expectations) and bottom-up (the brain's integration of sensory information) influences. Importantly, the enhancement of activity is also associated with improved behavioral performance and perceptual accuracy. For example, there are several studies that present evidence for a strong association in humans between gamma-band activity and behavioral response speed (Jokeit and Makeig, 1994; Haig et al., 1999; Gonzalez Andino et al., 2005; Frund et al., 2007; Schadow et al., 2009b) and response accuracy (Kaiser et al., 2008a; Kaiser et al., 2008b; Kaiser et al., 2009). In addition, in monkeys performing an attention task, the strength of this selective synchronization of neuronal groups processing relevant information has been shown to correspond to behavioral performance and changes in attentional demands (Taylor et al., 2005; Womelsdorf et al., 2006; Lakatos et al., 2008). The influence of local synchronization on behavioral responses was found to be spatially selective (Womelsdorf et al., 2006), suggesting that strength of synchronization is modulated at a fine spatial scale. The emerging view from these

findings is that neuronal coherences at fast frequencies subserves the selective and effective transmission of information among neuronal groups during the integration of sensory information (Laughlin and Sejnowski, 2003; Fries, 2005; Sejnowski and Paulsen, 2006; Womelsdorf and Fries, 2006) to ultimately trigger adaptive motor performance.

Corroborating the evidence that fast frequency synchronization of neuronal discharges is integral to healthy brain functioning, gamma activity is disrupted in diseases associated with sensory processing and attentional impairments, such as schizophrenia, autism, and ADHD [reviewed in (Uhlhaas and Singer; Spencer et al., 2003; Herrmann and Demiralp, 2005)]. For example, several studies have found that positive symptoms (hallucinations and delusions) of schizophrenia are correlated with enhanced amplitude and phase synchronization of evoked and induced gamma-band activity whereas negative symptoms (blunted affect, alogia, anhedonia, asoociality, avolition, etc) are related to reduced high-frequency oscillations [reviewed in (Uhlhaas and Singer; Herrmann and Demiralp, 2005)]. Furthermore, a reduction of gamma activity is observed in patients with Alzheimer's Disease, whereas an increase is found in patients with ADHD [reviewed in (Herrmann and Demiralp, 2005)].

Generation and modulation of gamma activity

Mounting evidence has demonstrated that the fast rhythmic signal is generated in the local circuit by a specialized class of interneurons: the fast-spiking parvalbumin positive inhibitory cells. The fast-spiking neurons form an extensive network, interconnected by gap junctions (specialized intracellular connection that allow direct

electrical communication between cells) (Gibson et al., 1999; Beierlein et al., 2000; Galarreta and Hestrin, 2001a, 2002), and fast inhibitory synaptic connections (Bartos et al., 2001; Bartos et al., 2002; Galarreta and Hestrin, 2002), which helps to synchronize action potential activity within the fast-spiking network. The cells can generate trains of high frequency (100+ Hz) narrow action potentials due to the expression of a fast-activating potassium channel (Kv3.1 /KCNC1) (Martina et al., 1998; Erisir et al., 1999), however the duration of the inhibitory post-synaptic potentials regulates the firing rate to the gamma frequency range (Whittington et al., 1995). Furthermore, the cells exhibit a high intrinsic resonance frequency and low attenuation of high frequency inputs (Fellous et al., 2001; Hasenstaub et al., 2005), suggesting that the cells are capable of following gamma frequency inputs. Experiments with pharmacologically isolated networks of inhibitory neurons and model simulations have shown that these networks can generate synchronized gamma-band oscillations on their own (Whittington et al., 1995; Vida et al., 2006) (reviewed in (Bartos et al., 2007; Fries et al., 2007), requiring only synaptic inhibition and gap junction coupling to be intact (Deans et al., 2001; Hormuzdi et al., 2001; Traub et al., 2003). The network of inhibitory cells is activated by excitatory inputs from pyramidal cells; driving the interneurons by activating principle cell activity even by non-rhythmic means, is sufficient to generate gamma-frequency rhythmicity (Adesnik and Scanziani; Cardin et al., 2009; Sohal et al., 2009).

Action potentials in fast-spiking interneurons trigger the release of GABA from pre-synaptic vesicles into the synaptic cleft. GABA then binds to kinetically fast GABA-A receptors (Bartos et al., 2001; Bartos et al., 2002) in post-synaptic cells,

resulting in fast hyperpolarizing fluctuations in the membrane potential, termed inhibitory post-synaptic potentials (IPSPs). The synchronized network of fast-spiking inhibitory neurons makes both divergent and convergent contacts onto the perisomatic compartments of other cortical neurons (Miles et al., 1996; Kawaguchi and Kubota, 1998; Papp et al., 2001; Tamas et al., 2004), producing strong and effective gamma-frequency hyperpolarizations in their targets (Hasenstaub et al., 2005; Cardin et al., 2009; Sohal et al., 2009). By synapsing near the spike initiation zone of its post-synaptic targets, the fast-spiking inhibitory network is able to effectively control the timing and probability of spike output in principal cells.

Because gamma activity is dependent upon the activation of this specialized inhibitory subclass, many factors can modulate and/or disrupt the oscillations. The fast-spiking neurons receive excitatory thalamocortical, corticocortical, and local excitatory inputs through NMDA (N-methyl-D-aspartate) receptors (Kinney et al., 2006), particularly the NR2A/NR2B subtype, and AMPA (α-amino-3-hydroxyl-5-methyl-4-isoxazole-propionate) receptors with rapid decay kinetics (Angulo et al., 2003), making them susceptible to changes in glutamatergic drive. In addition, pharmacological and pathological agents affecting GABAergic neurotransmission have been found to modulate gamma activity. For example, the frequency of the oscillation is controlled by the duration of individual inhibitory synaptic events (i.e., mainly dependent on decay constant $\tau_{GABA(A)}$). A wide range of general anesthetics which demonstrate a long increase in the decay time constant for the $GABA_A$ synaptic responses (including inhalational agents enflurane and isofurane, the opiates sufentanil and fentanyl, the GABAergic agents thiopental and propofol, and the

sedative/hypnotic agent diazepam) have all been shown to reduce gamma band activity [reviewed in (Whittington et al., 2000; Deco and Thiele, 2009)]. The power of the oscillations is controlled by changes in the amplitude of the $GABA_A$ response, making it susceptible to agents which affect the release and availability of GABA. Interestingly, a selective agonist for the α_2 subunit containing $GABA_A$ receptors (the receptors selectively expressed in the fast-spiking synapses) improves behavioral and electrophysiological measures of prefrontal function in individuals with schizophrenia (Lewis et al., 2008).

Additionally, cholinergic modulators have been found to modulate strength of gamma. For instance, in isolated slices, bath application of a acetylcholine receptor agonist generated gamma activity (Roopun et al.; Buhl et al., 1998; Fellous and Sejnowski, 2000). *In vivo* application of a cholinergic agonist with synchrony-inducing light increased the probability that the stimulated cells engaged in gamma oscillations and response synchronization (Rodriguez et al., 2004). In addition, *in vivo* activation of cholinergic cells in the basal forebrain with neurotensin lead to enhanced gamma activity in the cortical EEG (Cape et al., 2000). Cholinergic activity can be signal driven, but it can also be driven by top-down mechanisms emanating from the prefrontal cortex which influence acetylcholine levels in the parietal attention system and in sensory cortices (Sarter et al., 2005). In fact, the cholinergic input to the cortex is able to specifically target selected cortical areas in a task- and context-dependent manner (Zaborszky and Duque, 2000; Zaborszky, 2002). Thus, acetylcholine may play an important role in locally modulating the temporal interactions of neurons in a given area [reviewed in (Deco and Thiele, 2009)].

Possible functions of gamma-frequency activity

The brain is relatively hard wired: anatomical connections between and within brain regions exist in stereotyped ways creating a connectome to route information. For instance, sensory information is routed to a particular thalamic nucleus, then to layer 4 of the appropriate sensory cortex (e.g. visual information is routed to the lateral geniculate nucleus of the thalamus then to layer 4 of the visual cortex). Layer 4 sends projections to Layer 2/3 (which sends and receives information from other cortical areas), Layer 5 (which projects to subcortical regions), and Layer 6 (which projects back to the thalamus). While the signal travels in a manner dictated by the anatomical connectivity, the activity traversing the anatomical routes at a given moment determine the functional connectivity. The functional connectome is remarkably flexible, constantly changing to efficiently interact with a dynamic environment. The same sensory input can be differentially processed depending upon the state of the system and the contextual demands.

Because gamma activity is correlated to active cognitive processes and reflects the coordinated activity of a large ensemble of inhibitory neurons that make both divergent and convergent contacts near the spike initiation zone of its post-synaptic targets, it has been hypothesized to act as a mechanism to dynamically regulate the functional connectome. Consider a cell receiving input from a set of neurons, when those inputs are synchronized the effect on the post-synaptic target is enhanced because the post-synaptic potentials integrate. The coordinated activity of fast-spiking cells results in gamma-frequency windows of increased and decreased excitation (Hasenstaub et al., 2005; Cardin et al., 2009; Sohal et al., 2009), providing a

mechanism for regulating the spike output of neurons with high temporal precession. Synchronization at lower frequencies is more temporally smeared, resulting in a less pronounced summation of the PSPs. Thus, the fast-frequency inhibitory input may act as a mechanism to regulate the probability and timing of spike output.

Spike rate. Even though inhibitory inputs to a neuron typically lower a neuron's firing rate, changes in input synchrony of the fast-spiking inhibitory neurons may actually increase the spike rates of their post-synaptic targets. Temporally correlated inputs summate creating large fluctuations in a cell's membrane potential. It has been shown that the post-synaptic cell is more likely to spike when the membrane potential rises quickly immediately preceding a spike due to high coherence of the inputs (Azouz and Gray, 2000, 2003). Even though fast-spiking cell activity acts to hyperpolarize the neuron, windows of opportunity for spiking are created during the relief of inhibition. Therefore changes in the coherence of inhibitory inputs has been theorized to act as a gain control—enhancing or suppressing the number of spikes generated to the same input stimulus—which may be used as a code to downstream neurons. In fact, computational experiments have shown that increases in synchronous input enhance neuronal sensitivity and the gain of neuronal spiking responses (Salinas and Sejnowski, 2000; Galarreta and Hestrin, 2001b; Salinas and Sejnowski, 2001; Tiesinga et al., 2004; Borgers et al., 2005; Tiesinga and Toups, 2005). In other words, even small increases in synchronization increase the impact of a given input, and small increases of stimulus strength can result in multiplicatively scaled increases in spiking responses during coherent activity (Tiesinga et al., 2004). This effect of input synchronization on the gain of spiking activity appears particularly

pronounced for oscillatory synchronization in the gamma-frequency band (Burchell et al., 1998; Deans et al., 2001; Csicsvari et al., 2003; Tiesinga and Toups, 2005).

Spike time. Changes in input synchrony may also affect timing of the spike discharges in the post-synaptic targets. The oscillatory fluctuations in the membrane potential of a cell periodically elevates the membrane potential close to threshold, providing discrete windows of opportunity for the neuron to respond. If the input is not appropriately timed, the response may be delayed or ignored altogether. Indeed various studies have shown that the post-synaptic spike times are aligned to the phase of the oscillations, with the strongest output evident in the rising phase of the depolarization (Burchell et al., 1998; Chrobak and Buzsaki, 1998; Pouille and Scanziani, 2001; Csicsvari et al., 2003). It has been theorized that restricting the timing of the spike outputs of the inhibitory cells' post-synaptic targets acts to group or bind subsets of neurons together for further joint processing and enhance their impact through feedforward coincidence detection (Salinas and Sejnowski, 2000, 2001). In other words, correlated or temporally bound discharges have a stronger impact on neuronal populations than temporally disorganized inputs (Abeles, 1982; Konig et al., 1996; Engel et al., 2001). This binding tag has been hypothesized to act as a flexible code for linking neurons into flexible cell assemblies. Information could be processed, transferred, and stored by transiently linking subgroups of neurons together (Engel and Singer, 2001; Fries, 2005).

It has also been hypothesized that the fast oscillatory activity may act as a timing code, in which the amplitude of excitation is recorded in the time of occurrence of output spikes relative to the gamma cycle; stronger inputs leading to earlier

responses (Fries et al., 2007). In other words, given the same oscillatory input, a neuron that is more depolarized will reach threshold sooner and thereby fire earlier than a neuron that is less depolarized. This gamma-phase shift would provide an instantaneous analog representation of excitation. Indeed, one study in monkeys found that neurons that are more strongly activated by the preferred stimulus orientation, fire earlier in the LFP gamma cycle than neurons that are less strongly activated (Vinck et al.). excitation. Because pyramidal cell activity actively recruits the fast-spiking inhibitory network, a neuron that fires earlier in the gamma cycle is then in a position to suppress the activity of neurons receiving weaker input through disynaptic feedforward inhibition. It has been proposed that within each gamma cycle there is a race among the pyramidal cells in which the most excited pyramidal cells will compete against the less excited ones. The winner suppresses the weak response and improve the signal-to-noise ratios (Olufsen et al., 2003; Borgers et al., 2005; Fries et al., 2007). In addition, gamma activity as a timing code has been proposed to enable spike-time dependent plasticity. Spike time dependent plasticity requires that the presyanptic neuron is either leading or lagging the postsynaptic neuron by a few milliseconds (Markram et al., 1997; Bi and Poo, 1998; Caporale and Dan, 2008), which could be achieved by gamma-phase shifting (Vinck et al.)

However, the ability of gamma-frequency inhibition to control the responsiveness of their targets will depend on their target's integrative properties. The way a neuron processes its synaptic inputs depends on its membrane filtering properties and its ion channels' distribution, densities, and kinetics, which varies considerably within and between neuronal types. As discussed previously, the fast-

spiking parvalbumin neurons posses a unique combination of ion channels that enable them to efficiently follow and disseminate high frequency activity, whereas other neuronal types with particular integrative properties and circuit positions, are likely to serve different computational or functional roles. The next two chapters of this dissertation focus on how the integrative properties of a variety of neuronal types interact with fast-frequency oscillatory inhibition to control response rate and timing.

Gamma Oscillations and Energy Consumption

Gamma-frequency activity have been shown to be energetically expensive (Niessing et al., 2005; Huchzermeyer et al., 2008; Zaehle et al., 2009). The high-frequency activity requires enhanced activation of Na^+/K^+-ATPases to restore ionic gradients after spike generation to maintain excitability. Most of the ATP that is used in the brain is produced by oxidative phosphorylation in mitochondria. Neurons exhibit significant heterogeneity in mitochondrial number, size, distribution, and enzymatic activity (Wong-Riley, 1989; Waagepetersen et al., 1999; Popov et al., 2005). The fast-spiking parvalbumin inhibitory neurons express abundant mitochondria (Carr et al., 1989; Martinez-Guijarro et al., 1993; Toida et al., 1996), which could contribute to the remarkable vulnerability of gamma oscillations during pathological processes (Huchzermeyer et al., 2008).

Expensive functions prompt the evolution of expense-minimizing adaptations (Weibel, 2000), and energy availability does appear to have constrained the evolution of macroscopic brain features, resulting in minimization of brain volume subject to functional requirements (Aiello and Wheeler, 1995; Fish and Lockwood, 2003; Isler

and van Schaik, 2006; Barrickman et al., 2008). We therefore asked whether differences on the microscopic level (i.e differences in neuronal properties) may also serve to minimize energy consumption subject to functional constraints (Chapter 4).

CHAPTER II

CELL-TYPE SPECIFIC CONTROL OF NERUONAL RESPONSIVENESS BY GAMMA BAND OSCILLATORY INHIBITION

Summary

Neocortical networks are composed of diverse populations of cells that differ in their chemical content, electrophysiological characteristics, and connectivity. Gamma frequency oscillatory activity of inhibitory sub-networks has been hypothesized to regulate information processing in the cortex as a whole. Inhibitory neurons in these sub-networks synchronize their firing and selectively innervate the perisomatic compartments of their target neurons transmitting both slow tonic and fast fluctuating inhibition. How do different types of cortical neurons respond to changes in the level (slow changes in inhibitory tone) and structure (fast changes in synchronized inhibition) of perisomatic inhibition? What accounts for the heterogeneity between cell types, and are they fixed or flexible? To answer these questions, we use in vitro electrophysiology to study six distinct types of cortical neurons. We demonstrate that different types of neurons systematically vary in their receptiveness to fast changes in the structure of inhibition and the range over which changes in inhibitory tone affect their output. Using simple neuron models and model-neuron hybrids (dynamic clamp), we determine which intrinsic differences between cell types lead to these variations in receptiveness. These results suggest important differences in the way cell types are affected by gamma frequency inhibition, which may have important circuit level implications. Although intrinsic differences observed in vitro are useful for the elucidation of basic cellular properties and differences between cell types, we also demonstrate how the integrative properties of neurons are likely to be rapidly modulated in the context of active networks *in vivo*.

Introduction

Synchronization of neocortical neuronal activity, particularly at gamma (30-80Hz) frequencies, is related to cognitive functions such as working memory maintenance, attentional selection, sensory-motor integration, and memory retrieval (reviewed in (Herrmann and Demiralp, 2005; Womelsdorf and Fries, 2006; Jensen et al., 2007)), while disruption of oscillatory synchronization is associated with attention and cognition disorders, including schizophrenia, epilepsy, and ADHD (reviewed in (Herrmann and Demiralp, 2005; Basar and Guntekin, 2008)). However, the physiological and functional consequences of gamma activity on individual neurons remain unclear.

The generation of these oscillations depends critically upon inhibitory neuronal interactions ((Cardin et al., 2009; Sohal et al., 2009); reviewed in (Bartos et al., 2007; Fries et al., 2007; Fries, 2009)). Indeed, the intracellular correlate of these population-level oscillations is synchronized, phase-locked inhibition (Klausberger et al., 2003; Hasenstaub et al., 2005) believed to play a role in timing or coordinating the activity of other neurons in the cortical circuit (Galarreta and Hestrin, 2002; Fries et al., 2007). Further, fast changes in oscillatory synchronization are often enveloped by slow changes in overall local circuit activity and inhibitory tone (Hasenstaub et al., 2005; Lakatos et al., 2008). Thus, in order to understand how gamma activity contributes to cortical information processing, we must determine how fast changes in inhibitory synchrony, in concert with slow changes in inhibitory tone, interact with the integrative properties of target neurons.

There are many different types of cortical neurons, each having specific neurochemical properties, patterns of connectivity, laminar distribution, and electrophysiological characteristics (Kawaguchi, 1993; Kasper et al., 1994; Markram et al., 2004). Therefore, different cells are likely to respond differently to changes in inhibition. For example, different types of neurons may vary in the amplitude and timing of the synchronized inhibition they receive during a given epoch of gamma, as well as in their temporal filtering and integration of a given pattern of inhibitory inputs. Consistent with these expectations, experiments in cortical brain slices have demonstrated that spatiotemporal filtering of inhibitory synaptic inputs differs between inhibitory cell types (Tamas et al., 2000; Szabadics et al., 2001), and modeling and experimental studies have revealed that changes in fluctuating input affect a cell's spike rate (Aradi et al., 2002; Chance et al., 2002; Kuhn et al., 2004; Tiesinga et al., 2004). Here we further investigate the integrative properties of inhibitory and excitatory neuronal types, focusing on the interactions between slow and fast changes in inhibition and the properties that are likely to underlie differences between cells.

We use intracellular recordings from a variety of excitatory and inhibitory cortical neuron types in vitro to characterize the diverse relationships between slow changes and fast fluctuations in a cell's inhibitory inputs, and its output. We then use a simple single-compartment model to predict which intrinsic electrophysiological differences can account for the observed relationship differences. Next, we modify neurons' intrinsic properties, using dynamic clamp, to test these predictions in multiple neuron types. Finally, we demonstrate how these relationships may be flexibly altered by factors such as neuromodulation and local circuit activity.

Results

Integration of Tonic and Fluctuating Inhibition Depends on Cell Type. Whole-cell current clamp recordings were performed on three types of projection neurons (Fig. 2.1A) and three types of inhibitory neurons (Fig. 2.1B). Projection neurons were identified by their pyramidal shaped cell body, and separated into three classes based on their laminar location and spiking phenotype: layer 5 pyramidal neurons capable of generating intrinsic burst discharges (Fig. 2.1A, L5B)(Kasper et al., 1994), layer 5 pyramidal neurons generating regular trains of single spikes (Fig. 2.1A, L5R)(Kasper et al., 1994), and layer 2/3 pyramidal neurons generating regular-spiking adapting trains of action potentials (Fig. 2.1A, L2/3). In addition, three types of local-circuit inhibitory neurons were identified by GFP expression in the GIN, G42 and G30 lines of mice (Oliva et al., 2000; Chattopadhyaya et al., 2004; Lopez-Bendito et al., 2004) and confirmed by their spiking phenotype. GFP+ cells in G42 mice generated rapid, non-adapting trains of action potentials (Fig. 2.1B, G42), and are parvalbumin-positive (Chattopadhyaya et al., 2004). GFP+ cells in the GIN mice generated slower, accommodating trains of action potentials (Fig. 2.1B, GIN), and are somatostatin-positive Martinotti neurons (Oliva et al., 2000; Xu et al., 2006; Xu and Callaway, 2009). GIN neurons are heterogeneous in their spike parameters and expression of other chemical markers (Halabisky et al., 2006; Xu et al., 2006), but were not further subdivided in this study. While the G30 line labels many neuron types with various morphologies and firing patterns, only irregular-spiking GFP+ cells were used in this

study (Fig. 1B, G30). These cells are multipolar, cholecystokinin-positive, and express type 1 cannabinoid receptors (Galarreta et al., 2004; Xu and Callaway, 2009).

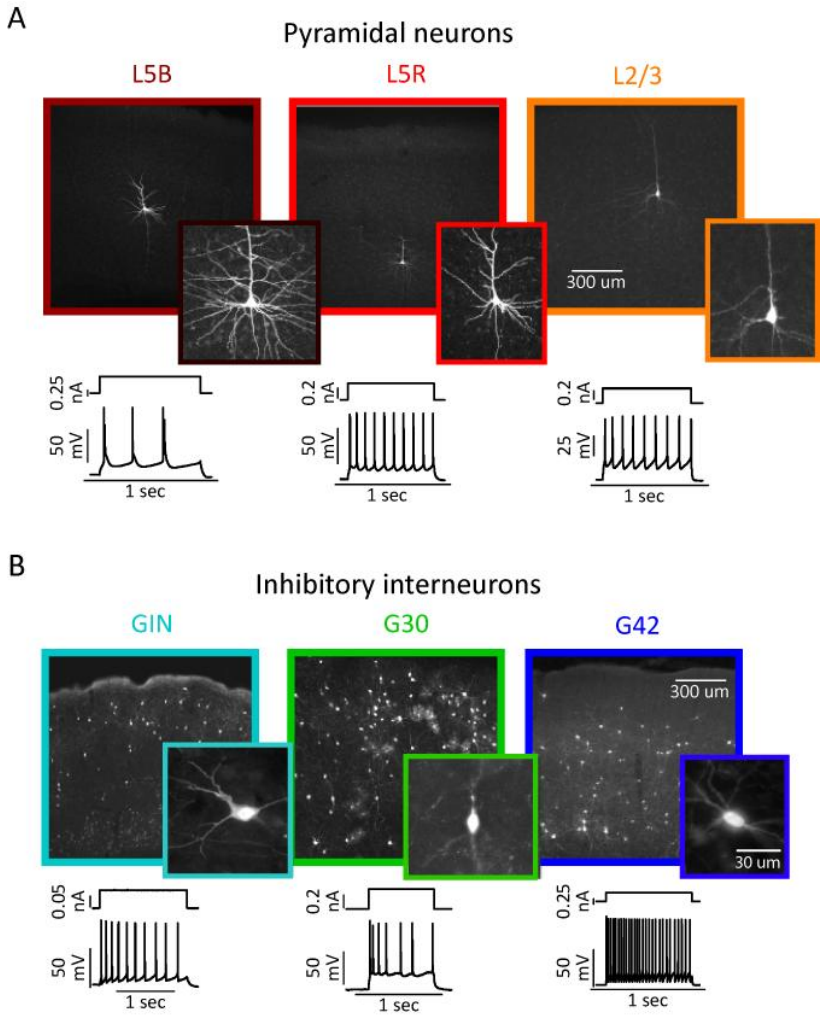

Figure 2.1. Six electrically and morphologically distinct types of neurons in mouse somatosensory cortex.

A. Biocytin-filled reconstructions (top) and intracellular recordings (bottom) showing the laminar location, morphology, and spiking responses typical of Layer 5 bursting (left, dark red), Layer 5 regular-spiking (center, red) and Layer 2/3 regular-spiking (right, orange) pyramidal neurons
B. Biocytin-filled reconstructions (top) and intracellular recordings (bottom) showing the laminar location, morphology, and spiking responses typical of GFP+ inhibitory neurons in the GIN (left, cyan, adapting-spiking), G30/SZ (center, green, irregular-spiking), and G42 (right, blue, fast-spiking).

Our experimental approach and data analysis methods are first exemplified in figure 2.2, for a representative irregular spiking inhibitory neuron. To examine how slow changes in the level of network activity interact with changes in fast synchronized inhibition to affect the responsiveness of these different neuronal types, each neuron was depolarized (Fig. 2.2A, tonic excitation) until it fired action potentials at least 3Hz (example trace in Fig. 2.2Ba). Superimposed on this stimulus was a fluctuating 40Hz sinusoidal hyperpolarizing current whose mean offset and amplitude varied randomly from trial to trial (Fig. 2.2A, fluctuating inhibition). To mimic changes in the synchrony of the cell's inhibitory inputs without changes to the overall drive to the neuron, the mean level of hyperpolarizing current was maintained while changing the amplitude of the gamma frequency sine wave, and spike rate was measured in each condition (e.g. Fig. 2.2Bd, green horizontal overlay). To mimic changes in the overall amount of inhibitory drive to a neuron without changes in the fast temporal structure, the mean level of hyperpolarizing current was changed without changing the amplitude of the superimposed sine wave, and spike rate was measured in each condition (Fig. 2.2Bd, green vertical overlay). Trials with differing levels of tonic inhibition and input synchrony were randomly interleaved to avoid systematic changes that might affect the cells' responses (see Methods).

For each neuron, the response to changing levels of inhibition and changing levels of input synchrony was displayed as a summary grid (e.g. Fig. 2.2Bd). Each combination of input mean and input synchrony is represented by one box in the grid, brighter boxes represent combinations that typically elicit more action potentials. Horizontal slices through the grid represent the effect on spike output of changes in

input synchrony, for a given mean (e.g. 2.2Bd, green horizontal overlay; 2.2Ca, green line). Vertical slices through the grid represent the effect of changes in mean inhibition, for a given level of inhibitory synchrony (e.g. 2.2Bd, green vertical overlay; 2.2Cb, green line). The full families of input-output curves are shown in figure 2.2C.

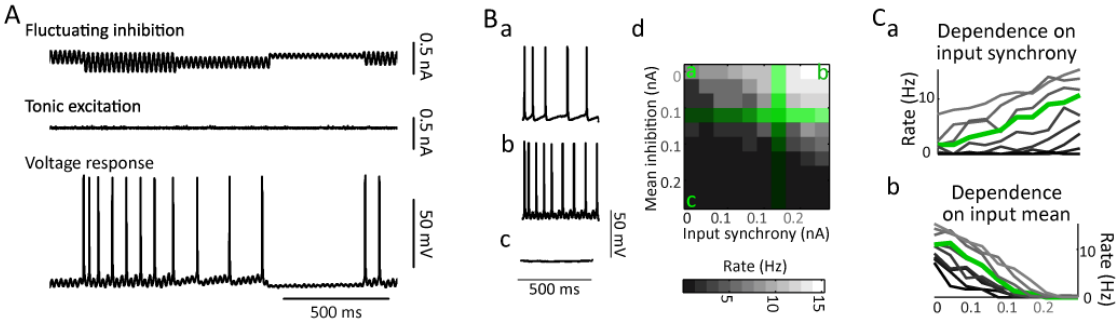

Figure 2.2. Gamma oscillation stimulation protocol and analysis.

A. Neurons were stimulated with a constant level (I_{base}) of depolarizing current (middle) and a fluctuating hyperpolarizing current (top). On each 500 ms long trial, stimuli were constructed by randomly adding one of ten levels of tonic inhibition ("input mean") (equal intervals, ranging from 0 to I_{base}) to a zero-mean 40 Hz oscillatory current ("input synchrony") with a amplitude of a one of ten randomly selected values (equal intervals, ranging from 0 to I_{base}).
B. Sample responses to low-mean, low-synchrony inputs (a), low-mean, high-synchrony inputs (b), and high-mean, low-synchrony inputs (c). d: The cell's responsiveness (black to white) systematically varied with mean inhibitory current (vertical axes) and inhibitory synchrony (horizontal axes). Responsiveness was reduced as the amount of inhibition increased (green vertical overlay), and increased as the inhibition became more synchronized (green horizontal overlay).
Ca. Dependence of spike rate on input synchrony, for each level of mean inhibition. Green line represents the green-highlighted horizontal segment of Bd. Lighter grey = less mean inhibition. b: Dependence of output spike rate on mean inhibition, for each level of input synchrony. Green line represents the green-highlighted vertical segment of Bd. Lighter gray = more inhibitory synchrony.

Typical responses from the six types of neurons are shown in figures 2.3AB, and population responses are shown in figure 2.3CD. The different types of neurons systematically differed in their relative responses to changes in input mean and

synchrony. Neurons whose response was relatively synchrony-independent (Fig. 2.3 Aa and Ba) showed roughly horizontal grid isoclines, roughly flat input-output curves for spike rate as a function of input synchrony (shown above the grids) and their input-output curves for spike rate as a function of mean inhibition (shown to the right of the grids) overlapped. Conversely, neurons whose response was relatively synchrony-dependent (Fig. 2.3 Abc, Bbc) showed diagonal grid isoclines and sloped input-output curves for spike rate as a function of input synchrony. Each neuron's spike rate dependence on input mean and synchrony was calculated by taking the median of the slopes of the F-I relationship about the midpoint for each condition. Relative synchrony dependence was quantified by dividing the neuron's synchrony dependence by its mean dependence.

G42 fast-spiking neurons (Fig. 2.3Bc; 2.3C, blue circles, n=7) had the largest normalized synchrony dependence (Kruskal-Wallis $p<0.05$); these neurons were nearly as sensitive to changes in inhibitory synchrony as to changes in inhibitory mean. Bursting layer 5 pyramidal neurons (Fig. 2.3Aa; 3.3C, dark red up-triangles, n=6) and GIN regular-spiking inhibitory neurons (Fig. 2.3Ba; 2.3C, cyan squares, n=7) had the smallest synchrony to mean ratios (Kruskal-Wallis $p<0.05$); these neurons were much more sensitive to changes in the overall drive to the cell than to changes in the synchrony of the inputs, and increases in the amplitude of the fast fluctuating input had little impact on their spike rate (Fig. 2.3Aa and 2.3Ba). L5R (Fig. 2.3Ab; 2.3C, red triangles, n=6) and L2/3 (Fig. 2.3Ac; 2.3C, orange triangles, n=9) excitatory neurons, and G30 (Fig. 2.3Bb; 2.3C, green diamonds, n=6) inhibitory

neurons, increased their spike rate as the amplitude of the gamma oscillation increased, and had intermediate synchrony to mean ratios.

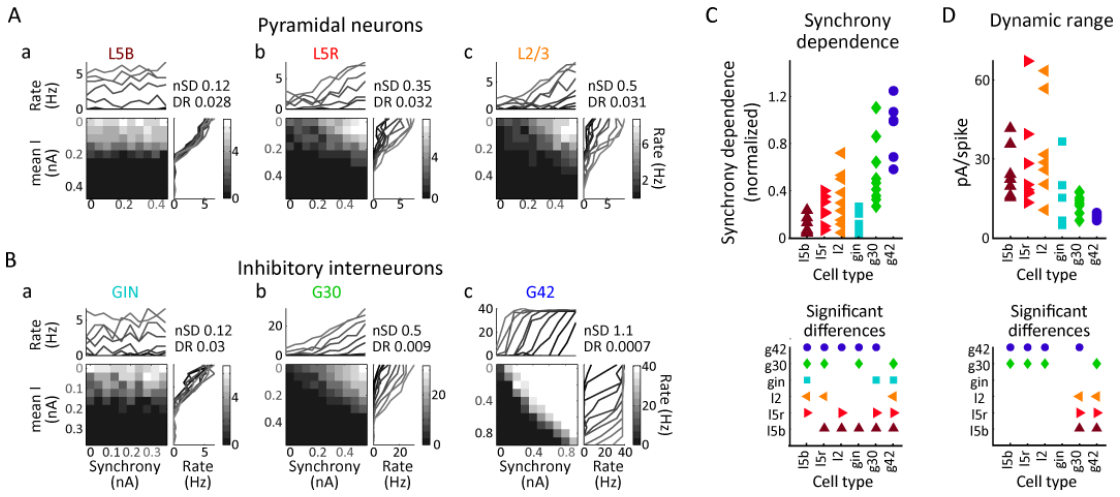

Figure 2. 3. Systematic, cell type specific differences in responsiveness to gamma-band oscillatory synchronized inhibition.

A. Typical responses of three types of pyramidal neurons: Layer 5 bursting (L5B, a), Layer 5 regular spiking (L5R, b), and Layer 2/3 regular spiking (L2/3, c). All of the example pyramidal cells' firing rates change gradually with changes in mean drive indicating a high dynamic range (DR) in spikes/nA: L5B= 0.028; L5R =0.032; L2/3 = 0.031. The example L2/3 and L5R pyramidal neurons' firing rates also change gradually with changing level of input synchrony (normalized synchrony dependence or "NSD": L2/3= 0.5; L5R=0.35), while the L5B neuron's firing rate is relatively unaffected by changes in input synchrony (NSD= 0.12).

B. Typical responses of three types of inhibitory interneurons from the GIN, G30, and G42 mouse lines. The GIN and G30 neurons' firing rates gradually change with changes in mean drive (DR in spikes/nA: GIN= 0.03; G30=0.009), however the GIN neuron's firing rate is unaffected by changes in input synchrony (NSD=0.12), while the G30 neuron's firing rate gradually increases with changing level of input synchrony (NSD=0.5). The G42 neuron's firing rate changes abruptly with changes in mean drive (DR=0.007 spikes/nA), and is strongly affected by changes in input synchrony (NSD = 1.1).

C. Top: The six cell types differed in the relative dependence of firing rates on changes in input synchrony, normalized by changes in input mean ("normalized synchrony dependence"; n=44 cells). L5B, dark red▲; L5R, red►; L2/3, orange ◄; GIN, cyan ■; G30, green ♦; and G42, blue ●. Bottom: Significant differences in normalized synchrony dependence between cell types (Kruskal-Wallis $p<0.05$) are indicated by the corresponding cell marker.

D. Top: The median dependence of firing rate on changes on input mean (nS per spike, n=43 cells). Bottom: Significant differences (Kruskal-Wallis $p<0.05$) are indicated by the corresponding cell marker.

The cell types also differed in their dynamic range: some neurons' responses were all-or-none (i.e., changes in input mean or synchrony abruptly shifted them from never firing to firing at their maximum rate), while some showed graded responses. Because L5B (Fig. 2.3Aa) and GIN (Fig. 2.3Ba) neurons were insensitive to changes in the synchrony of inhibitory input, all neurons' dynamic ranges were quantified by measuring the shallowness of the slope of the spike rate dependence on changes in mean inhibition. G42 fast-spiking neurons had the smallest dynamic range of the cell types (Fig. 2.3D, blue circles), either firing at every cycle of gamma or not at all. Pyramidal neurons of all types had the largest dynamic range (Fig. 2.3A; 2.3D, triangles); these neurons' responses changed gradually with changes in inhibitory mean or synchrony. GIN regular spiking inhibitory neurons exhibited the most variable dynamic ranges (Fig. 2.3D, cyan squares), and did not significantly differ from any other neuronal types. These results suggest that there are cell-type specific variations in the range over which changes in the level of tonic inhibition can affect neuronal responsiveness. What features of the cells' electrophysiology might account for these differences?

Synchrony dependence and passive membrane properties. A cell's input resistance and membrane capacitance act as a low-pass filter attenuating responses to inputs at high frequencies (Hutcheon and Yarom, 2000), leading us to hypothesize that the differences in relative synchrony dependence between cell types was due to differences in their average time constants. Consistent with this hypothesis, in a simple Hodgkin-Huxley style model neuron stimulated with the same current protocol as the real neurons, output spike rate was nearly independent of input synchrony (Fig.

2.4Aa). Decreasing the time constant, either by decreasing the membrane capacitance (Fig. 2.4Aa →b) or by decreasing the total input resistance (Fig. 2.4Aa →c), increased the model cell's relative responsiveness to changes in input synchrony.

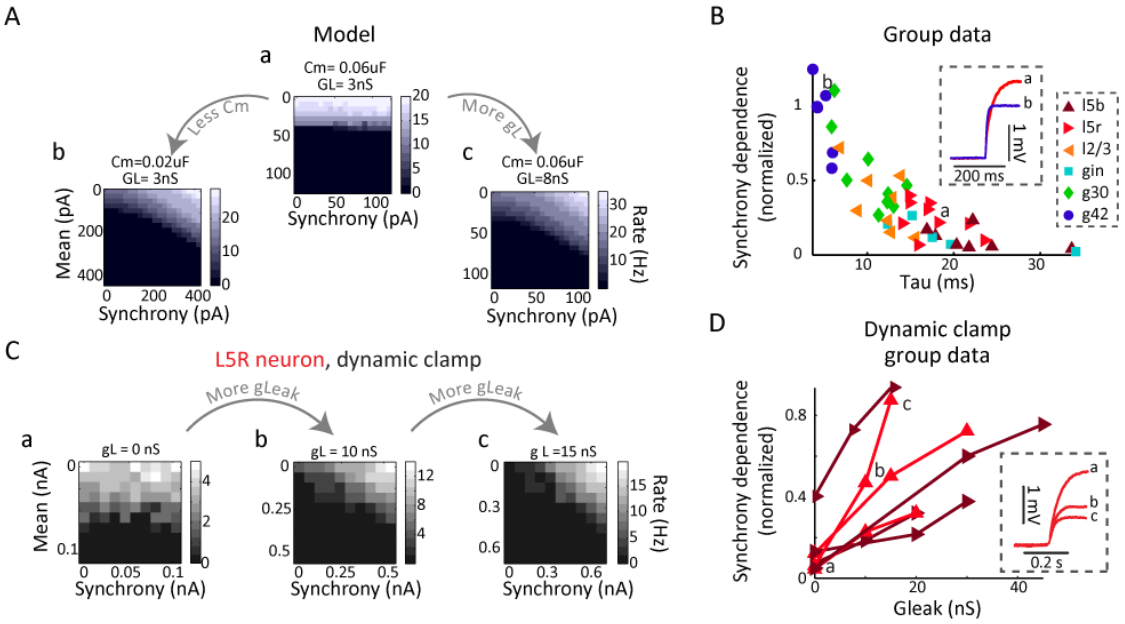

Figure 2.4. Neurons' relative synchrony dependence depends on passive membrane filtering properties.

A. A single compartment Hodgkin-Huxley style model neuron's response to the stimulation protocol is relatively synchrony independent. (a). Decreasing its time constant either by decreasing the capacitance (a→b) or increasing the leak conductance (a→c) increases synchrony dependence.

B. Across n=38 cells, time constant correlates with normalized synchrony dependence (Spearman's R=-0.88; $p<0.05$). An example voltage trace from a Layer 5 regular spiking neuron with a short time constant (a) and an example G42 fast-spiking with a long time constant (b) are illustrated and corresponding points marked.

C. Changing membrane filtering properties changes synchrony dependence. An example L5 regular spiking cell's response is weakly dependent on input synchrony; reducing its time constant by the addition of leak conductance (a→b→c) increases its relative synchrony dependence.

D. Across n =7 L5R (red) and L5B cells (dark red), increasing the leak conductance reliably increased the neuron's synchrony to mean ratio ($p<0.05$). Trial blocks shown in inset are marked. Inset: Example voltage traces from Ca, Cb, Cc.

To assess these relationships in our experimental data, for 44 recorded neurons, we compared their time constants with their normalized synchrony dependences, revealing a strong correlation (Spearman's R:-0.88; p = 5.04e-013; Fig. 2.4B). These results suggest that neurons with long time constants (e.g. Fig. 2.4Ba) filter out the fast fluctuations in their inputs and simply respond to the mean level of inhibition, while neurons with short time constants (e.g. Fig. 2.4Bb) can follow both slow changes in network activity and fast fluctuations in inhibitory drive.

To confirm our hypothesis that the neuron's time constant controls the ability of gamma frequency input to affect neuronal responsiveness, in layer V pyramidal neurons that were initially unresponsive to input synchrony, dynamic clamp was used to add a leak conductance (a constant conductance whose reversal potential matched the cell's resting potential). The addition of leak conductance effectively decreased the cells' membrane resistance and time constants (e.g. Figure 2.4D, a→b→c). This manipulation caused synchrony-independent neurons to develop synchrony dependence. Across n=7 Layer 5 neurons, increasing leak conductance reliably increased the neuron's normalized synchrony dependence (Friedman's p = .0009**)** (Figure 2.4D).

Dynamic range and spike afterhyperpolarizations. Medium- and long-duration afterhyperpolarizations (AHPs) affect both the minimum achievable spike rate frequency and the frequency range that cells respond to (Schreiber et al., 2004; Prescott and Sejnowski, 2008). Different neurons vary greatly in the shape and amplitude of their AHPs, from a few milliseconds to several seconds (Sah and Faber, 2002). We thus hypothesized that differences in the range over which changes in

network activity and fast fluctuating input affected neuronal responsiveness might be due to differences in their AHPs. To determine the potential impact of AHP conductances on a neuron's dynamic range, we varied the amount and duration of the AHP conductance in a simple single compartment Hodgkin-Huxley style model neuron. Increasing the AHP conductance (Fig. 2.5Aa→b) or AHP duration (Fig. 2.5Aa→c) increased the model cell's dynamic range: the model cell became responsive to a larger range of changes in mean inhibition (Fig. 2.5bc, top to bottom) and inhibitory synchrony (Fig. 2.5bc, left to right).

Consistent with this hypothesis, in 44 recorded cells, the AHP duration was closely correlated with the dynamic range (Spearman's R=0.68; p = 4.25e-007) (Fig. 2.5Ba). However, because the shallowness of the mean dependence, which is measured as spikes/nA, can be distorted by combining neurons with drastically different conductances, we separately analyzed the data for cells with a more narrow range of input resistances. When only neurons with similar input resistance between 50-200 MΩ are plotted (Fig. 2.5Bb) an even stronger correlation between dynamic range and AHP duration is revealed (R=0.87; p = 1.85e-006). Neurons with a short AHP duration (e.g. Fig. 2.1B, G42) are able to fire every time there is a relief of inhibition, provided that the neuron is sufficiently excited; conversely, neurons with a long AHP duration (e.g. Fig. 2.1A, pyramidal neurons) are still hyperpolarized during the next peak of the gamma cycle after firing an action potential, but increased levels of excitation can counteract this accumulated AHP, leading to an increased range over which neurons are responsive to changes in the level of inhibitory input.

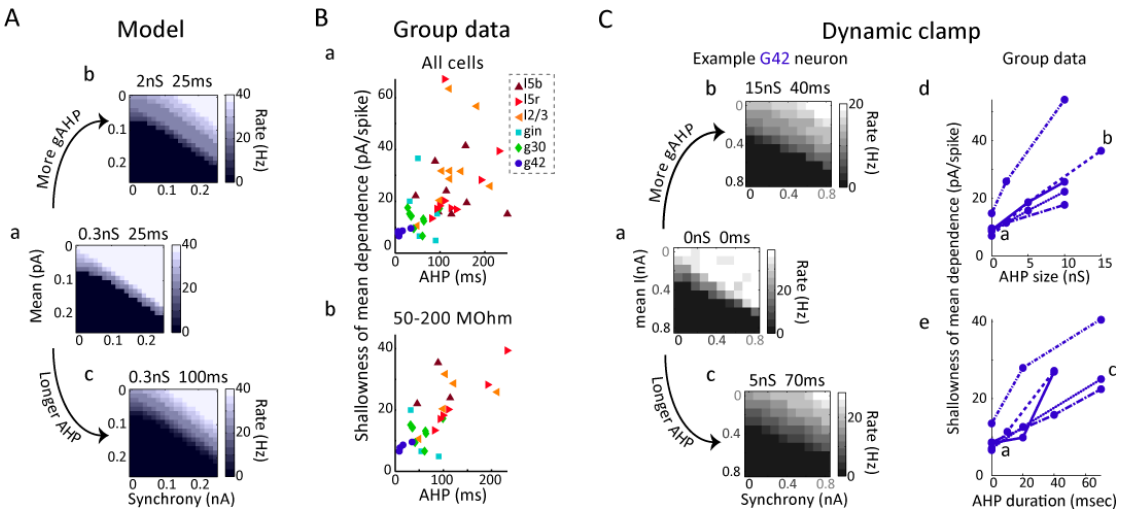

Figure 2.5. Neurons' dynamic range depends on afterhyperpolarization amplitude and duration.

A. In a single-compartment Hodgkin-Huxley style model neuron with a brief, weak afterhyperpolarization (AHP), response rate depends steeply on input strength (a). Either increasing the AHP conductance amplitude (a→b), or the AHP duration (a→c), makes the input-output relationship shallower.

B. The correlation of the shallowness of the input-output relationship with AHP duration (a) for n=44 neurons (Spearman's R: 0.68; p 4.25e-007), and (b) in the n=26 neurons with input resistances between 50-200 MΩ (Spearman's R: 0.87; p 1.85e-006). Neuronal types are color- and marker-coded as in figures 3 and 4.

C. Dynamic clamp was used to add an artificial AHP conductance to a sample G42 neuron (a). Either increasing the amplitude (a→b) or increasing the duration (a→c) of the artificial AHP conductance increases the neuron's dynamic range. Across n=5 cells, increasing either the amount of AHP (d) or the duration of the AHP (e) reliably increased the neurons' dynamic range.

To confirm these results, we used dynamic clamp to add an AHP conductance to G42 fast-spiking neurons, which initially all exhibited a small dynamic range (Fig. 3D, blue circles). Increasing the amount (in nS; Fig. 5Ca→b) or the duration (Fig. 5Ca→c) of the additional AHP clearly increased the range over which changes in the level and structure of the inhibition affected the neurons' responses. In n=5 G42 cells,

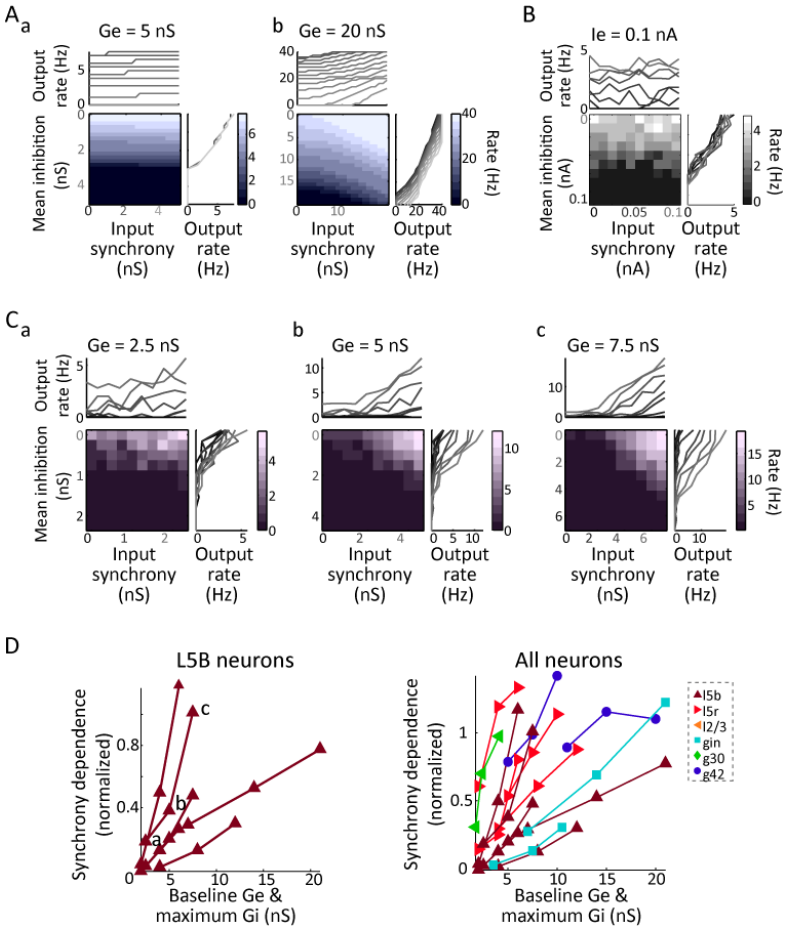

Figure 2.6. The relative synchrony dependence of neurons changes with background conductance input.

A. a) In a model neuron stimulated with constant excitatory conductance and randomly varying inhibitory conductance, spike responses are only weakly dependent on input synchrony, compared to input mean. b) Proportionately increasing the model neuron's inhibitory and excitatory conductance causes its output to become synchrony dependent.
B. In a L5B, changing the synchrony of the current stimulus has little effect on spike output.
C. Driving the same neuron in B with stronger artificial synaptic drive (i.e. proportionately scaling up the mean inhibitory and excitatory conductances) creates synchrony dependence in the cell's spike output.
D. a) In n=6 large bursting pyramidal neurons, adding artificial synaptic drive changed their response profiles from relatively synchrony-independent to relatively synchrony-dependent.
b) In n=13 neurons, including G42, GIN, L2/3, and L5R neurons, scaling up the excitatory and inhibitory conductances that the neuron received increased its synchrony dependence, whether or not the neuron's response was initially synchrony dependent.

increasing the AHP amount (in nS, 2.5Cd, Friedman's $p<0.01$) or duration (in ms, 2.5Ce, Friedman's $p<0.01$) reliably increased the neuron's dynamic range.

Network activity changes neurons' responsiveness to gamma oscillations. Different neuron types differ in the degree to which they are intrinsically responsive to gamma-band synchrony in their inputs, but all cortical neurons are embedded in recurrent networks. When these networks are active, their constituent neurons deluge one another with excitatory and inhibitory synaptic inputs. These inputs, taken together, can be large enough to substantially alter neurons' effective input resistances and time constants (Pare et al., 1998; Shu et al., 2003; Haider et al., 2006; Cardin et al., 2008); reviewed in (Haider and McCormick, 2009)). Since membrane time constant is a key determinant of neuronal filtering properties, can increases in local network activity permit gamma oscillatory synaptic inputs to control neurons' output, even for neurons whose intrinsic properties ordinarily make them unresponsive to gamma oscillations?

In a model neuron whose output is initially unaffected by gamma-frequency input synchrony (Fig. 2.6Aa), increasing the neuron's level of synaptic input, by scaling up the inhibitory and excitatory conductance stimuli, causes the neuron's output to become relatively more dependent on input synchrony (Fig. 2.6Ab). The same effect can also be seen in real neurons, by using dynamic clamp to generate artificial excitatory and inhibitory conductance stimuli (rather than depolarizing and hyperpolarizing current stimuli). An example L5 neuron whose response rate is unaffected by gamma-frequency input synchrony (Fig. 2.6B) becomes progressively more affected by changes in input synchrony as the excitatory and inhibitory

conductance inputs are scaled up (Fig. 2.6Ca→c). Across n=6 large bursting pyramidal neurons, scaling up the artificial synaptic drive significantly increased the normalized synchrony dependence by an average of 0.59 +-0.37 (unitless; Friedman's p=0.0025) (Fig. 2.6Da). In n=13 neurons, including bursting and regular spiking Layer 5 and Layer 2/3 pyramidal neurons, and G30, GIN and G42 inhibitory neurons, additional drive increased the synchrony to mean ratio in all cases (by an average of 0.58 +- 0.26 unitless, Friedman's p=7.7e-007, Fig. 2.6Db).

Discussion

Many groups have found that the generation of gamma-frequency oscillations depends critically on the activation of fast-spiking inhibitory neuronal networks, which changes both the level and structure of inhibition in the local network ((Cardin et al., 2009; Sohal et al., 2009); for review see: (Bartos et al., 2007; Fries et al., 2007; Fries, 2009)). Fast-spiking interneurons make both divergent and convergent contacts onto the perisomatic compartments of other cortical neurons, producing strong and effective hyperpolarizations in their post-synaptic targets (Miles et al., 1996; Kawaguchi and Kubota, 1998; Papp et al., 2001). Because of their gap junction coupling (Galarreta and Hestrin, 2001a, 2002), fast inhibitory synaptic connections (Bartos et al., 2001; Bartos et al., 2002; Galarreta and Hestrin, 2002), rapid spiking conductances (Erisir et al., 1999), and reduced filtering of high frequency fluctuations (Fellous et al., 2001; Hasenstaub et al., 2005), these neurons tend to synchronize their firing at gamma (30-80 Hz) frequencies, generating oscillatory inhibition (Hasenstaub

et al., 2005; Cardin et al., 2009; Sohal et al., 2009). Because cortical neurons vary in their laminar distribution and patterns of connectivity, different types of neurons may vary in the amplitude and timing of the synchronized inhibition they receive during gamma activity. In addition, because of differences in electrophysiological and neurochemical properties between cells, neurons will likely differ in their integration of these inhibitory inputs. Here, we examined how changes in inhibitory tone and changes in inhibitory structure interact to control neuronal responsiveness, and how these interactions differ in different elements of the cortical circuit.

Cell-type specific differences in gamma frequency input integration. Cell types differed considerably in both their relative dependence on slowly changing inhibition compared to fast changing inhibitory structure (Figure 2.3C) as well as the range over which changes in the level of inhibition and structure of inhibition affected their spike rate (Figure 2.3D). Differences between the neurons' passive filtering properties (Figure 2.4) and active conductances (Figure 2.5) help explain these cell-type specific variations.

G42 fast-spiking inhibitory neurons are the most sensitive to changes in fast fluctuating input and have the smallest dynamic range. Their short time constant and brief AHP duration allow them to integrate gamma frequency inputs and, if sufficiently excited, spike on every cycle of gamma. This supports the finding of several previous studies showing that these cells are able to follow fast frequency inputs (Fellous et al., 2001; Hasenstaub et al., 2005), and are likely to be the generators of gamma activity in the cortex ((For review see: (Bartos et al., 2007; Fries et al., 2007; Fries, 2009)); (Cardin et al., 2009; Sohal et al., 2009)). G30 irregular

spiking inhibitory neurons also had relatively short time constants and AHP durations, owing to their relatively high synchrony to mean ratios and small dynamic ranges. Both of these cell types make inhibitory synaptic contacts on the somatic compartments of other neuronal types (Freund, 2003), which is the preferred location for regulating the spike output of their post-synaptic targets. If these neurons receive gamma frequency input, they are likely able to transmit this fast fluctuating input to their post-synaptic targets, suggesting that these cells are capable of amplifying gamma activity in the local network.

GIN regular spiking inhibitory neurons are the least sensitive of the inhibitory types to changes in gamma frequency input synchrony, due to their relatively long time constants. Since changes in input synchrony cannot increase these neurons' spike rates, networks of GIN neurons will likely only be inhibited, not entrained, by increases in activity of FS networks, suggesting an inverse relationship between the activity in these two populations of interneurons. The GIN inhibitory neurons have the most variation in their dynamic ranges between cells. GFP+ cells in the GIN line of mice have been shown to vary greatly in their afterhyperpolarization characteristics, which plausibly accounts for this variation (Halabisky et al., 2006).

Of the pyramidal neurons, Layer 5 bursting neurons (L5B) were the least dependent on changes in gamma-band input synchrony, due to their relatively long time constants in the resting state (Figure 2.3C). Increases in gamma-frequency inhibition have a minimal influence on L5B cells' responsiveness, while gamma-frequency inhibition can more easily excite L5R and L2/3 pyramidal neurons. Even though some of the pyramidal neurons are able to integrate gamma frequency

information, the relatively long AHP duration of all the pyramidal types tested prevents the neurons from firing on every gamma cycle. Decreasing the level of inhibition can overcome the hyperpolarizing effects of the AHP conductances, effectively expanding the "dynamic range" over which the cell's responsiveness can be modified.

Fast, flexible control of gamma-frequency input integration**.** Although intrinsic differences observed in vitro are useful for the elucidation of basic cellular properties and differences between cell types, it is important to note that the passive filtering properties of the neuron are in fact under rapid control. A cell's time constant is dynamically regulated by the opening and closing of ion channels in its membrane. The addition or subtraction of any synaptic or ionic conductances will change the neuron's frequency response, and, as we have shown here, affect the ability of gamma-frequency input to control its firing. Therefore, neurons bombarded by synaptic conductances during active brain states will likely be more strongly affected by gamma frequency input synchrony. Indeed, we found that using dynamic clamp to simulate increases in synaptic drive created the ability to respond to gamma-frequency oscillatory input in cells, such as L5 bursting neurons, that are not ordinarily responsive to gamma (Figure 2.6). Additionally, neurons of all types become relatively more responsive to gamma-oscillatory input, compared to slowly fluctuating inputs, as their overall synaptic drive scales up. These results suggest that increased synaptic activity will likely increase the whole network's ability to generate and transmit gamma oscillations. Consistent with this, increases in gamma activity often occur during periods of high network activity, including the peak of slower

oscillations (Csicsvari et al., 2003; Freeman et al., 2003; Hasenstaub et al., 2005; Lakatos et al., 2005; Canolty et al., 2006; Lakatos et al., 2008), or periods of increased arousal or attention (Fries et al., 2001b; Womelsdorf et al., 2006; Buschman and Miller, 2007; Lakatos et al., 2008).

Further, neurons' afterhyperpolarization amplitude and kinetics can be dynamically modulated (reviewed in(Vogalis et al., 2002)). For instance, the slow AHP conductance (g_{sAHP}) is regulated by a balance of phosphorylation and dephosphorylation in which activation of the cAMP/PKA pathway causes a reduction in the I_{sAHP}, whereas activation of phosphatases leads to an increase in the current (Pedarzani et al., 1998). The slow AHP conductance in many neurons is strongly inhibited by neurotransmitters that act through G-protein coupled receptors, such as noradrenaline (McCormick et al., 1991), serotonin (Higgs et al., 2006), glutamate (Nicoll, 1988), and acetylcholine (Blitzer et al., 1994). These same neurotransmitters have also been shown to increase network activity (Nicoll, 1988; McCormick et al., 1991; McCormick, 1992a; Wang and McCormick, 1993; Steriade et al., 2001). The current study implies that increasing the overall excitability of the network and decreasing the duration of the AHP conductance should increase the probability of the neuron firing at the termination of the IPSPs, thus enhancing the transmission of gamma oscillatory activity through the whole network. Consistent with this hypothesis, cholinergic agonists have been found to enhance gamma activity in vivo (Rodriguez et al., 2004) . In addition, isolated slices are evoked using agonists for metabotropic glutamate receptors (Whittington et al., 1995), muscarinic acetylcholine

receptors (Fisahn et al., 1998; Fellous and Sejnowski, 2000) and kainate receptors (Hajos et al., 2000; Fisahn et al., 2004).

The studies described here delve further into the complex interactions that occur between highly interconnected networks of diverse populations of cortical neuron types. We found that in some cell types, fast changes in inhibitory structure can overcome the suppressive effects of increases in inhibitory tone; this variable effect is modulated by the cell's passive filtering properties. We also found cell type differences in the range over which changes in inhibitory tone and inhibitory structure affect neuronal responsivenss; the "dynamic range" is modulated by the active conductances in the cell that control the cell's intrinsic periodicity. Because these passive and active conductances are dynamically regulated in vivo by feedforward and recurrent synaptic activity and intracellular signaling molecules, neuronal responsiveness to inhibitory tone and structure can be changed over a range of time scales to suit the network's changing computational requirements. Future studies will better reveal how each cell type contributes to and is regulated by dynamic changes in vivo as well as how dysregulation of these circuits at the genetic, molecular, cellular and network levels contributes to neurological disease.

Methods

In vitro slice experiments

All animal use was approved by the Institutional Animal Care and Use Committee at The Salk Institute for Biological Studies. The G42 transgenic mice

were originally generated by Josh Huang at Cold Spring Harbor (Chattopadhyaya et al., 2004) and were obtained from Jackson Labs (http://www.jax.org). G30 transgenic mice were originally generated by Gabor Szabo at the Department of Functional Neuroanatomy at the Institute of Experimental Medicine in Budapest, Hungary (Lopez-Bendito et al., 2004) and obtained from Sascha Nelson at Brandeis University. GIN transgenic mice were generated in John Swan's laboratory at the Baylor College of Medicine (Oliva et al., 2000) and obtained from Jackson Labs. The C57/Bl6 mice were obtained from Jackson Labs.

To prepare brain slices, mice aged P18-P26 were deeply anesthetized with Nembutal (100mg/kg i.p.) and rapidly decapitated. A vibratome (Series 1000, Vibratome) was used to cut 300 μm thick coronal brain slices from the somatosensory cortex (S1). Slices were cut in ice-cold artificial cerebral spinal fluid (ACSF; 24mM NaCl, 5mM KCl, 26mM NaHCO3, 1mM KH2PO4, 1mM MgSO4, 10mM glucose, 1.2mM CaCl2, and 1mM kynurenic acid) and incubated at 35 degrees C for at least 30 minutes in ACSF bubbled with 95% O2/ 5% CO2 before transferring to a room-temperature submerged chamber for recording.

Whole cell recordings. Neurons were visualized at 40X magnification using a DIC/fluorescent Olympus microscope and a video camera (VE 1000; MTI-Dage). Pyramidal neurons from layer III and V were identified by their laminar location, pyramidal-shaped cell bodies and long apical dendrite. GFP+ cells from G42, G30, and GIN mice were identified by their fluorescence. Whole-cell recordings were performed using glass pipettes pulled on a P-97 micropipette puller (Sutter Instruments, Novato, CA) from borosilicate glass (Sutter Instruments) to 3- 5MΩ,

filled with 130mM K-gluconate, 0.2mM EGTA, 2mM MgCl2, 6mM KCl, 10mM HEPES, 2.5mM Na-ATP, 0.5mM Na-GTP, and 10mM K-phosphocreatine (pH 7.2). Signals were amplified with a MultiClamp 700B amplifier (Molecular Devices). Data were acquired and digitized using the Spike2 Power 1401 collection system (Cambridge Electronic Designs, Cambridge, UK). All recordings were performed in current-clamp mode. Intracellular recordings were accepted if they showed a stable resting membrane potential below −50 mV throughout the experiment, and had stable-size action potentials with heights at least 60 mV (for pyramidal neurons) or 40 mV (for interneurons) and widths at half-height of less than 2 ms.

Cell characterization. The membrane time constant and input resistance were evaluated using current pulses sufficient to cause 2-5 mV hyperpolarizations. AHP duration and amplitude were measured from the average of >5 action potentials separated by at least 200ms. AHP amplitude was measured as the maximum negative voltage deflection relative to spike threshold. AHP duration was measured as the time when mean voltage was 2/3 recovered towards rest.

Stimulus protocol. Cells were stimulated with a constant depolarizing current I_{base} sufficient to maintain firing at 3-5 Hz. To characterize cells' relative dependence on inhibitory synchrony, compared to tonic inhibition, cells were simultaneously stimulated with a hyperpolarizing current whose mean offset randomly varied every 500 msec, and a zero-mean 40 Hz sine wave current whose amplitude randomly varied every 500 msec. Ten levels of tonic inhibition (equal intervals, ranging from 0 to I_{base}), and ten levels of gamma-wave amplitude (equal intervals, ranging from 0 to

I_{base}), were tested in each block of trials. Each block lasted at least 600 sec, for at least 10 repeats of each trial condition.

Dynamic clamp

In some blocks, as indicated in the results, the same protocol was repeated using conductance rather than current injections. Fast real-time dynamic clamp was implemented using RTLDC (Boston University; (Dorval et al., 2001)) combined with the Real-Time Application Interface (www.rtai.org), device drivers from the COMEDI project (www.comedi.org), and a NI DAQ PCI-MIO-16XE-50 board (National Instruments). The dynamic clamp was used to generate two conductances, one with a reversal potential of 0mV (mimicking excitation), and another with a reversal potential of -80mV (mimicking inhibition) (Figure 2.6). Cells were simultaneously stimulated with a constant excitatory conductance, a fluctuating inhibitory conductance, and a sine-varying inhibitory conductance, as in the current-injection protocol above. In some blocks, as indicated in the results, dynamic clamp was also used to add a leak conductance (Figure 2.4CD) or an AHP conductance (Figure 2.5CD) to the neurons. Each cell's leak conductance was changed by adding a constant conductance whose reversal potential was set to match the resting membrane potential of the recorded neuron. The strength and duration of each cell's afterhyperpolarization (AHP) was changed by adding a conductance that reversed at -80 mV and decayed as a single exponential.

Analysis

The slope of the rate-mean inhibition or rate-synchrony relationships were quantified by measuring the slope of the input-firing rate relationship about the midpoint, for all points with firing rates between 20 and 80% of the cell's maximum. A separate slope was calculated for each rate-mean or rate-synchrony curve, and the median of these slopes was used for display and statistical analysis. To measure the neuron's relative synchrony dependence, the median slope of the rate-synchrony relationship was normalized by dividing by the median slope of the rate-mean relationship.

Model

A single compartment neuron model was implemented in Matlab. The model contained a Hodgkin-Huxley style transient Na+ conductance and delayed rectifier potassium conductance (Erisir et al., 1999). The default maximum sodium and potassium conductances were 700 and 1400 nS, respectively, and the corresponding currents reversed at 50 and -80 mV, respectively. The model also contained a constant leak conductance of 3 nS which reversed at –70mV, and an afterhyperpolarization conductance which was modeled as a single exponential reversing at -80 mV, with a default maximum conductance of 10% of the cell's leak conductance and a default time constant of 40ms. The model neuron was stimulated with the same experimental protocol as the real neurons. The model cell's capacitance (Figure 2.4A), leak conductance (Figure 2.4A), AHP duration (Figure 2.5A), and AHP amplitude (Figure 2.5A) were systematically changed as indicated in the results.

Acknowledgments

We thank members of the Callaway lab, Terry Sejnowski, and Massimo Scanziani for helpful discussions. We are grateful for support from NIH grant MH063912, the Crick-Jacobs Center for Theoretical and Computational Biology, the Aginsky Foundation, and the Kavli Institute for Brain and Mind.

Publication Acknowledgments

Chapter 2, in full, is a reprint of the material as it appears in J Neuroscience 2010; Otte S, Hasenstaub A, Callaway EM. J Neuroscience 30:2150-2159. The dissertation author was co-primary authors of this material. Secondary author is thesis advisor.

CHAPTER III

NEURONAL BIOPHYSICS MODULATE THE ABILITY OF GAMMA OSCILLATIONS TO CONTROL RESPONSE TIMING

Summary

Cortical function emerges from interactions among diverse neuron types that vary in their molecular identity, intrinsic biophysics, and circuit function. Synchronized gamma-frequency oscillatory activation of fast-spiking inhibitory neurons has been hypothesized to regulate the timing and probability of spike output. The functional consequences of such inhibition will depend on the integrative properties and circuit locations of the recipient neurons. Here, we study the interactions between neurons' intrinsic properties, the degree of gamma-band synchrony among their inhibitory inputs, and spike timing. We find that neuronal types systematically vary in the phase and precision of their spike timing relative to the peak of gamma frequency input, and the degree to which their spike time output time precesses with changes in inhibitory synchrony or level of activation. Using simple neuron models and model-neuron hybrids (dynamic clamp), we determine which intrinsic differences between cell types lead to these variations in responsiveness. These results suggest important differences in the way cell types are affected by gamma frequency inhibition. Although intrinsic differences observed in vitro are useful for the elucidation of basic cellular properties and differences between cell types, we also demonstrate how the integrative properties of neurons are likely to be rapidly modulated in the context of active networks *in vivo*.

Introduction

Cortical network function emerges from interactions among diverse neuron types. One window into these interactions is the rhythmic or oscillatory signals they generate: various cortical rhythms are associated with different cognitive, behavioral, or motivational states, are generated through different intrinsic and circuit mechanisms, and likely reflect different types of cell-cell or cell-network interactions. It is therefore of interest to understand precisely what types of interactions these rhythms reflect, and the mechanistic relationship (if any) between their presence or absence and the cognitive functions with which they are associated.

Oscillatory activity in the gamma (Y) band (30-80 Hz) is of particular interest, both because of its clear association with processing of salient stimuli, and because of its frequent disruption in diseases of cognition or attention, most notably schizophrenia (). This rhythm has been proposed to serve numerous roles in circuit function, many of which rely on its ability to provide a framework for temporally organizing activity. Among these, it has been proposed to implement network-level amplification or routing, by synchronizing neurons' spiking to facilitate coincidence detection in their targets; to facilitate learning, by restricting neurons' relative spike times to those optimal for inducing spike-timing dependent plasticity; to underlie a winner-take-all selection scheme, where earlier-firing neurons recruit widespread inhibition that blocks other neurons' firing for the duration of the oscillation; to provide the carrier wave for a phase code, in which information is carried in neurons' phase of firing with respect to the oscillation; as well as to be an epiphenomenon. These hypotheses have vastly different implications for our understanding of cortical operation.

Resolving these possibilities is made more difficult by the complexity of the cortical architecture: cortex contains numerous types of neuron, which differ in their laminar positioning, local and long-distance connectivity, intrinsic biophysics, sensitivity to neuromodulation, and expression of peptides and calcium binding proteins. These neurons need not all participate in, or be affected by, oscillatory activity in the same ways. Indeed, in vivo and in vitro recordings have demonstrated that while many neurons' firing is to some extent synchronized with gamma-band oscillations in the local field, neuron types vary in the strength and phase of these relationships. These studies have also demonstrated that synchronized activity among one type of interneuron, the soma-targeting parvalbumin-positive basket neuron, is critical for generating these oscillations, and that synchronized, rhythmic inhibition of cells' somata is an intracellular correlate of the extracellularly recorded gamma oscillations. This implies that the potential computational roles of these oscillations may be limited by the ability of rhythmic synchronized inhibition to modulate spike timing, in various cell types, in ways consistent with these functional hypotheses – in other words, by the ability of rhythmic inhibition to restrict action potential timing to occur in specific time windows, to encode the strength of other inputs in spike phase with respect to the oscillation, or both.

To investigate these possibilities, we use intracellular recordings from several types of cortical excitatory and inhibitory neurons to characterize the relationship between slow and fast fluctuations in cells' somatic inputs and the phase and precision of their spike timing. We then use a simple model to predict which intrinsic biophysical differences can account for the observed differences in control of spike timing. Next, we test these predictions in multiple neuron types by using dynamic clamp to modify these

intrinsic properties. Finally, we demonstrate how these relationships can be flexibly altered by factors such as neuromodulation and local circuit activity.

Results

Cell-type differences in entrainment and precession to fast fluctuating inhibition. Whole-cell current clamp recordings were performed on three types of projection neurons (Fig. 3.1A) and three types of inhibitory neurons (Fig. 3.1B). Projection neurons were identified by their pyramidal shaped cell body and long apical dendrites, and separated into three classes based on their laminar location and spiking phenotype: layer 5 pyramidal neurons capable of generating intrinsic burst discharges (Fig. 3.1A, L5B)(Kasper et al., 1994), layer 5 pyramidal neurons generating regular trains of single spikes (Fig. 3.1A, L5R), and layer 2/3 pyramidal neurons generating regular-spiking adapting trains of action potentials (Fig. 3.1A, L2/3). In addition, three types of local-circuit inhibitory neurons were identified by GFP expression in the GIN, G42 and G30 lines of mice (Oliva et al., 2000; Chattopadhyaya et al., 2004; Lopez-Bendito et al., 2004) and confirmed by their spiking phenotype. GFP+ cells in G42 mice generated rapid, non-adapting trains of action potentials (Fig. 3.1B, G42), and are parvalbumin-positive (Chattopadhyaya et al., 2004). GFP+ cells in the GIN mice generated slower, accommodating trains of action potentials (Fig. 3.1B, GIN), often exhibited low-threshold spiking (LTS) behavior, and are somatostatin-positive Martinotti neurons (Oliva et al., 2000; Xu et al., 2006; Xu and Callaway, 2009). GIN neurons are heterogeneous in their spike parameters and expression of other chemical markers (Halabisky et al., 2006; Xu et al., 2006), but were not further subdivided in this study.

While the G30 line labels many neuron types with various morphologies and firing patterns, only irregular-spiking GFP+ cells were used in this study (Fig. 3.1B, G30). These cells are multipolar, cholecystokinin-positive, and express type 1 cannabinoid receptors (Galarreta et al., 2004; Xu and Callaway, 2009).

Our experimental approach and data analysis methods are first exemplified in figure 3.1C, for a representative irregular spiking G30 neuron. To examine how slow changes in the level of network activity interacts with fast synchronized inhibition to affect the timing of spike output for these different neuronal types, each neuron was depolarized (Figure 3.1C, tonic excitation), until it fired action potentials at a rate of at least 3Hz. Superimposed on the stimulus was a fluctuating 40Hz hyperpolarizing current, whose mean offset and amplitude varied randomly from trial to trial (Figure 3.1C, fluctuating inhibition). For each stimulus parameter the results were displayed as a circular histogram of the spike output times relative to the gamma-frequency input (e.g Fig 3.1D). Superimposed on each histogram is a best-fit von Mises distribution whose color indicates the average spike time, and whose color saturation indicates the standard deviation of the spike times. To mimic changes drive to a neuron without changes in the fast temporal structure, the mean level of hyperpolarizing current was changed without changing the amplitude of the superimposed sine wave (e.g. 3.2 ABab). For this example neuron, decreasing the mean level of hyperpolarizing current resulted in more spikes that occurred on average earlier in the gamma cycle (Fig. 3.2 Bab). To mimic changes in the synchrony of the cell's inhibitory inputs without changes to the overall drive to a neuron, the mean level of hyperpolarizing current was maintained while changing the amplitude

of the gamma frequency input (e.g. Fig. 3.2 ABbc). For this example neuron, decreasing the amplitude of the gamma frequency sine wave resulted in less precisely timed spikes.

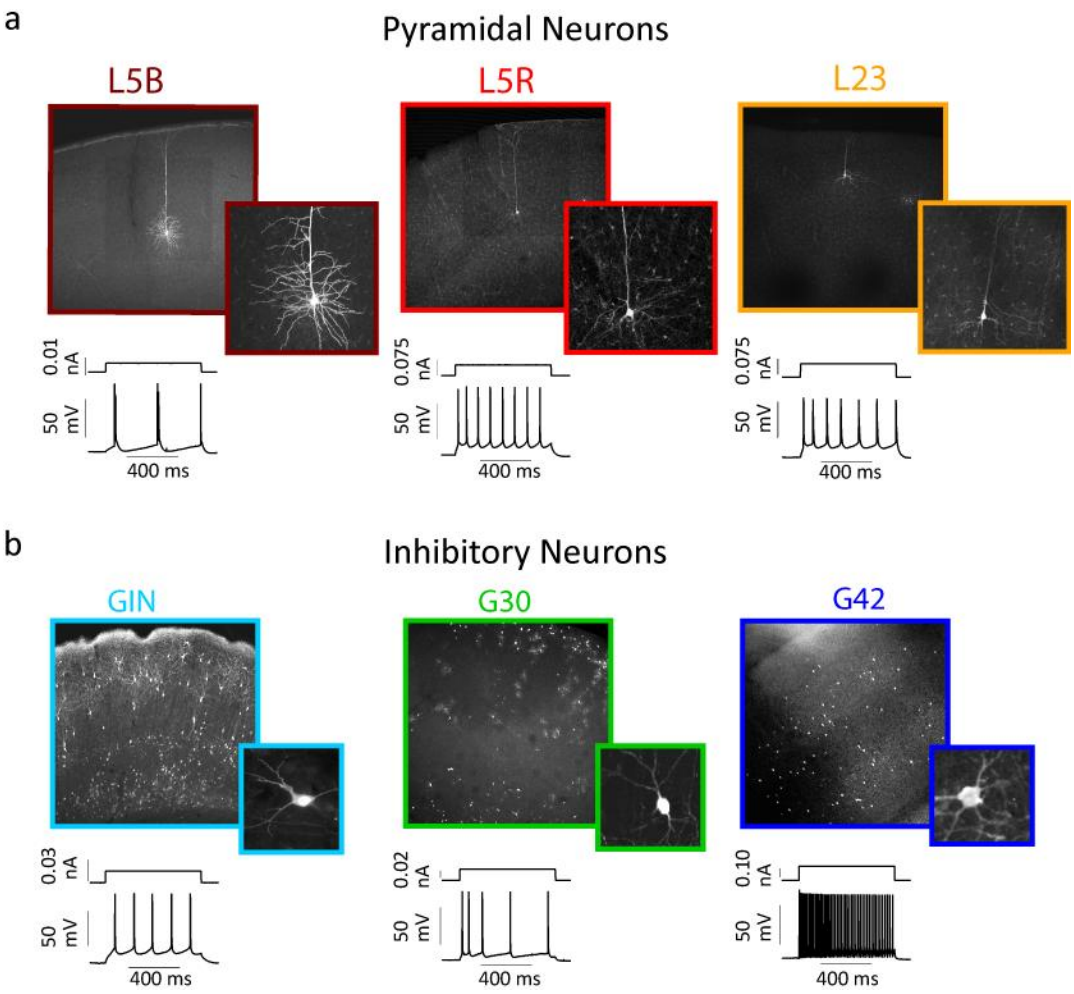

Figure 3.1. Six distinct cell types in the mouse somatosensory cortex

A. Biocytin-filled reconstructions (top) and intracellular recordings (bottom) showing the laminar location, morphology, and spiking responses typical of Layer 5 bursting (left, dark red), Layer 5 regular-spiking (center, red) and Layer 2/3 regular-spiking (right, orange) pyramidal neurons
B. Biocytin-filled reconstructions (top) and intracellular recordings (bottom) showing the laminar location, morphology, and spiking responses typical of GFP+ inhibitory neurons in the GIN (left, cyan, adapting-spiking), G30/SZ (center, green, irregular-spiking), and G42 (right, blue, fast-spiking).

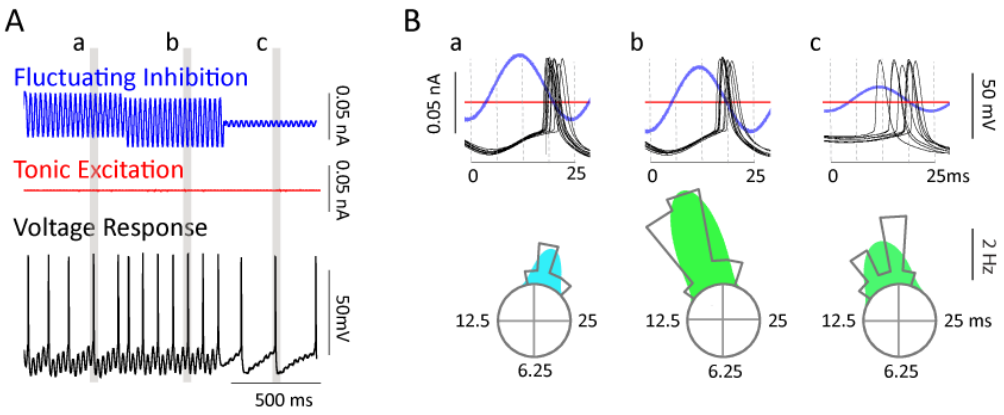

Figure 3.2. Stimulation protocol and analysis

C. Neurons were stimulated with a constant level (I_{base}) of depolarizing current (middle) and a fluctuating hyperpolarizing current (top). On each 500 ms long trial, stimuli were constructed by randomly adding one of ten levels of tonic inhibition ("input mean") (equal intervals, ranging from 0 to I_{base}) to a zero-mean 40 Hz oscillatory current ("input synchrony") with a amplitude of a one of ten randomly selected values (equal intervals, ranging from 0 to I_{base}).
D. Overlays of the spike output (top) and circular histograms of the spike times relative to the gamma frequency input (bottom) to high-mean, high-synchrony inputs (a), low-mean, high-synchrony inputs (b), and low-mean, low-synchrony inputs (c) (top).

Typical responses from the six neuronal types are displayed as a summary grid in Figure 3.3. Horizontal slices through the grids represent the effects of changing the mean level of hyperpolarizing current for a given carrier amplitude. Vertical slices through the grid represent the effects of changing the carrier amplitude for a given level of input mean. The different neuronal types systematically differed in the timing (Figure 3.4ab) and precision (Figure 3.4cd) of spike outputs relative to the gamma frequency input.

Across all stimulus conditions, the pyramidal neurons fired at similar phases in the gamma cycle (Fig. 3.3a; 3.4a, triangles); however cell-type differences were observed in the spike phase dependence on the level of excitation. As the mean level of hyperpolarizing current decreased (decreasing DC), many of the regular spiking

pyramidal neurons (8 of 10 L5R, and 5 of 9 L23) fired earlier in the gamma cycle (e.g. Fig. 3.2a L5R and L23) demonstrating a significant amount of phase precession (Fig. 3.4b, fully saturated yellow and orange triangles); while few of the Layer 5 bursting neurons (3 of 9)`advanced their phase of firing (e.g. Fig. 3.3a, L5B) (Fig 3b, red triangles). Significant group differences in DC phase precession were observed between the L5B and L5R spiking pyramids (Fig 3.4b) (Kruskal-Wallis $p<0.05$). Of the inhibitory cell types, the G42 fast-spiking cells (n=12) fired on average earlier in the gamma cycle (stats $p<0.05$) and exhibited significantly more phase precession than the other inhibitory cell types (Figure 3.4ab) (Kruskal-Wallis $p<0.05$). Although there was no difference in average phase of firing between the GIN regular and G30 irregular spiking inhibitory cells (Fig. 3.4a, green squares and blue diamonds), significant differences in phase precession were observed between the two populations (Figure 3.4b, green squares and blue diamonds) (Kruskal-Wallis $p<0.05$).

Cell-type differences in the spike time precision were also observed. Of the pyramidal neurons, the regular spiking cells (L23 and L5R) fired more precisely timed spikes than the L5B neurons (Fig. 3.4c) (Kruskal-Wallis $p<0.05$), however nearly all pyramids improved their level of precision as the amplitude of the carrier wave increased (Fig 3.4d, fully saturated triangles). Of the inhibitory cell types, the fast-spiking cells (G42) fired the most precisely timed spikes, followed by the other soma-targeting interneuron type: the irregular-spiking (G30) cells. Increasing the amplitude of the carrier signal (AC) decreased the spike time variability in most inhibitory cells (Fig3.4d). However, the decrease in spike time variability was strongest in the GIN neurons (Fig. 3.4d, green squares), because the GIN interneurons started off poorly entrained and

modestly improved their spike time precession as the carrier signal amplitude increased, while the soma targeting neurons were well entrained even to a small amplitude signal.

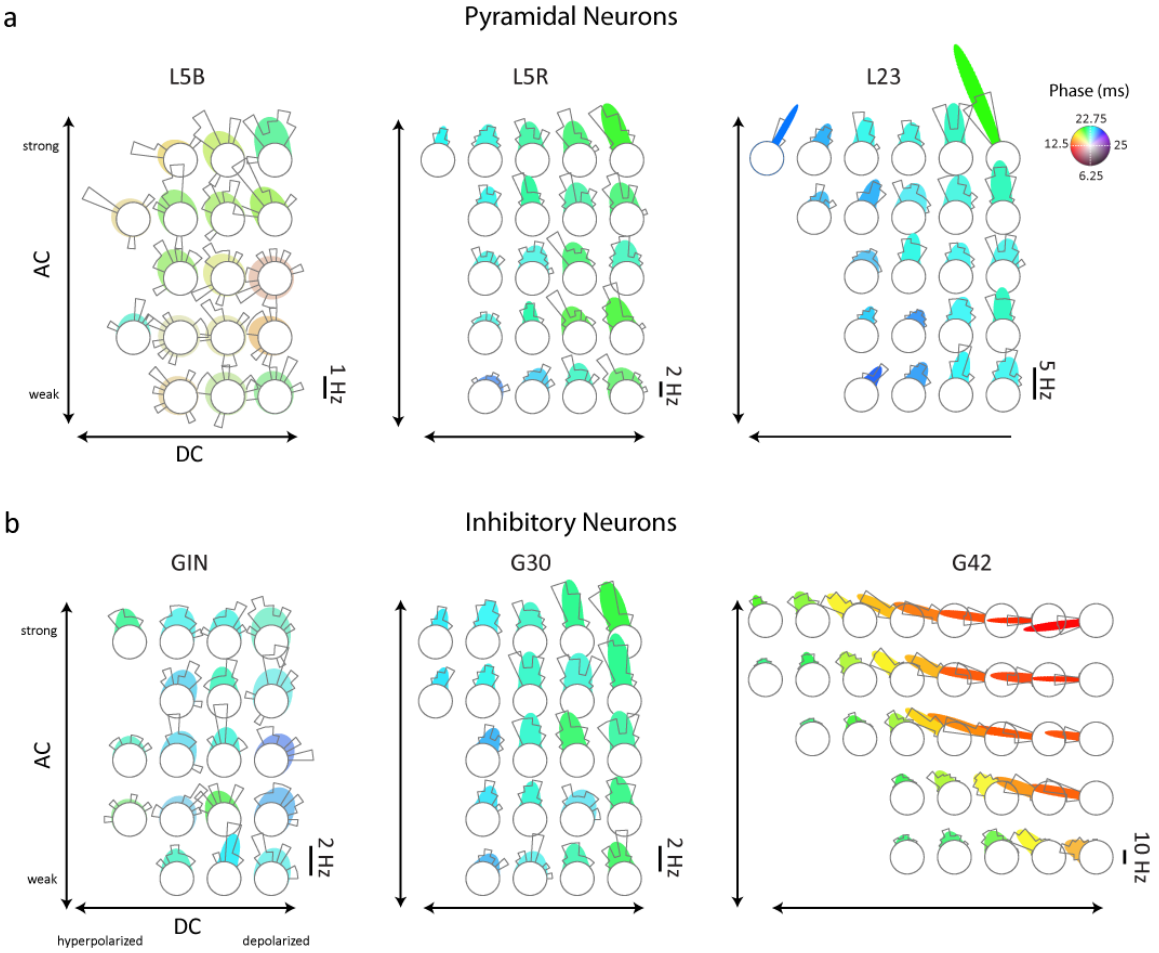

Figure 3.3. Representative responses of different neuronal types to gamma-band synchronized inhibition

A. Typical responses of three types of pyramidal neurons: Layer 5 bursting (a,L5B), Layer 5 regular spiking (b,L5R), and Layer 2/3 regular spiking (c,L2/3) of the spike output timing for changing the mean level of hyperpolarizing current (x-axis) and the amplitude of the superimposed gamma wave (y-axis).
B. Typical responses of three types of inhibitory interneurons from the GIN(a), G30(b), and G42(c) mouse lines of the spike output timing for changing the mean level of hyperpolarizing current (x-axis) and the amplitude of the superimposed gamma wave (y-axis).

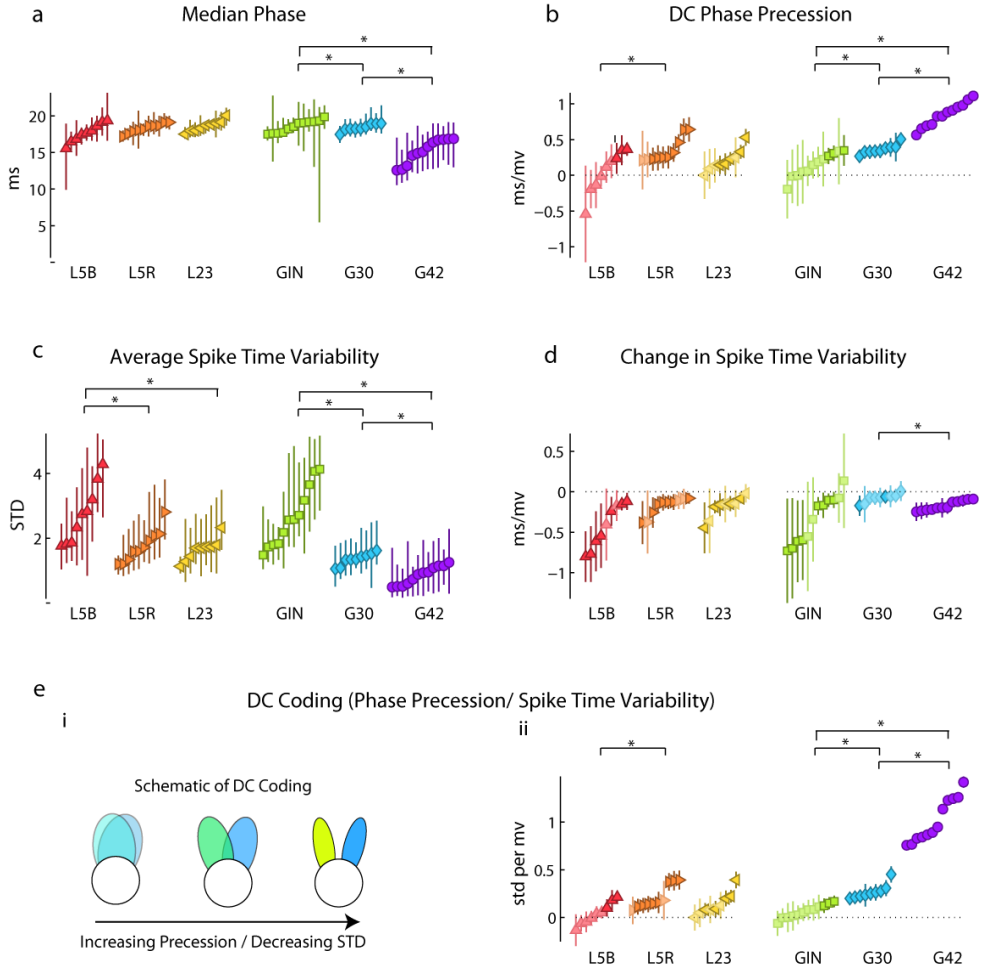

Figure 3.4. Cell-type differences in average phase, precession, and entrainment.

For each recorded cell (L5B (red ▲, n= 9), L5R (orange ►, n=10), L23 (yellow ◄, n=9), GIN (greeen ■, n=12), G30 (cyan ♦, n=9), and G42 (purple ●, n=12) several measurements were taken.

A. The median spike time ("median phase") across all stimulus conditions.

B. The slope of the phase change as the inhibitory DC decreases ("DC phase precession"). Significant changes in DC phase precession for a neuron are indicated by full color saturation (95% CI ≠ 0).

C. The median trial by trial circular standard deviation for all trial conditions "Average spike time jitter".

D. The slope of the change in spike time jitter as the amplitude of the gamma-frequency input increases ("AC entrainment"). Significant changes in AC entrainment a neuron are indicated by full color saturation (95% CI ≠ 0). Significant difference between the three pyramidal cell types and the three interneuron types for each measurement are indicated by an asterisk (Kruskal-Wallis nonparametric ANOVA, $p<0.05$).

The G42 fast-spiking inhibitory neurons fired on average earlier in the gamma cycle (Fig. 3.3Bc; 3.4A, blue box) than the other neuronal types (multiple comparisons Anova, $p<0.05$). Their spike outputs occurred before or at the peak of the gamma cycle, which corresponds to the time of maximum depolarization. The other cell types typically fired action potentials several milliseconds later.

Interactions of intrinsic properties determine cell-type differences in responsiveness. Using a simplified adaptive exponential integrate and fire model it was determined that an interaction between the cell's time constant and the time constant of the adaptation variable predict the cell's ability to entrain and phase code the level of excitation (Figure 5). Faster time constants allow the cell to follow and entrain well to the fast-frequency input; as the time constant increases the cell generally becomes more poorly entrained (Figure 5A). Adding a artificial leak conductance into pyramidal cell using dynamic clamp confirmed these results: decreasing the constant improved the cell's ability to entrain to gamma (Figure 5A, dynamic clamp). The adaptation time constant determines the left over hyperpolarizing conductance on each successive gamma cycle. With sufficiently small adaptation time constant, <10ms, no hyperpolarizing currents are active to compete with the gamma- initiated depolarization, however as the adaptation time constant increases, the adaptive conductances either acts to inhibit spike generation or delay the phase of firing. The effect of the adaptation conductance is most apparent in the fast-spiking cell range; decreasing their ability to precess as the level of excitation increases. Dynamic clamp experiments confirm these results, adding longer AHP conductance into fastspiking cells decreased their ability to phase precess (Figure 5B).

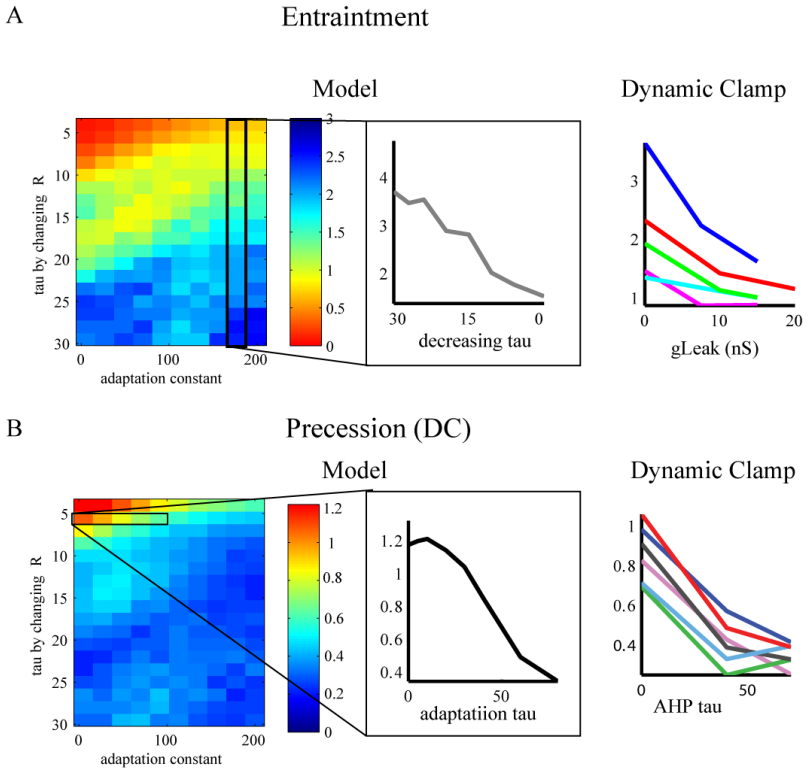

Figure 3.5. Interactions between intrinsic properties determine cell-type differences in average phase, precession, and entrainment.

A. The average entrainment for a model neuron (left) as the time constant of the cell (y axis) and the adaptation time constant changes (x axis). Decreasing the time constant of the cell increases the ability of the cell to entrain. Adding an artificial leak conductance to pyramidal neurons, thereby decreasing the neuron's time constant, also increases the ability of the cell to entrain to gamma-frequency input (right).

B. The average phase precession for a model neuron (left) as the time constant of the cell (y axis) and the adaptation time constant changes (x axis). Increasing the adaptation time constant delays the spike phase and decreases the ability of the cell to phase precess as the level of excitation increases. Increasing the duration of artificial after-hyperpolarization conductances in fast-spiking neurons also decreases the ability of the cell to phase prcess as the level of excitation increases.

Network activity changes neurons' responsiveness to gamma oscillations. Neuronal types differ in their responsiveness to synchronous gamma-frequency inputs, however neurons exist in highly interconnected networks. When the networks are active,

their constituent neurons deluge one another with excitatory and inhibitory synaptic inputs. These inputs, taken together, can be large enough to substantially alter neurons' intrinsic properties (Pare et al., 1998; Shu et al., 2003; Haider et al., 2006; Cardin et al., 2008); reviewed in (Haider and McCormick, 2009)), and likely their responsiveness to gamma frequency input. Using dynamic clamp to generate artificial excitatory and inhibitory conductance stimuli (rather than depolarizing and hyperpolarizing current stimuli), an example L5 neuron becomes progressively more entrained, phase advances as the level of excitation increases, and encodes in its phase the level of excitation Across n=13 neurons, scaling up the artificial synaptic drive significantly increased the entrainement, ability to precession, and phase code the level of excitation. (Data not shown).

Discussion

Several lines of evidence suggest that neuroelectric oscillations, rhythmic shifts in neuronal excitability, in the gamma frequency range, may play a role in or reflect the selective and effective processing of information. For instance, brain regions (Tiitinen et al., 1993; Tallon-Baudry et al., 1997; Gruber et al., 1999; Muller et al., 2000; Ray et al., 2008) and individual neurons (Fries et al., 2001a; Womelsdorf et al., 2006) processing relevant and/or salient information have been shown to exhibit enhanced gamma-band activity. In addition, the strength of gamma activity has been shown to correspond to behavioral performance and changes in attentional demands (Taylor et al., 2005; Womelsdorf et al., 2006; Lakatos et al., 2008). Furthermore, gamma activity has been shown to be disrupted in diseases associated with sensory processing and attentional

impairments, such as schizophrenia, autism, and ADHD (Uhlhaas and Singer; Herrmann and Demiralp, 2005).

A mechanistic understanding of the generation of gamma oscillations has lead to numerous hypotheses about its functional role. These fast oscillations are generated by the coordinated activity of fast-spiking interneurons (Cardin et al.; Hasenstaub et al., 2005; Sohal et al., 2009) which synapse on or near the soma of their targets (cite), resulting in gamma-frequency windows of increased and decreased excitation (Cardin et al.; Hasenstaub et al., 2005; Sohal et al., 2009). Thus, it has been suggested that gamma activity may provide a mechanism for regulating the spike output of neurons with high temporal precision. Indeed various studies have shown that post-synaptic spike times are aligned to the phase of the oscillations, with the strongest output evident in the rising phase of the depolarization (Burchell et al., 1998; Chrobak and Buzsaki, 1998; Pouille and Scanziani, 2001; Csicsvari et al., 2003). However the ability and degree to which gamma-frequency input can regulate the spike output timing will likely depend on their target's identity, given that neurons are not homogenous entities, but differ considerably in their biochemical, electrical, synaptic, and functional properties. Here we explored how precisely gamma activity can regulate spike output time in several different neuronal types and discuss the possible functional implications of these findings.

Gamma-frequency input of sufficient amplitude was able to restrict the spike outputs times of all the cell types tested (fig 3.4ab), however some neurons were much better entrained, i.e. the action potentials were tightly time-locked to a particular phase of the gamma cycle. For instance, the somatic targeting inhibitory cells (Fig3.4c, G30 and G42) were strongly entrained even at low carrier amplitudes, implying that these cells are

capable of transforming gamma-band synchrony in their inputs into gamma-band oscillatory inhibition in their targets. In addition, the regular spiking pyramids in Layer 2/3 and 5 were also well entrained, supporting the hypothesis that gamma activity may be acting to synchronize the firing of cells to enhance their impact through feed-forward coincidence detection (Salinas and Sejnowksi, 2000 and 2001).

It has also been hypothesized that the fast oscillatory activity may act as a timing code, in which the amplitude of excitation is recorded in the time of occurrence of output spikes relative to the gamma cycle; stronger inputs leading to earlier responses (Fries et al., 2007). The timing code could act to suppress the activity of neurons receiving weaker input through disynaptic feed-forward inhibition (Olufsen et al., 2003; Borgers et al., 2005; Fries et al., 2007) or enable spike-time dependent plasticity, which depends on the presyanptic neuron either leading or lagging the postsynaptic neuron by a few milliseconds (Markram et al., 1997; Bi and Poo, 1998; Caporale and Dan, 2008). We found that many of the regular spiking pyramidal neurons in Layer 2/3 and 5 did exhibit phase precession as the level of excitation increased (fig3.4b), while most of the layer 5 bursting neurons did not advance their phase of firing (fig3.4b, L5B). Because the regular spiking neurons are also reasonably well entrained (fig 3.4b), the phase advancement they are able to exhibit may be enough to encode the level of excitation in the timing of their spike output (fig3.4e). However, fast-spiking inhibitory cells exhibit the largest amount of phase precession (fig3.4b), and are able to encode in their phase the level of excitation (fig3.4e). The post-synaptic targets of the fast-spiking cells are in a position to take advantage of the phase precession, escaping from inhibition and firing

earlier than neurons receiving fluctuating inhibition from less excited or less synchronized fast-spiking inhibitory populations.

Dynamic regulation of responsiveness. Although intrinsic differences observed in vitro are useful for the elucidation of basic cellular properties and differences between cell types, it is important to note that because cells are embedded in highly interconnected circuits, their integrative properties are in fact dynamically regulated. Changes in ionic concentrations and currents (Bean, 2007), synaptic plasticity (Dan and Poo, 2004), and the actions of neuromodulators (McCormick, 1992b) affect the way a cell integrates and responds to its inputs. Here, we found that using dynamic clamp to simulate increases in synaptic drive created the enhanced a cell's entrainment, precession, and ability to phase code the level of excitation (Fig. 3.5). These results suggests that neurons bombarded by synaptic conductances during active brain states will likely be more strongly affected by gamma frequency input synchrony and will likely increases the whole network's ability to generate and transmit gamma oscillations. Consistent with this, increases in gamma activity often occur during periods of high network activity, including the peak of slower oscillations (Csicsvari et al., 2003; Freeman et al., 2003; Hasenstaub et al., 2005; Lakatos et al., 2005; Canolty et al., 2006; Lakatos et al., 2008), or periods of increased arousal or attention (Fries et al., 2001b; Womelsdorf et al., 2006; Buschman and Miller, 2007; Lakatos et al., 2008).

The studies described here delve further into the complex interactions that occur between highly interconnected networks of diverse populations of cortical neuron types. We find that the spike outputs of some cell types are highly entrained to gamma-

frequency input even for small amplitudes of gamma, while all cell types can improve their entrainment given a large enough fast-oscillatory input. We also found that phase precession was considerably more difficult. Only the perisomatic targeting interneurons and a small subset of pyramids are capable of a significant amount of phase advancement, or have the ability to phase code information. Because the integrative properties of neurons are dynamically regulated in vivo by feedforward and recurrent synaptic activity and intracellular signaling molecules, neuronal responsiveness to inhibitory tone and structure can be changed over a range of time scales to suit the network's changing computational requirements. Future studies will better reveal how each cell type contributes to and is regulated by dynamic changes in vivo as well as how dysregulation of these circuits at the genetic, molecular, cellular and network levels contributes to neurological disease.

Methods

In vitro slice experiments

All animal use was approved by the Institutional Animal Care and Use Committee at The Salk Institute for Biological Studies. The G42 transgenic mice were originally generated by Josh Huang at Cold Spring Harbor (Chattopadhyaya et al., 2004) and were obtained from Jackson Labs (http://www.jax.org). G30 transgenic mice were originally generated by Gabor Szabo at the Department of Functional Neuroanatomy at the Institute of Experimental Medicine in Budapest, Hungary (Lopez-Bendito et al., 2004) and obtained from Sascha Nelson at Brandeis University. GIN transgenic mice were generated in John Swan’s laboratory at the Baylor College of Medicine (Oliva et al.,

2000) and obtained from Jackson Labs. C57/Bl6J mice were obtained from Jackson Labs.

To prepare brain slices, mice aged P18-P26 were deeply anesthetized with Nembutal (100mg/kg i.p.) and rapidly decapitated. A vibratome (Series 1000, Vibratome) was used to cut 300 μm thick coronal brain slices from the somatosensory cortex (S1). Slices were cut in ice-cold artificial cerebral spinal fluid (ACSF; 24mM NaCl, 5mM KCl, 26mM NaHCO3, 1mM KH2PO4, 1mM MgSO4, 10mM glucose, 1.2mM CaCl2, and 1mM kynurenic acid) and incubated at 35 degrees C for at least 30 minutes in ACSF bubbled with 95% O2/ 5% CO2 before transferring to a room-temperature submerged chamber for recording.

Whole cell recordings. Neurons were visualized at 40X magnification using a DIC/fluorescent Olympus microscope and a video camera (VE 1000; MTI-Dage). Pyramidal neurons from layer III and V were identified by their laminar location, pyramidal-shaped cell bodies and long apical dendrite. GFP+ cells from G42, G30, and GIN mice were identified by their fluorescence. Whole-cell recordings were performed using glass pipettes pulled on a P-97 micropipette puller (Sutter Instruments, Novato, CA) from borosilicate glass (Sutter Instruments) to 3- 5MΩ, filled with 130mM K-gluconate, 0.2mM EGTA, 2mM MgCl2, 6mM KCl, 10mM HEPES, 2.5mM Na-ATP, 0.5mM Na-GTP, and 10mM K-phosphocreatine (pH 7.2). Signals were amplified with a MultiClamp 700B amplifier (Molecular Devices). Data were acquired and digitized using the Spike2 Power 1401 collection system (Cambridge Electronic Designs, Cambridge, UK). All recordings were performed in current-clamp mode. Intracellular recordings were accepted if they showed a stable resting membrane potential below −50

mV throughout the experiment with a standard deviation of less than 0.9mV, and had stable-size action potentials with heights at least 60 mV (for pyramidal neurons) or 40 mV (for interneurons) and widths at half-height of less than 2.5 ms.

Cell characterization. The membrane time constant and input resistance were evaluated using current pulses sufficient to cause 2-5 mV hyperpolarizations. Afterhyperpolarization (AHP) duration and amplitude were measured from the average of >5 action potentials separated by at least 200ms. AHP amplitude was measured as the maximum negative voltage deflection relative to spike threshold. AHP duration was measured as the time when mean voltage was 2/3 recovered towards rest. The upstroke velocity was measured by averaging the derivatives of the action potential upstrokes for each spike in a trial.

Stimulus protocol. Cells were stimulated with a constant depolarizing current I_{base} sufficient to maintain firing at 3-5 Hz. To characterize how the amplitude of the gamma-frequency oscillatory inhibition and the level of tonic inhibition affect a neuron's spike output time relative to the gamma wave, cells were simultaneously stimulated with a hyperpolarizing current whose mean offset randomly varied every 500 msec, and a zero-mean 40 Hz sine wave current whose amplitude randomly varied every 500 msec. Ten levels of tonic inhibition (equal intervals, ranging from 0 to I_{base}), and ten levels of gamma-wave amplitude (equal intervals, ranging from 0 to I_{base}), were tested in each block of trials. Each block lasted at least 600 sec, for at least 10 repeats of each trial condition.

Dynamic clamp

In some blocks, as indicated in the results, the same protocol was repeated using conductance rather than current injections. Fast real-time dynamic clamp was implemented using RTLDC (Boston University; (Dorval et al., 2001)) combined with the Real-Time Application Interface (www.rtai.org), device drivers from the COMEDI project (www.comedi.org), and a NI DAQ PCI-MIO-16XE-50 board (National Instruments). The dynamic clamp was used to generate two conductances, one with a reversal potential of 0mV (mimicking excitation), and another with a reversal potential of -80mV (mimicking inhibition) (Figure 3.5). Cells were simultaneously stimulated with a constant excitatory conductance, a fluctuating inhibitory conductance, and a sine-varying inhibitory conductance, as in the current-injection protocol above.

Analysis

Normalization. In order to compare the effects of differently-sized stimuli across neurons with different input resistances, all sizes of current stimuli were expressed in terms of the voltage change, in millivolts, induced by that amount of DC current. This conversion was calculated from the IV curve for the four smallest 0-AC stimulus sizes that did not evoke action potentials.

Phase and jitter. Each time the stimulus conditions changed, the next four trials (e.g. the next 100 ms) were excluded. The average phase of action potential generation for each AC/DC combination was calculated as the circular mean of the phase of all remaining spikes generated during all trials with that AC and DC. The average jitter of action potential generation for each AC/DC combination was calculated as the circular

standard deviation of all remaining spikes generated during all trials with that AC and DC.

Cell by cell phase and jitter. Each cell's overall mean phase was defined as the median of the phases for all ACs and DCs tested. Each cell's overall mean jitter was defined as the median of the trial by trial jitters, for the largest AC sizes tested.

Precession and coding. Each cell's tendency to precess, in ms/mV, was calculated as the slope of the relationship between mean phase (in ms) and input (in mV). 95% confidence intervals (CI) of the mean were also calculated, and a cell was counted as "significantly precessing" if its CI did not include 0. Each cell's ability to increase entrainment as AC input increased was calculated in the same way. Coding quality was calculated by dividing each cell's precession (in ms/mV) by its average jitter (in ms), to obtain a measure (in mV) of how much depolarization would be required, on average, to advance the mean spike phase by one standard deviation.

Cell type comparisons. The three pyramidal cell types, and the three interneuron types, were each compared by performing a multiple comparisons corrected Kruskal-Wallis nonparametric ANOVA with p=0.05 (adjusted).

Model

A single compartment adaptive exponential integrate and fire neuron model was implemented in Matlab (Brette and Gerstner, 2005; Touboul and Brette, 2008) The model is describes by two differential equations, where where V is the membrane potential, w the adaptation variable, I the input current, C the membrane capacitance, g_L the leak

conductance, E_L the leak reversal potential, V_T the threshold, Δ_T the slope factor, a the adaptation coupling parameter and τ_w is the adaptation time constant.

$$C\frac{dV}{dt} = -g_L(V - E_L) + g_L\Delta_T \exp(\frac{V - V_T}{\Delta_T}) - w + I$$

$$\tau_w\frac{dw}{dt} = a(V - E_L) - w$$

The leak conductance of the model neuron was set at 30nS, the leak reversal potential at -70mV, threshold at -50mV, the slope factor at 2, and the adaptive coupling parameter at 4. The model neuron was stimulated with the same experimental protocol used in the real cells. To analyze the effect of changing the membrane time constant and the afterhyperpolarization duration, the membrane capacitance and the adaptation variable were systematically changed as indicated in the results.

Acknowledgments

We are grateful for support from NIH grant MH063912, the Crick-Jacobs Center for Theoretical and Computational Biology, the Aginsky Foundation, and the Kavli Institute for Brain and Mind

Publication Acknowledgements

Chapter 3, in part, is currently being prepared for submission for publication of the material. Otte SL, Hasenstaub AR, Callaway EM. The dissertation author is co-primary author of this material. Secondary author is thesis advisor.

CHAPTER IV

METABOLIC COST AS A UNIFYING PRINCIPLE GOVERNING NEURONAL BIOPHYSICS

Summary

The brain contains an astonishing diversity of neurons, each expressing only one set of ion channels out of the billions of potential channel combinations. Simple organizing principles are required for us to make sense of this abundance of possibilities and wealth of related data. We suggest that energy minimization subject to functional constraints may be one such unifying principle. We compared the energy needed to produce action potentials singly and in trains for a wide range of channel densities and kinetic parameters, and examined which combinations of parameters maximized spiking function while minimizing energetic cost. We confirmed these results for sodium channels using a dynamic current clamp in neocortical fast spiking interneurons. We find further evidence supporting this hypothesis in a wide range of other neurons from several species and conclude that the ion channels in these neurons minimize energy expenditure in their normal range of spiking.

Introduction/Results

The mammalian genome contains genes encoding hundreds of types of ion channels, most of which can be produced in multiple splice variants and regulated at multiple phosphorylation sites by numerous intrinsic and extrinsic factors (Coetzee et al., 1999; Jentsch et al., 2002; Lee and Irizarry, 2003; Schulz et al., 2008). Which combination of these ion channels will be expressed by any particular neuron, with any particular computational or behavioral role? Since any given electrical phenotype can be produced by many combinations of ion channels (Swensen and Bean, 2005;

Achard and De Schutter, 2006; Marder and Goaillard, 2006; Schulz et al., 2006), on functional grounds alone, this question is severely underconstrained. What other constraints might govern ion channel expression, and can exploring these constraints help us understand how cells or circuits are constructed?

Energy consumption may be one such constraint. The brain is one of the most energetically demanding organs in the body (Holliday et al., 1967; Ames et al., 1992): the human brain uses more than twice as much glucose per day as the heart (Holliday et al., 1967). Neuronal activity -- action potential generation, input integration, and synaptic transmission--accounts for 50-80% of this energy use (Astrup et al., 1981b, a; Sokoloff, 1999; Shulman et al., 2004). Potential energy is stored in transmembrane ion gradients, which creates a cellular battery whose maintenance accounts for most of the brain's ATP consumption (Astrup et al., 1981b; Sokoloff, 1999; Attwell and Laughlin, 2001; Lennie, 2003). Action potential generation taps into these gradients and expends some of this potential energy, which needs to be actively restored. How can this energy be most efficiently used to generate activity or carry out computation? This question has inspired a body of research on how to encode a signal, or perform a computation, using as few action potentials-and thus as little energy-- as possible (Mitchison, 1991; Levy and Baxter, 1996; Laughlin et al., 1998; Balasubramanian et al., 2001; Balasubramanian and Berry, 2002; Levy and Baxter, 2002; Chklovskii and Koulakov, 2004; Niven et al., 2007). The combinations of ion channels that most efficiently generate action potentials depends on function of the neuron, such as the average firing rate, and the detailed kinetics of the channels (Alle et al., 2009). Here, we combine biophysical modeling with dynamic-clamp electrophysiology to

understand the constraints on the kinetics and density of the ion channels underlying action potential generation. Ion channel expression in various species, neural structures, and cell types support the hypothesis that they may be constrained to minimize energy use, subject to functional requirements.

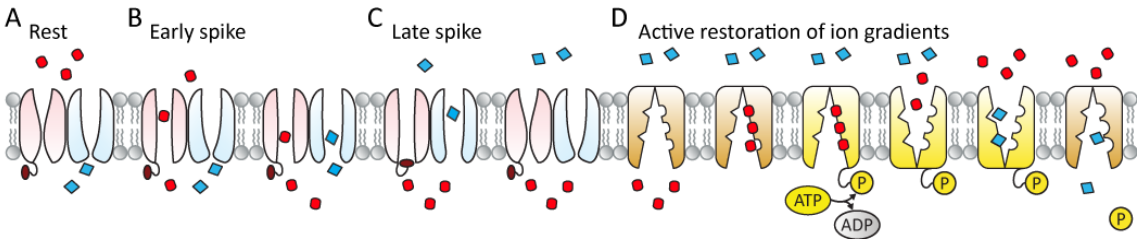

Figure 4.1. Sodium and potassium channels during action potential generation.

(A) At rest , both sodium channels (light red) and K+ channels (light blue) are closed, Na+ ions (red ovals) are concentrated extracellularly, and K+ ions (blue diamonds) are concentrated intracellularly. (B) Depolarization causes Na+ channels to open, permitting Na+ ions to flow down their concentration gradients into the cell. This influx of positive charge depolarizes the neuron. (C) This depolarization causes K+ channels to open, letting K+ leave the cell, hyperpolarizing the membrane potential; at the same time, depolarization causes Na+ channel inactivation gates (dark red ball-and-chain) to close, limiting Na+ influx. Eventually the hyperpolarization is sufficient to close and de-inactivate the Na+ channels, and close the K+ channels, restoring the channel states to baseline. (D) The Na+ influx and K+ efflux are reversed by the Na^+,K^+ ATPase.

Basics of action potential generation**.** The Hodgkin-Huxley model of action potential generation uses fast voltage-gated sodium (Na+) channels, delayed rectifier potassium (K+) channels, and voltage-independent ("leak") potassium channels. At rest (Figures 1A, 2A-1), the cell's batteries are already charged — Na^+ ions are more concentrated outside the cell than inside (red ovals), while K^+ ions (blue diamonds) are more concentrated inside the cell than outside. The action potential is triggered when modest depolarization (Figure 2A-2) causes the sodium channels'

activation/deactivation gates ("m" gates, Figure 2B, light red) to enter the "open state" (Figure 1B). This increases the membrane's permeability to Na+ ions (Figure 1B; Figure 2C, red), permitting Na+ ions to passively flow down their concentration gradient and enter the cell. This influx of positive charge (Figure 2D, red) depolarizes the membrane, bringing the membrane potential up to the Na+ ions' reversal potential, roughly 50 mV (Figure 2A-3).

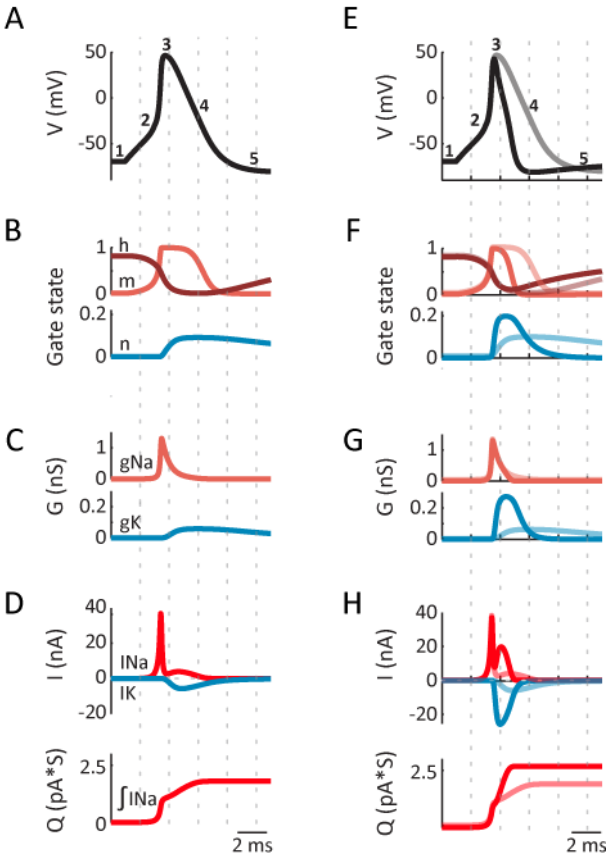

Figure 4.2. Membrane Dynamics During Action potential generation.

(A and E): voltage waveforms. (B and F): gate states. Light red: "m" (Na+ channel activation) gate; dark red: "h" (Na+ channel inactivation) gate; blue, "n" (K+ channel activation) gate. 1=fully open, 0=fully closed or inactivated. (C and G): Na+ (red) and K+ (blue) conductances. (D and H): Na+ (red) and K+ (blue) currents, top; cumulative Na+ current influx, bottom. Right: the traces from the broad action potential in A-D are overlaid on the corresponding traces from a narrower action potential, generated by tripling the rate of K+ channel activation/deactivation.

This strong depolarization triggers the potassium channel activation/deactivation gates ("n" gates, Figure 2B, blue) to open, increasing the membrane's permeability to K^+ ions (Figure 2C, blue), which lets potassium exit the cell (Figure 2D, blue). This efflux of K+ ions competes with the influx of Na+ ions to control the membrane potential; the net effect is to hyperpolarize the neuron (Figure 2A-4). At the same time, the sodium channels' inactivation gates ("h" gates, Figure 1C; Figure 2B, dark red) begin to block the sodium channels, slowly reducing the membrane's sodium permeability. Eventually, sufficient hyperpolarization causes the "m" and "n" gates both to enter the de-activated state, (Figure 2A-5, Figure 2B), bringing the membrane's sodium and potassium permeability back to baseline levels. These changes in gate states, channel conductances, and current flow were fueled by the energy stored in the cell's Na+ and K+ gradients: no ATP was expended during the generation of the action potential itself. These gradients are now partly run down, and must be actively restored. The sodium-potassium pump (Na^+,K^+ ATPase) is primarily responsible for this restoration. It imports two K+ ions and extrudes three Na^+ ions (Figure 1D), at the cost of one ATP. There is thus a direct relationship between the number of Na+ ions that enter the cell during action potential generation, and the energy cost of recovering from the action potential.

Spike cost and spike rate. The ionic currents underlying the action potential are plotted in Figure 2D (top), and the cumulative Na+ influx is plotted in Figure 2D (bottom). Note that action potential repolarization (between times 3 and 5), not just depolarization (between times 2 and 3), accounts for a substantial portion of this Na+

influx. Intuitively, this occurs because during depolarization, sodium conductance far exceeds potassium conductance. Sodium entry during depolarization is thus approximately limited to what is required to charge the cell's capacitance. But during repolarization, both sodium and potassium channels are open and sodium enters the cell at the same time that potassium exits the cell. These fluxes mostly cancel each other, so that only a small part of the charge exchanged goes into changing the cell's membrane potential.

Second, note that the duration of this repolarization, and thus the duration of the action potential itself, limits the rate at which the neuron can spike. Partial sodium channel de-inactivation is required to replenish the pool of sodium channels available for action potential generation, and this de-inactivation can only occur when the membrane is sufficiently hyperpolarized. Indeed, narrowing the action potential by tripling the rate of potassium channel activation (detailed in Figures 2E-H) does increase the rate at which the model neuron is able to spike (Figure **3A**). However, because sodium channel inactivation accumulates slowly, sodium channels are less inactivated earlier in the action potential. If potassium channels activate earlier, sodium and potassium conductances will overlap more extensively (Figure 2G). Earlier hyperpolarization will therefore be opposed by a greater sodium current flow, increasing the total Na+ influx during repolarization, and thus increasing the metabolic cost of the action potential (Figure 2H). These two factors thus imply a trade-off between the energy cost of action potential generation, particularly repolarization, and neurons' functional capacity—their ability to spike rapidly, or their bandwidth.

Kinetics, rates, and costs. For the model shown in Figure 3A, systematically speeding (curves and points on curves labeled 'a' in Figure 3A) or slowing (curves and points on curves labeled 'c' in same panels) the time constants of potassium channel activation speeds or slows the maximum action potential rate. Both for single action potentials (solid) and for action potentials generated in trains (50 Hz shown, dotted), faster K+ channels increase Na+ influx – and thus increase energy cost- and slower K+ channels decrease Na+ influx and energy cost. In other words, although fast-activating potassium channels do give cells the ability to spike quickly, this increased bandwidth comes at a cost, and this cost must be paid every time the neuron generates any action potential. This implies that neurons whose computational role does not require the ability to spike quickly need not pay this cost to perform their function. We thus predict that naturally slow-spiking neurons should not express fast-activating potassium channels.

Are there other strategies that cells might adopt to achieve the fast-spiking phenotype, and how metabolically expensive are they? This minimal model has two other gates, whose kinetics may be varied. Faster sodium channel activation/deactivation (i.e., faster “m” gates) somewhat increases the rate at which neurons can spike, with almost no effect on metabolic cost (Figure 3B). Intuitively, this occurs because the total Na+ influx during the upstroke of the action potential is nearly independent of sodium channel activation speed, since during this period the sodium conductance depolarizes the cell without significant opposition. The contribution of sodium channel deactivation to Na+ influx during the action potential downstroke is also relatively small — by the time that the cell has hyperpolarized

enough to cause m-gates to reenter the closed state (deactivation), the sodium current is sufficiently inactivated (h-gate) to keep the sodium current low, irrespective of how long this transition takes.

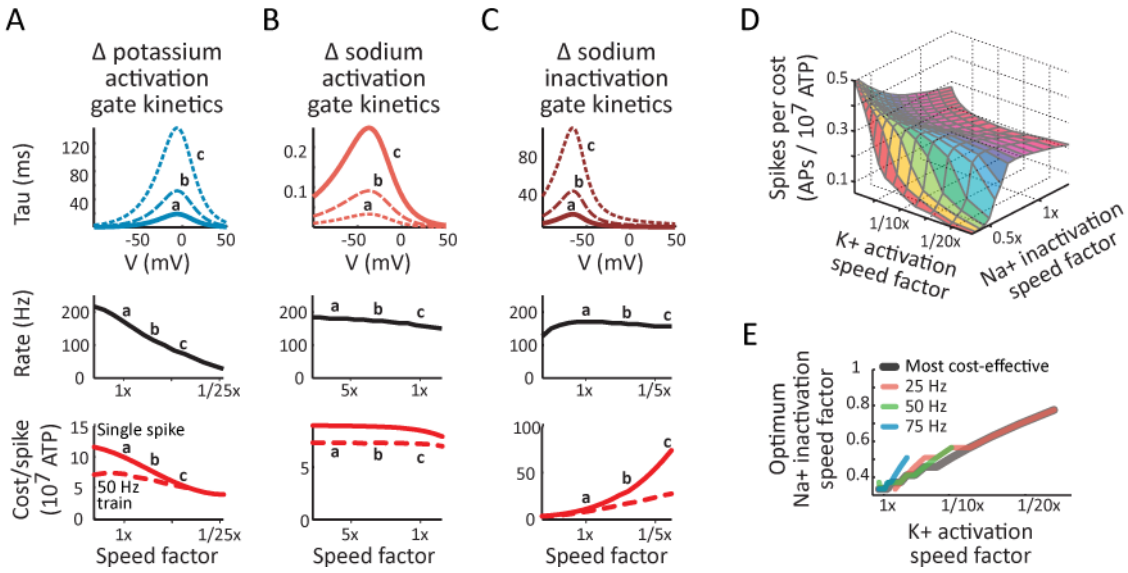

Figure 4.3. Model: Effects of changing the kinetics of the spike generating conductance on spike rate and spike cost.

(A, B, and C), top: time constants as a function of membrane potential. Gate kinetics were systematically speeded or slowed by multiplying the time constants at all voltages by the same constant speed factor. Middle: maximum spike rate as a function of speed factor. Bottom: cost (in ATP) for a single action potential (solid) or for an action potential in a 50 Hz train (dotted) as a function of speed factor. (D): maximum number of spikes per 10^7 ATP (z-axis) as a function of n-gate speed factor (x-axis) and h-gate speed factor (y-axis and surface color). (E): Na+ channel inactivation speed factor that maximizes the spikes/cost, for spikes generated as efficiently as possible (black), and for spikes generated in 25, 50, and 75 Hz trains (red, green, blue).

Differences in sodium channel inactivation/deinactivation (i.e., faster "h" gate) kinetics also have little effect on the rate at which neurons can spike, outside of the degenerate range in which inactivation occurs too quickly for the neuron to support action potential generation (Figure 3c). However, faster sodium channel inactivation limits the degree to which sodium and potassium currents overlap during

repolarization, limiting waste current; slower inactivation increases this overlap, increasing waste. These differences thus have an enormous effect on action potential cost. This implies that to minimize metabolic cost (while preserving the ability to spike quickly) sodium current inactivation must occur as fast as possible, outside of the degenerate range. This relationship between τ_n, τ_h, and metabolic efficiency (i.e., spikes per ATP) is characterized in Figure 3D. Note that optimum inactivation rate – the point at which inactivation becomes too fast to sustain spike generation -- varies with potassium channel activation speed: if potassium channels activate more slowly, the speed of sodium channel inactivation must be reduced, so that sodium-mediated depolarization still lasts long enough to activate the potassium channels. Conversely, if potassium channels activate more rapidly, then sodium channels must also inactivate rapidly to minimize waste current. The sodium inactivation speed that minimizes cost per spike is a linear function of potassium activation speed, both when action potentials are generated as fast as possible, and when they are generated at a given rate (Figure 3E). This is another prediction of the model.

Densities, rates, and costs. Cells can also express different densities of the same ion channels. Does changing channel density permit rapid action potential generation, and if so, at what cost? Increasing potassium channel density, like speeding potassium channel kinetics, increases the rate at which a cell can spike by narrowing its action potential, with a roughly proportional increase in the cost per action potential (Figure 4B). Conversely, increasing sodium conductance also increases the rate at which a cell can spike, but without narrowing action potentials (Figure 4C). Instead, increased sodium conductance reduces the refractory period by

decreasing the voltage threshold for spike generation, allowing spikes to be generated even when a smaller proportion of the total sodium conductance is available. However, the combination of wider action potentials with increased sodium flow at each stage of the action potential makes this an expensive strategy.

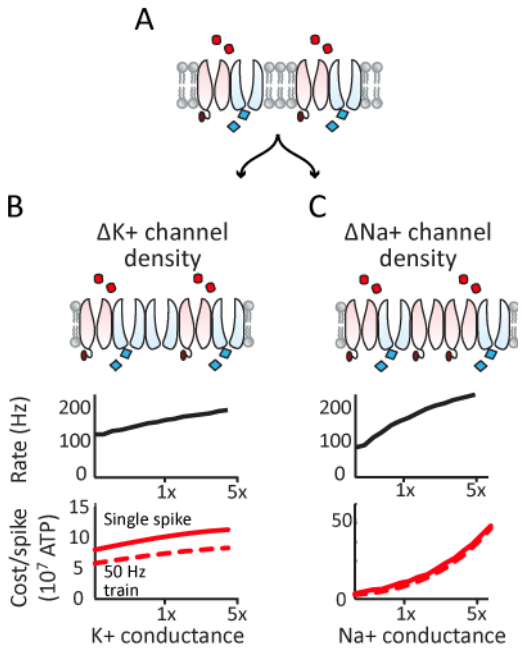

Figure 4.4. Model: Effects of changing the densities of the spike generating conductances on spike rate and spike cost.

The default membrane Na+ and K+ channel densities (A) can be changed by adding or removing K+ channels (B, top), or by adding or removing Na+ channels (C, top). (B and C), middle: maximum spike rate as a function of channel density. (B and C), bottom: cost (in ATP) for a single action potential (solid) or for an action potential in a 50 Hz train (dotted) as a function of speed factor.

These relationships between metabolic cost, functional capabilities, and channel kinetics and density allow us to make predictions about what biophysical strategies cells with different firing properties will adopt, if their aim is to minimize metabolic cost and meet their functional requirements. But these trade-offs are derived from a greatly reduced model, while real neurons are morphologically

complicated and contain numerous, diverse voltage-gated channels. It is therefore unclear to what extent we should expect these relationships to hold in real neurons. Two factors make this question difficult to address experimentally. First, in real neurons, individual channel or gate kinetics cannot be systematically varied, which makes parameter sweeps impossible. Further, in any given neuron, one cannot simultaneously measure the voltage response to a given current input and reverse-engineer the contributions of different ionic currents to this response, which complicates estimation of energy costs.

Rate and costs in real neurons. Both problems can be resolved using dynamic voltage clamping. In a dynamic clamp, a computer is reciprocally connected to a neuron through an amplifier. At each time step, the computer reads the cell's membrane potential from the amplifier, calculates how much current would be flowing through the simulated conductance at that membrane potential, commands the amplifier to apply that amount of current, and updates the state of the simulated conductance (Figure 5A). We first blocked cells' intrinsic voltage gated sodium channels with tetrodotoxin (TTX) and then used high-speed dynamic clamp to re-insert simulated sodium channels, modeled using the same equations as in our parameter sweeps above (Figure 5). Of all the ion channels in a cell the sodium channel has the fastest time constants, which requires a comparably fast dynamic clamp.

After sodium channel replacement, cells could generate action potential-like waveforms in response to depolarizing current steps. The upsweeps of these waveforms were generated by the user defined, artificial sodium conductances — but

the repolarization was mediated by the cell's own potassium channels, whose kinetics, densities, positions, and diversity were unchanged. "Sodium" influx was now measurable, simply by tracking the amount of current injected by the dynamic clamp system over time. Because the simulated sodium current had user-definable kinetics and density, it was now possible to systematically alter the kinetics of the underlying modeled gates and the density of the modeled channels. This enabled parameter sweeps over sodium channel properties, in real neurons, similar to those performed in the model. We were thus able to test how similar the relationships between sodium channel properties, cellular function, and energy cost, observed in our simple model, were to the relationships among these factors found in real neurons.

We found that both modeled and real neurons displayed qualitatively similar relationships between sodium channel properties, bandwidth, and metabolic cost (Figure 5C). Faster-activating sodium channels moderately increased the rate at which cells could fire, with little effect on action potential cost (a); faster-inactivating sodium channels had little effect on the rate at which cells could fire, but decreased spike cost (b); and increased sodium current density increased the rate at which cells could fire, but increased spike cost (c). We thus conclude that the trade-offs between kinetics, rates, and cost that we observed in the model are robust to variations in channel kinetics, voltage dependence, and subcellular localization, and are therefore likely to hold in real neurons. We propose that if the energy cost of action potential generation is a constraint on brain volume, coding strategy, or computational capacity, then cellular ion channel expression will be optimized not merely to achieve function, but

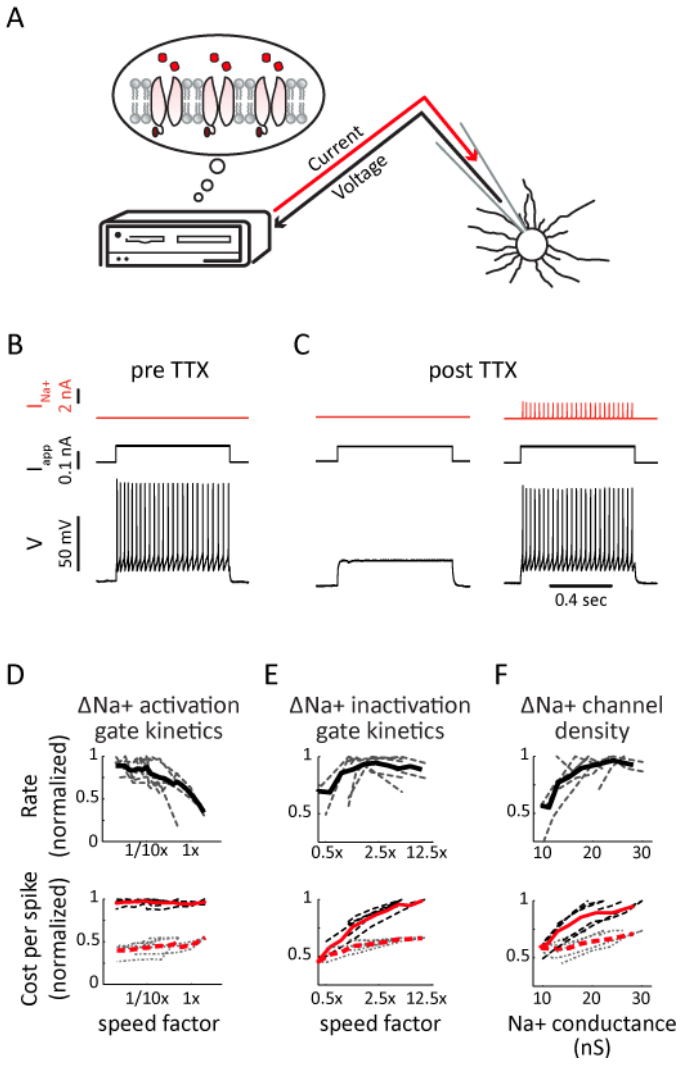

Figure 4.5. Effects of changing the kinetics and densities of dynamic clamp generated sodium conductance on spike rate and spike cost.

(A) Dynamic clamp schematic: a computer (left), simulating a voltage-gated sodium conductance is reciprocally connected to a neuron (right). The cell's voltage determines the driving force on the simulated conductance, and thus the current command sent to the amplifier; at each time step, the dynamic clamp computer uses the cell's voltage to update the state of its sodium conductance model.
(B) intracellular recording of a fast-spiking interneuron showing its ability to generate fast, non-adapting trains of action potentials. TTX application (middle) blocks action potential generation. Dynamic clamp restoration of sodium conductance (right; command current in red) permits the neuron to generate fast, non-adapting trains of action potential like waveforms.
(C) Maximum spike rate (top) and spike cost (bottom) as a function of Na+ channel activation rate (a), inactivation rate (b), and channel density (c). Black traces, average of normalized values for all cells; gray traces, normalized values for each cell.

to achieve function while minimizing metabolic cost; and that if this is the case, then ion channel expression patterns will obey the trade-offs predicted by our model and experiments.

Comparisons across cell types, structures, and species. We found two biophysical strategies, speeding potassium channel activation and increasing the sodium conductance density, which could strongly increase the rate at which neurons were able to fire. Both strategies also increased the energy cost of action potential generation. But the two strategies were very different in their energy efficiency: doubling a cell's maximum spike rate from 100 to 200 Hz by speeding potassium channel activation roughly doubles the energy cost per spike, but doubling the rate by adding sodium conductance multiplies the energy cost per spike by a factor of twenty. We therefore predict that cells with higher spike-rate requirements will fulfill these requirements by expressing faster potassium channels, and not by expressing more sodium channels. Further, because faster potassium channels are expensive even in a cell that spikes slowly, we predict that only cells whose operation requires them to be able to spike quickly will express fast potassium channels. This is the principle of minimally acceptable bandwidth. Many brain regions contain multiple cell types with different in vivo spike rates, from which we can infer differences in their functional or bandwidth requirements. Do faster-spiking neurons achieve these spike rates through faster-activating potassium channels or through greater expression of sodium channels?

In the cerebral cortex, parvalbumin-positive (Pv+) interneurons are tonically active at comparatively high rates, while regular-spiking pyramidal neurons spike relatively infrequently and irregularly (Figure 6A). The faster spiking neurons display far narrower action potentials – to the degree that Pv+ neurons are one of only a few cell types identifiable in extracellular recording. These action potentials are made narrow specifically by the expression of the fast-activating potassium channel Kv3.1/KCNC1. A far greater proportion of Pv+ interneurons, compared to pyramidal neurons, contain mRNA for KCNC1 (Figure 6Ba, (Martina et al., 1998)), and KCNC1 RNA levels are tenfold higher in Pv+ interneurons than in regular spiking Thy1+ pyramidal neurons (Figure 6B, (Sugino et al., 2006)). These neurons do not adopt the dense-sodium strategy to permit fast spiking: in vivo, maximal action potential upstroke velocities, a proxy for available sodium current, are not significantly different between fast- and regular- spiking cortical neurons (Figure 6C (Nowak et al., 2003)). A similar pattern is found in a wide variety of neural structures. In the hippocampus, neurons that spontaneously fire faster (Tukker et al., 2007) have narrower action potentials (Kawaguchi and Hama, 1987), mediated by faster-activating potassium currents (Erisir et al., 1999). Similarly, thinner-spiking neurons have higher *in vivo* firing rates in both the striatum (Kawaguchi, 1993; Mallet et al., 2005) and amygdala (Washburn and Moises, 1992; Pare and Gaudreau, 1996; Likhtik et al., 2006). In the songbird high-vocal center thinner-spiking neurons have faster spiking rates *in vivo* (Del Negro and Edeline, 2001). In the lateral parabrachial nucleus, central lateral neurons, compared to external lateral neurons, have briefer action potentials mediated by faster repolarization, and also far less spike frequency adaptation (permitting

comparatively fast sustained spiking), with no difference in rate of rise (Hayward and Felder, 1999).

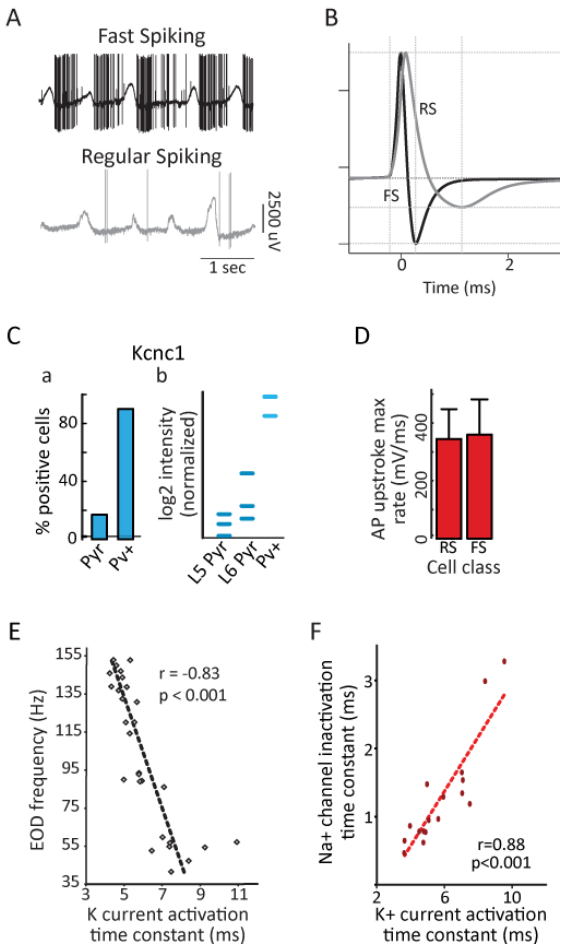

Figure 4.6. Survey of the literature: spike generating conductances in neurons.

(A) Action potential rate (left) and shape (right) in a thin-spiking interneuron (black) and a regular-spiking neuron (gray) during Up and Down states *in vivo*. (Ba) Percentage of pyramidal neurons and PV+ interneurons identified as KCNC1-positive through single-cell PCR. (Bb) Microarray measurements of KCNC1 RNA levels in pyramidal neurons and PV+ interneurons. (C) Maximum action potential upstroke velocity in regular spiking (RS) and fast spiking (FS) cortical neurons. (Da) electric organ discharge (EOD) frequency in the electric organ of n= 28 different fish, versus K+ current activation time constant in EOD cells of the same fish (measured at 25mV above threshold). (Db) Na+ current inactivation time constant versus K+ activation time constant in n=17 fish. (A) adapted from (Hasenstaub et al., 2005). (Ba) adapted from (Martina et al., 1998). (Bb) adapted from (Sugino et al., 2006). (C) adapted from

Although faster potassium channels can endow a cell with the ability to spike quickly, this comes with increased energy cost. The extra cost can be kept to a minimum by speeding sodium channel inactivation, which minimizes the overlap between sodium and potassium conductance opening. But this speeding is only beneficial up to a point, and this point is proportional to potassium conductance activation speed. We thus predict that, all else being equal, cells with faster potassium channel activation kinetics will display faster sodium channel inactivation kinetics.

These comparisons are difficult to make between neurons with different action potential heights, spike thresholds, and resting potentials – i.e., between neurons with sodium channels that experience vastly different ranges of voltage before the repolarizing phase of the action potential. However, we can straightforwardly compare kinetics across neurons with similar pre-spike and early-spike voltages. An example of an entire family of cells with similar resting membrane potential, action potential height, and spike threshold, but with variable firing rate requirements, is found in the electric organ of weakly electric fish. The electrically active cells (electrocytes) in these fish generate the electric organ discharge (EOD): each fish generates the EOD at a characteristic frequency, but different fish generate this discharge at different frequencies, spanning a wide range from 50 to 200 Hz, and the same fish may change its frequency with hormonal shifts. In fish with faster EOD frequencies, electrocytes contain potassium channels with faster activation kinetics ((McAnelly and Zakon, 2000), Figure 6Da). This can be predicted from functional considerations alone. Yet cells with faster-activating potassium channels, and thus with thinner action potentials, also contain faster-inactivating sodium channels (Figure

6Db). This relationship cannot be predicted from functional constraints alone, because fast sodium inactivation is not required for thin spikes or fast action potential generation. Yet this relationship is required for cells to minimize energy costs subject to functional constraints (i.e., while preserving the ability to spike quickly). Similarly, during development, the calyx of Held develops the ability to spike progressively faster, through progressive speeding of its potassium channel kinetics (as predicted above). During the same period, sodium channel inactivation kinetics become faster (Leao et al., 2005). Again, this relationship is predicted by mixed functional and metabolic, not purely functional, considerations.

Discussion

Neural tissue is inordinately expensive. Brain ranks behind only heart and kidney in glucose used per gram (Holliday et al., 1967; Holliday, 1971; Lieberman et al., 2009), and the human brain accounts for one fifth of the body's total energy consumption ((Kinney et al., 1992; Aiello and Wheeler, 1995), . Much of this cost derives from the essential ongoing neural activity (Shulman et al., 2004; Raichle, 2006; Logothetis, 2008) which maintains the circuit context in which sensory processing, planning, decision-making, and motor control can occur (Llinas and Pare, 1991; Kenet et al., 2003; Fiser et al., 2004; Kording and Wolpert, 2004; Olshausen and Field, 2005; Raichle, 2006; Raichle and Mintun, 2006; Fox et al., 2007; Hasenstaub et al., 2007; Haider and McCormick, 2009). Expensive functions prompt the evolution of expense-minimizing adaptations (Weibel, 2000), and energy availability does

appear to have constrained the evolution of macroscopic brain features, resulting in minimization of brain volume subject to functional requirements (Aiello and Wheeler, 1995; Fish and Lockwood, 2003; Isler and van Schaik, 2006; Barrickman et al., 2008). We propose that the same principle holds on a microscopic level. One aspect of this optimization involves the kinetics and densities of the ion channels underlying spikes, but this principle may have driven other aspects of ion channel expression. Substantial energy is expended on ion transport in nonspiking neural tissue such as retina (Ames et al., 1992; Okawa et al., 2008), and on synaptic and integrative activity in spiking neurons (Attwell and Laughlin, 2001; Lennie, 2003; Logothetis and Wandell, 2004; Buzsaki et al., 2007; Viswanathan and Freeman, 2007; Goense and Logothetis, 2008; Alle et al., 2009). If evolution has optimized the expression of the spike- generating ion channels to minimize metabolic cost while preserving spiking bandwidth, perhaps it has also optimized expression of the ion channels involved in subthreshold input integration to minimize metabolic cost while preserving computational ability. This is an extremely general framework for interpreting neurons' biophysical specializations.

We have not found any data to contradict the broader conclusion that evolution has honed the properties of ion channels and their densities to minimize energy consumption while ensuring sufficient bandwidth to perform necessary computation. This analysis focused on ATP consumption, the coin of the cellular realm, and should not depend on details regarding glucose consumption, such as whether activity-related glycolysis occurs in glia or neurons. The results are also independent of the fraction

of energy used for action potential generation, compared to that needed to support other activity-dependent processes such as dendritic integration and vesicle recycling.

The results presented here build on a long tradition of research on optimality in neural signaling (Hodgkin, 1975; Mitchison, 1991; Aiello and Wheeler, 1995; Laughlin et al., 1998; Niven et al., 2007), including more recent studies examining the cost of single action potentials (Alle et al., 2009; Carter and Bean, 2009). Consistent with prior studies, our results confirm that mismatches between Na+ and K+ kinetics are likely to be a primary contributor to the cost of action potential generation. Our results extend the previous work in several major ways. First, by using dynamic clamp, we assessed, in actual neurons, how their diverse ensembles of hyperpolarizing currents interact with simple depolarizing conductances to control spike cost and function. Second, by using Hodgkin-Huxley style models rather than bulk conductance models (24), we linked our models to the actual biophysical mechanisms -- channel gating kinetics and voltage dependence -- that could be altered in each cell type in order to optimize energy cost, and by using dynamic clamp to simulate changes in gating parameters, we confirmed these models' predictions in real neurons. Third, we considered not only the cost of a single action potential, but also energetic cost in the context of broader functional requirements, such as the ability to support sustained spiking. For example, we showed that high maximum spike rates carry a high metabolic cost. This implies that neurons which do not need to fire at high frequencies are likely to adopt different solutions to optimization of spike cost. Finally, by examining neurons' biophysical specializations in the context of cost optimization, we combined data from functionally diverse neurons spanning brain structures and species to support the

hypothesis that neurons' biophysics are tuned to minimize metabolic cost subject to functional constraints. We propose that this principle generalizes broadly, and constrains the range of solutions neurons might adopt to satisfy competing functional and energetic requirements.

Materials and Methods

Model

Simulations were performed using a single compartment, Hodgkin-Huxley style model (details given in Supplement). Action potentials were required to begin and end below -50 mV and cross at least 0 mV at maximum. The cost of a single action potential was determined by finding the smallest-amplitude 1 ms current pulse that evoked an action potential, integrating the sodium current during the 20 ms post-stimulus, and converting integrated sodium current to ATP required to transport the Na+ ions using the 3:1 stoichiometry of the Na^+,K^+ ATPase. Spike trains were elicited from 200 ms current pulses. The cost per spike for spikes in a train was determined by applying a 200 ms current pulse, integrating the sodium current over the pulse and the following 20 ms, and dividing by the number of spikes evoked. In Figures 2 and 3, gate kinetics were speeded or slowed by multiplying the time constants calculated at each time step by a constant factor. In Figure 4, maximum sodium or potassium conductances were scaled by a constant factor.

Dynamic clamp

Slices were prepared and neurons recorded using standard patch-clamp techniques (detailed in Supplement). 1 uM TTX was applied to block voltage-gated

sodium currents, and sodium current block was confirmed using current pulses. To "replace" the blocked sodium current, fast real-time dynamic clamp was implemented using RTLDC-based dynamic clamp (Boston University;(Dorval et al., 2001)) with cycle speed of 25-35 microseconds. This system generated an artificial sodium conductance (kinetics described in Supplement) that interacted with the cell's intrinsic potassium conductances to produce action potential like waveforms (as in Figure 5). Dynamic-clamp generated spikes were required to be at least 80% as tall as the cell's natural spikes. Single spikes were elicited from 0.2 ms current pulses. Spike trains were elicited from 500 ms current pulses. Costs were determined by integrating the dynamic clamp "sodium" current over the duration of the spike or train. To aggregate data from cells with different sizes and potassium channel kinetics, group data was constructed by normalizing each parameter-rate curve to have a maximum of 1, or normalizing each parameter-cost curve by the maximum cost per spike for a single spike.

Supplemental material

Model

Simulations were performed using a single compartment, Hodgkin-Huxley style model. The model parameters were as follows:

$$R_{in} = 10M\Omega; C_M = 0.1\mu F$$
$$E_{leak} = -70mV;\ E_{Na} = 50\ mV;\ E_K = -90\ mV$$
$$g_{Na,max} = g_{K,max} = 7\mu S$$

Sodium channel activation (m), sodium channel inactivation (h), and potassium channel activation (n) gate kinetics were given by:

$$\alpha_m = -40\frac{-75.5+v}{e^{\frac{-75.5+v}{-13.5}}-1};\ \beta_m = \frac{1.2262}{e^{\frac{v}{42.24}}}$$

$$\alpha_h = \frac{0.00315}{e^{\frac{v}{24.186}}};\beta_h = -0.0153\frac{51.2+v}{e^{\frac{-(51.2+v)}{5.2}}-1}$$

$$\alpha_n = -\frac{-95+v}{e^{\frac{-95+v}{-11.8}}-1};\beta_n = \frac{0.025}{e^{\frac{v}{22.222}}}$$

$$\tau = \frac{1}{\alpha+\beta};n_{\infty} = \alpha\tau$$

Gate states were updated according to the rule:

$$state(t+\Delta t) = n_{\infty} + (state(t) - n_{\infty}) * e^{-\frac{\Delta t}{\tau}}$$

Sodium and potassium conductances were given by:

$$g_{Na} = m^3h;g_k = n^2$$

Action potentials were required to begin and end below -50 mV and cross at least 0 mV at maximum. The cost of a single action potential was determined by finding the smallest-amplitude 1 ms current pulse that evoked an action potential, integrating the sodium current during the 20 ms post-stimulus, and converting integrated sodium current to ATP required to transport the sodium ions using the 3:1 stoichiometry of the Na^+,K^+ ATPase. Spike trains were elicited from 200 ms current pulses. The cost per spike for spikes in a train was determined by applying a 200 ms current pulse, integrating the sodium current over the pulse and the following 20 ms, and dividing by the number of spikes evoked. In Figures 2 and 3, gate kinetics were speeded or slowed by multiplying the time constants calculated at each time step by a constant factor. In Figure 4, maximum sodium or potassium channel conductances were scaled by a constant factor.

Slice preparation

All animal use was approved by the Institutional Animal Care and Use Committee. To prepare brain slices, mice aged P18-P26 were deeply anesthetized with Nembutal (100mg/kg i.p.) and rapidly decapitated. A vibratome (Series 1000, Vibratome) was used to cut 300 micron coronal brain slices from somatosensory cortex (S1). Slices were cut in ice-cold artificial cerebral spinal fluid (ACSF: 24 mM NaCl, 5mM KCl, 26m M NaHCO3, 1mM KH_2PO_4, 1mM $MgSO_4$, 10 mM glucose, 1.2 mM $CaCl_2$, and 1 mM kynurenic acid) and incubated at 35 C^o for at least 30 minutes in ACSF bubbled with 95% O2/ 5% CO_2 before transferring to a room-temperature submerged chamber for recording. Two types of mice were used in these experiments: G42 transgenic mice, generated in the lab of Josh Huang at Cold Spring Harbor (Chattopadhyaya et al., 2004), and C57/Bl6 mice, obtained from Jackson Laboratory.

Recordings

Neurons were visualized at 40X magnification using a DIC/fluorescent Olympus microscope and a video camera (VE 1000; Mti-Dage). Neurons were patched using glass pipettes pulled from borosilicate glass (Sutter Instruments) on a P-97 micropipette puller (Sutter Instruments, Novato, CA) to 3- 5MOhm, filled with 130mM D-gluconate, 0.2 mM EGTA, 2mM $MgCl_2$, 6mM KCl, 10mM HEPES, 2.5 mM Na-ATP, 0.5mM Na-GTP, and 10mM K-phosphocreatine (pH 7.2). Neurons were chosen for patching based on their fluorescence (for G42 slices) or round,

multipolar morphology (for C57 slices). Signals were amplified with a MultiClamp 700B amplifier (Molecular Devices) in current-clamp mode. Data was acquired and digitized using the Spike2 Power1401 collection system (Cambridge Electronic Designs, Cambridge, UK). Cell health and the fast-spiking phenotype were confirmed by injecting 500 ms long constant current pulses. Recordings were accepted if they showed a stable membrane potential below −50 mV at rest, and had action potentials of at least 40 mV (for fast-spiking interneurons).

Dynamic clamp

1 micromolar TTX was applied to block voltage-gated sodium currents, and sodium current block was confirmed using current pulses. To "replace" the blocked sodium current, fast real-time dynamic clamp was implemented using RTLDC (Boston University; Dorval et al, Ann Biomed Eng 29: 897-907) combined with the Real-Time Application Interface (www.rtai.org), device drivers from the COMEDI project (www.comedi.org), and a NI DAQ board (National Instruments). Dynamic clamp cycle speed was 25-35 microseconds. The dynamic clamp was used to generate an artificial sodium conductance with the same base kinetics as in the model, above. Kinetics were speeded or slowed, or total maximum conductance scaled, as in the model, above. The interaction of this synthetic sodium conductance with the cell's intrinsic potassium conductances produced action potential like waveforms (as in Figure 5). Dynamic-clamp generated spikes were required to be at least 80% as tall as the cell's natural spikes. Single spikes were elicited from 0.2 ms current pulses. Spike trains were elicited from 500 ms current pulses. Costs were determined by

integrating the dynamic clamp current (i.e., the model sodium current) over the duration of the spike or train. To aggregate data from cells with different sizes and potassium channel kinetics, group data was constructed by normalizing each parameter-rate curve to have a maximum of 1, or normalizing each parameter-cost curve by the maximum cost per spike for a single spike.

Acknowledgements

We thank members of the Crick-Jacobs Center for illuminating discussions and James Wing for technical support. Supported by the Crick-Jacobs Center for Theoretical and Computational Biology, HHMI, NIH MH063912, the Aginsky Foundation, and the Kavli Institute for Brain and Mind.

Publication Acknowledgements

Chapter 4, in full, is a reprint of the material as it appear in PNAS 2010; Hasenstaub A, Otte S, Callaway E, and Sejnowski T. PNAS 2010 : 0914886107v1-200914886. The dissertation author and thesis advisor were contributing investigators and authors of this material. The primary author is Andrea Hasenstaub, the secondary author is Terry Sejnowski, thesis committee member.

REFERENCES

Abeles M (1982) Role of the cortical neuron: integrator or coincidence detector? Isr J Med Sci 18:83-92.

Achard P, De Schutter E (2006) Complex parameter landscape for a complex neuron model. PLoS Comput Biol 2:e94.

Adesnik H, Scanziani M Lateral competition for cortical space by layer-specific horizontal circuits. Nature 464:1155-1160.

Aiello LC, Wheeler P (1995) The expensive-tissue hypothesis—the brain and the digestive-system in human and primate evolution. . Current Anthropology 36:199-221.

Alle H, Roth A, Geiger JR (2009) Energy-efficient action potentials in hippocampal mossy fibers. Science 325:1405-1408.

Ames A, 3rd, Li YY, Heher EC, Kimble CR (1992) Energy metabolism of rabbit retina as related to function: high cost of Na+ transport. J Neurosci 12:840-853.

Angulo MC, Staiger JF, Rossier J, Audinat E (2003) Distinct local circuits between neocortical pyramidal cells and fast-spiking interneurons in young adult rats. J Neurophysiol 89:943-953.

Aradi I, Santhakumar V, Chen K, Soltesz I (2002) Postsynaptic effects of GABAergic synaptic diversity: regulation of neuronal excitability by changes in IPSC variance. Neuropharmacology 43:511-522.

Astrup J, Sorensen PM, Sorensen HR (1981a) Inhibition of cerebral oxygen and glucose consumption in the dog by hypothermia, pentobarbital, and lidocaine. Anesthesiology 55:263-268.

Astrup J, Sorensen PM, Sorensen HR (1981b) Oxygen and glucose consumption related to Na+-K+ transport in canine brain. Stroke 12:726-730.

Attwell D, Laughlin SB (2001) An energy budget for signaling in the grey matter of the brain. J Cereb Blood Flow Metab 21:1133-1145.

Azouz R, Gray CM (2000) Dynamic spike threshold reveals a mechanism for synaptic coincidence detection in cortical neurons in vivo. Proc Natl Acad Sci U S A 97:8110-8115.

Azouz R, Gray CM (2003) Adaptive coincidence detection and dynamic gain control in visual cortical neurons in vivo. Neuron 37:513-523.

Balasubramanian V, Berry MJ, 2nd (2002) A test of metabolically efficient coding in the retina. Network (Bristol, England) 13:531-552.

Balasubramanian V, Kimber D, Berry MJ, 2nd (2001) Metabolically efficient information processing. Neural computation 13:799-815.

Barrickman NL, Bastian ML, Isler K, van Schaik CP (2008) Life history costs and benefits of encephalization: a comparative test using data from long-term studies of primates in the wild. J Hum Evol 54:568-590.

Bartos M, Vida I, Jonas P (2007) Synaptic mechanisms of synchronized gamma oscillations in inhibitory interneuron networks. Nat Rev Neurosci 8:45-56.

Bartos M, Vida I, Frotscher M, Geiger JR, Jonas P (2001) Rapid signaling at inhibitory synapses in a dentate gyrus interneuron network. J Neurosci 21:2687-2698.

Bartos M, Vida I, Frotscher M, Meyer A, Monyer H, Geiger JR, Jonas P (2002) Fast synaptic inhibition promotes synchronized gamma oscillations in hippocampal interneuron networks. Proc Natl Acad Sci U S A 99:13222-13227.

Basar E, Guntekin B (2008) A review of brain oscillations in cognitive disorders and the role of neurotransmitters. Brain Res 1235:172-193.

Bean BP (2007) The action potential in mammalian central neurons. Nat Rev Neurosci 8:451-465.

Beierlein M, Gibson JR, Connors BW (2000) A network of electrically coupled interneurons drives synchronized inhibition in neocortex. Nat Neurosci 3:904-910.

Bi GQ, Poo MM (1998) Synaptic modifications in cultured hippocampal neurons: dependence on spike timing, synaptic strength, and postsynaptic cell type. J Neurosci 18:10464-10472.

Blitzer RD, Wong T, Nouranifar R, Landau EM (1994) The cholinergic inhibition of afterhyperpolarization in rat hippocampus is independent of cAMP-dependent protein kinase. Brain Res 646:312-314.

Borgers C, Epstein S, Kopell NJ (2005) Background gamma rhythmicity and attention in cortical local circuits: a computational study. Proc Natl Acad Sci U S A 102:7002-7007.

Brette R, Gerstner W (2005) Adaptive exponential integrate-and-fire model as an effective description of neuronal activity. J Neurophysiol 94:3637-3642.

Buhl EH, Tamas G, Fisahn A (1998) Cholinergic activation and tonic excitation induce persistent gamma oscillations in mouse somatosensory cortex in vitro. J Physiol 513 (Pt 1):117-126.

Burchell TR, Faulkner HJ, Whittington MA (1998) Gamma frequency oscillations gate temporally coded afferent inputs in the rat hippocampal slice. Neurosci Lett 255:151-154.

Busch NA, Debener S, Kranczioch C, Engel AK, Herrmann CS (2004) Size matters: effects of stimulus size, duration and eccentricity on the visual gamma-band response. Clin Neurophysiol 115:1810-1820.

Buschman TJ, Miller EK (2007) Top-down versus bottom-up control of attention in the prefrontal and posterior parietal cortices. Science 315:1860-1862.

Buzsaki G, Draguhn A (2004) Neuronal oscillations in cortical networks. Science 304:1926-1929.

Buzsaki G, Kaila K, Raichle M (2007) Inhibition and brain work. Neuron 56:771-783.

Canolty RT, Edwards E, Dalal SS, Soltani M, Nagarajan SS, Kirsch HE, Berger MS, Barbaro NM, Knight RT (2006) High gamma power is phase-locked to theta oscillations in human neocortex. Science 313:1626-1628.

Cape EG, Manns ID, Alonso A, Beaudet A, Jones BE (2000) Neurotensin-induced bursting of cholinergic basal forebrain neurons promotes gamma and theta cortical activity together with waking and paradoxical sleep. J Neurosci 20:8452-8461.

Caporale N, Dan Y (2008) Spike timing-dependent plasticity: a Hebbian learning rule. Annu Rev Neurosci 31:25-46.

Cardin JA, Palmer LA, Contreras D (2008) Cellular mechanisms underlying stimulus-dependent gain modulation in primary visual cortex neurons in vivo. Neuron 59:150-160.

Cardin JA, Carlen M, Meletis K, Knoblich U, Zhang F, Deisseroth K, Tsai LH, Moore CI Targeted optogenetic stimulation and recording of neurons in vivo using cell-type-specific expression of Channelrhodopsin-2. Nat Protoc 5:247-254.

Cardin JA, Carlen M, Meletis K, Knoblich U, Zhang F, Deisseroth K, Tsai LH, Moore CI (2009) Driving fast-spiking cells induces gamma rhythm and controls sensory responses. Nature.

Carr PA, Yamamoto T, Karmy G, Baimbridge KG, Nagy JI (1989) Analysis of parvalbumin and calbindin D28k-immunoreactive neurons in dorsal root

ganglia of rat in relation to their cytochrome oxidase and carbonic anhydrase content. Neuroscience 33:363-371.

Carter BC, Bean BP (2009) Sodium entry during action potentials of mammalian neurons: incomplete inactivation and reduced metabolic efficiency in fast-spiking neurons. Neuron 64:898-909.

Chance FS, Abbott LF, Reyes AD (2002) Gain modulation from background synaptic input. Neuron 35:773-782.

Chattopadhyaya B, Di Cristo G, Higashiyama H, Knott GW, Kuhlman SJ, Welker E, Huang ZJ (2004) Experience and activity-dependent maturation of perisomatic GABAergic innervation in primary visual cortex during a postnatal critical period. J Neurosci 24:9598-9611.

Chklovskii DB, Koulakov AA (2004) Maps in the brain: what can we learn from them? Annual review of neuroscience 27:369-392.

Chrobak JJ, Buzsaki G (1998) Gamma oscillations in the entorhinal cortex of the freely behaving rat. J Neurosci 18:388-398.

Coetzee WA, Amarillo Y, Chiu J, Chow A, Lau D, McCormack T, Moreno H, Nadal MS, Ozaita A, Pountney D, Saganich M, Vega-Saenz de Miera E, Rudy B (1999) Molecular diversity of K+ channels. Molecular and Functional Diversity of Ion Channels and Receptors 868:233-285.

Csicsvari J, Jamieson B, Wise KD, Buzsaki G (2003) Mechanisms of gamma oscillations in the hippocampus of the behaving rat. Neuron 37:311-322.

Dan Y, Poo MM (2004) Spike timing-dependent plasticity of neural circuits. Neuron 44:23-30.

Deans MR, Gibson JR, Sellitto C, Connors BW, Paul DL (2001) Synchronous activity of inhibitory networks in neocortex requires electrical synapses containing connexin36. Neuron 31:477-485.

Deco G, Thiele A (2009) Attention: oscillations and neuropharmacology. Eur J Neurosci 30:347-354.

Del Negro C, Edeline JM (2001) Differences in auditory and physiological properties of HVc neurons between reproductively active male and female canaries (Serinus canaria). The European journal of neuroscience 14:1377-1389.

Dorval AD, Christini DJ, White JA (2001) Real-Time linux dynamic clamp: a fast and flexible way to construct virtual ion channels in living cells. Ann Biomed Eng 29:897-907.

Engel AK, Singer W (2001) Temporal binding and the neural correlates of sensory awareness. Trends Cogn Sci 5:16-25.

Engel AK, Fries P, Singer W (2001) Dynamic predictions: oscillations and synchrony in top-down processing. Nat Rev Neurosci 2:704-716.

Erisir A, Lau D, Rudy B, Leonard CS (1999) Function of specific K(+) channels in sustained high-frequency firing of fast-spiking neocortical interneurons. J Neurophysiol 82:2476-2489.

Fellous JM, Sejnowski TJ (2000) Cholinergic induction of oscillations in the hippocampal slice in the slow (0.5-2 Hz), theta (5-12 Hz), and gamma (35-70 Hz) bands. Hippocampus 10:187-197.

Fellous JM, Houweling AR, Modi RH, Rao RP, Tiesinga PH, Sejnowski TJ (2001) Frequency dependence of spike timing reliability in cortical pyramidal cells and interneurons. J Neurophysiol 85:1782-1787.

Fisahn A, Pike FG, Buhl EH, Paulsen O (1998) Cholinergic induction of network oscillations at 40 Hz in the hippocampus in vitro. Nature 394:186-189.

Fisahn A, Contractor A, Traub RD, Buhl EH, Heinemann SF, McBain CJ (2004) Distinct roles for the kainate receptor subunits GluR5 and GluR6 in kainate-induced hippocampal gamma oscillations. J Neurosci 24:9658-9668.

Fiser J, Chiu C, Weliky M (2004) Small modulation of ongoing cortical dynamics by sensory input during natural vision. Nature 431:573-578.

Fish JL, Lockwood CA (2003) Dietary constraints on encephalization in primates. Am J Phys Anthropol 120:171-181.

Fox MD, Snyder AZ, Vincent JL, Raichle ME (2007) Intrinsic fluctuations within cortical systems account for intertrial variability in human behavior. Neuron 56:171-184.

Freeman WJ, Holmes MD, Burke BC, Vanhatalo S (2003) Spatial spectra of scalp EEG and EMG from awake humans. Clin Neurophysiol 114:1053-1068.

Freund TF (2003) Interneuron Diversity series: Rhythm and mood in perisomatic inhibition. Trends Neurosci 26:489-495.

Fries P (2005) A mechanism for cognitive dynamics: neuronal communication through neuronal coherence. Trends Cogn Sci 9:474-480.

Fries P (2009) Neuronal gamma-band synchronization as a fundamental process in cortical computation. Annu Rev Neurosci 32:209-224.

Fries P, Nikolic D, Singer W (2007) The gamma cycle. Trends Neurosci 30:309-316.

Fries P, Reynolds JH, Rorie AE, Desimone R (2001a) Modulation of oscillatory neuronal synchronization by selective visual attention. Science 291:1560-1563.

Fries P, Neuenschwander S, Engel AK, Goebel R, Singer W (2001b) Rapid feature selective neuronal synchronization through correlated latency shifting. Nat Neurosci 4:194-200.

Frund I, Busch NA, Schadow J, Korner U, Herrmann CS (2007) From perception to action: phase-locked gamma oscillations correlate with reaction times in a speeded response task. BMC Neurosci 8:27.

Fujioka T, Trainor LJ, Large EW, Ross B (2009) Beta and gamma rhythms in human auditory cortex during musical beat processing. Ann N Y Acad Sci 1169:89-92.

Galarreta M, Hestrin S (2001a) Electrical synapses between GABA-releasing interneurons. Nat Rev Neurosci 2:425-433.

Galarreta M, Hestrin S (2001b) Spike transmission and synchrony detection in networks of GABAergic interneurons. Science 292:2295-2299.

Galarreta M, Hestrin S (2002) Electrical and chemical synapses among parvalbumin fast-spiking GABAergic interneurons in adult mouse neocortex. Proc Natl Acad Sci U S A 99:12438-12443.

Galarreta M, Erdelyi F, Szabo G, Hestrin S (2004) Electrical coupling among irregular-spiking GABAergic interneurons expressing cannabinoid receptors. J Neurosci 24:9770-9778.

Gibson JR, Beierlein M, Connors BW (1999) Two networks of electrically coupled inhibitory neurons in neocortex. Nature 402:75-79.

Goense JB, Logothetis NK (2008) Neurophysiology of the BOLD fMRI signal in awake monkeys. Curr Biol 18:631-640.

Gonzalez Andino SL, Michel CM, Thut G, Landis T, Grave de Peralta R (2005) Prediction of response speed by anticipatory high-frequency (gamma band) oscillations in the human brain. Hum Brain Mapp 24:50-58.

Gray CM, Konig P, Engel AK, Singer W (1989) Oscillatory responses in cat visual cortex exhibit inter-columnar synchronization which reflects global stimulus properties. Nature 338:334-337.

Gruber T, Muller MM, Keil A, Elbert T (1999) Selective visual-spatial attention alters induced gamma band responses in the human EEG. Clin Neurophysiol 110:2074-2085.

Haider B, McCormick DA (2009) Rapid neocortical dynamics: cellular and network mechanisms. Neuron 62:171-189.

Haider B, Duque A, Hasenstaub AR, McCormick DA (2006) Neocortical network activity in vivo is generated through a dynamic balance of excitation and inhibition. J Neurosci 26:4535-4545.

Haig AR, De Pascalis V, Gordon E (1999) Peak gamma latency correlated with reaction time in a conventional oddball paradigm. Clin Neurophysiol 110:158-165.

Hajos N, Katona I, Naiem SS, MacKie K, Ledent C, Mody I, Freund TF (2000) Cannabinoids inhibit hippocampal GABAergic transmission and network oscillations. Eur J Neurosci 12:3239-3249.

Halabisky B, Shen F, Huguenard JR, Prince DA (2006) Electrophysiological classification of somatostatin-positive interneurons in mouse sensorimotor cortex. J Neurophysiol 96:834-845.

Hasenstaub A, Sachdev RN, McCormick DA (2007) State changes rapidly modulate cortical neuronal responsiveness. J Neurosci 27:9607-9622.

Hasenstaub A, Shu Y, Haider B, Kraushaar U, Duque A, McCormick DA (2005) Inhibitory postsynaptic potentials carry synchronized frequency information in active cortical networks. Neuron 47:423-435.

Hayward LF, Felder RB (1999) Electrophysiological properties of rat lateral parabrachial neurons in vitro. The American journal of physiology 276:R696-706.

Herrmann CS, Demiralp T (2005) Human EEG gamma oscillations in neuropsychiatric disorders. Clin Neurophysiol 116:2719-2733.

Higgs MH, Slee SJ, Spain WJ (2006) Diversity of gain modulation by noise in neocortical neurons: regulation by the slow afterhyperpolarization conductance. J Neurosci 26:8787-8799.

Hodgkin A (1975) The optimum density of sodium channels in an unmyelinated nerve. Philos Trans R Soc Lond B Biol Sci 270:297-300.

Holliday MA (1971) Metabolic rate and organ size during growth from infancy to maturity and during late gastation and early infancy. Pediatrics 47:Suppl 2:169+.

Holliday MA, Potter D, Jarrah A, Bearg S (1967) The relation of metabolic rate to body weight and organ size. Pediatr Res 1:185-195.

Hormuzdi SG, Pais I, LeBeau FE, Towers SK, Rozov A, Buhl EH, Whittington MA, Monyer H (2001) Impaired electrical signaling disrupts gamma frequency oscillations in connexin 36-deficient mice. Neuron 31:487-495.

Huchzermeyer C, Albus K, Gabriel HJ, Otahal J, Taubenberger N, Heinemann U, Kovacs R, Kann O (2008) Gamma oscillations and spontaneous network activity in the hippocampus are highly sensitive to decreases in pO2 and concomitant changes in mitochondrial redox state. J Neurosci 28:1153-1162.

Hutcheon B, Yarom Y (2000) Resonance, oscillation and the intrinsic frequency preferences of neurons. Trends Neurosci 23:216-222.

Isler K, van Schaik C (2006) Costs of encephalization: the energy trade-off hypothesis tested on birds. J Hum Evol 51:228-243.

Jensen O, Kaiser J, Lachaux JP (2007) Human gamma-frequency oscillations associated with attention and memory. Trends Neurosci 30:317-324.

Jentsch TJ, Stein V, Weinreich F, Zdebik AA (2002) Molecular structure and physiological function of chloride channels. Physiological Reviews 82:503-568.

Jokeit H, Makeig S (1994) Different event-related patterns of gamma-band power in brain waves of fast- and slow-reacting subjects. Proc Natl Acad Sci U S A 91:6339-6343.

Kaiser J, Heidegger T, Lutzenberger W (2008a) Behavioral relevance of gamma-band activity for short-term memory-based auditory decision-making. Eur J Neurosci 27:3322-3328.

Kaiser J, Rahm B, Lutzenberger W (2009) Temporal dynamics of stimulus-specific gamma-band activity components during auditory short-term memory. Neuroimage 44:257-264.

Kaiser J, Heidegger T, Wibral M, Altmann CF, Lutzenberger W (2008b) Distinct gamma-band components reflect the short-term memory maintenance of different sound lateralization angles. Cereb Cortex 18:2286-2295.

Kasper EM, Lubke J, Larkman AU, Blakemore C (1994) Pyramidal neurons in layer 5 of the rat visual cortex. III. Differential maturation of axon targeting, dendritic morphology, and electrophysiological properties. J Comp Neurol 339:495-518.

Kawaguchi Y (1993) Physiological, morphological, and histochemical characterization of three classes of interneurons in rat neostriatum. J Neurosci 13:4908-4923.

Kawaguchi Y, Hama K (1987) Two subtypes of non-pyramidal cells in rat hippocampal formation identified by intracellular recording and HRP injection. Brain Res 411:190-195.

Kawaguchi Y, Kubota Y (1998) Neurochemical features and synaptic connections of large physiologically-identified GABAergic cells in the rat frontal cortex. Neuroscience 85:677-701.

Kenet T, Bibitchkov D, Tsodyks M, Grinvald A, Arieli A (2003) Spontaneously emerging cortical representations of visual attributes. Nature 425:954-956.

Kinney JM, Tucker HN, Clintec International Inc. (1992) Energy metabolism : tissue determinants and cellular corollaries. New York: Raven Press.

Kinney JW, Davis CN, Tabarean I, Conti B, Bartfai T, Behrens MM (2006) A specific role for NR2A-containing NMDA receptors in the maintenance of parvalbumin and GAD67 immunoreactivity in cultured interneurons. J Neurosci 26:1604-1615.

Klausberger T, Magill PJ, Marton LF, Roberts JD, Cobden PM, Buzsaki G, Somogyi P (2003) Brain-state- and cell-type-specific firing of hippocampal interneurons in vivo. Nature 421:844-848.

Konig P, Engel AK, Singer W (1996) Integrator or coincidence detector? The role of the cortical neuron revisited. Trends Neurosci 19:130-137.

Kording KP, Wolpert DM (2004) Bayesian integration in sensorimotor learning. Nature 427:244-247.

Kuhn A, Aertsen A, Rotter S (2004) Neuronal integration of synaptic input in the fluctuation-driven regime. J Neurosci 24:2345-2356.

Lakatos P, Karmos G, Mehta AD, Ulbert I, Schroeder CE (2008) Entrainment of neuronal oscillations as a mechanism of attentional selection. Science 320:110-113.

Lakatos P, Shah AS, Knuth KH, Ulbert I, Karmos G, Schroeder CE (2005) An oscillatory hierarchy controlling neuronal excitability and stimulus processing in the auditory cortex. J Neurophysiol 94:1904-1911.

Laughlin SB, Sejnowski TJ (2003) Communication in neuronal networks. Science 301:1870-1874.

Laughlin SB, de Ruyter van Steveninck RR, Anderson JC (1998) The metabolic cost of neural information. Nature neuroscience 1:36-41.

Leao RM, Kushmerick C, Pinaud R, Renden R, Li GL, Taschenberger H, Spirou G, Levinson SR, von Gersdorff H (2005) Presynaptic Na+ channels: locus, development, and recovery from inactivation at a high-fidelity synapse. J Neurosci 25:3724-3738.

Lee CJ, Irizarry K (2003) Alternative splicing in the nervous system: An emerging source of diversity and regulation. Biological Psychiatry 54:771-776.

Lennie P (2003) The cost of cortical computation. Curr Biol 13:493-497.

Lenz D, Jeschke M, Schadow J, Naue N, Ohl FW, Herrmann CS (2008) Human EEG very high frequency oscillations reflect the number of matches with a template in auditory short-term memory. Brain Res 1220:81-92.

Levy WB, Baxter RA (1996) Energy efficient neural codes. Neural computation 8:531-543.

Levy WB, Baxter RA (2002) Energy-efficient neuronal computation via quantal synaptic failures. J Neurosci 22:4746-4755.

Lewis DA, Cho RY, Carter CS, Eklund K, Forster S, Kelly MA, Montrose D (2008) Subunit-selective modulation of GABA type A receptor neurotransmission and cognition in schizophrenia. Am J Psychiatry 165:1585-1593.

Lieberman M, Marks AD, Smith CM (2009) Marks' basic medical biochemistry : a clinical approach, 3rd Edition. Philadelphia: Wolters Kluwer Health/Lippincott Williams & Wilkins.

Likhtik E, Pelletier JG, Popescu AT, Pare D (2006) Identification of basolateral amygdala projection cells and interneurons using extracellular recordings. J Neurophysiol 96:3257-3265.

Llinas RR, Pare D (1991) Of dreaming and wakefulness. Neuroscience 44:521-535.

Logothetis NK (2008) What we can do and what we cannot do with fMRI. Nature 453:869-878.

Logothetis NK, Wandell BA (2004) Interpreting the BOLD signal. Annu Rev Physiol 66:735-769.

Lopez-Bendito G, Sturgess K, Erdelyi F, Szabo G, Molnar Z, Paulsen O (2004) Preferential origin and layer destination of GAD65-GFP cortical interneurons. Cereb Cortex 14:1122-1133.

Mallet N, Le Moine C, Charpier S, Gonon F (2005) Feedforward inhibition of projection neurons by fast-spiking GABA interneurons in the rat striatum in vivo. J Neurosci 25:3857-3869.

Marder E, Goaillard JM (2006) Variability, compensation and homeostasis in neuron and network function. Nat Rev Neurosci 7:563-574.

Markram H, Lubke J, Frotscher M, Sakmann B (1997) Regulation of synaptic efficacy by coincidence of postsynaptic APs and EPSPs. Science 275:213-215.

Markram H, Toledo-Rodriguez M, Wang Y, Gupta A, Silberberg G, Wu C (2004) Interneurons of the neocortical inhibitory system. Nat Rev Neurosci 5:793-807.

Martina M, Schultz JH, Ehmke H, Monyer H, Jonas P (1998) Functional and molecular differences between voltage-gated K+ channels of fast-spiking interneurons and pyramidal neurons of rat hippocampus. J Neurosci 18:8111-8125.

Martinez-Guijarro FJ, Soriano E, Del Rio JA, Blasco-Ibanez JM, Lopez-Garcia C (1993) Parvalbumin-containing neurons in the cerebral cortex of the lizard Podarcis hispanica: morphology, ultrastructure, and coexistence with GABA, somatostatin, and neuropeptide Y. J Comp Neurol 336:447-467.

McAnelly ML, Zakon HH (2000) Coregulation of voltage-dependent kinetics of Na(+) and K(+) currents in electric organ. J Neurosci 20:3408-3414.

McCormick DA (1992a) Neurotransmitter actions in the thalamus and cerebral cortex. J Clin Neurophysiol 9:212-223.

McCormick DA (1992b) Neurotransmitter actions in the thalamus and cerebral cortex and their role in neuromodulation of thalamocortical activity. Prog Neurobiol 39:337-388.

McCormick DA, Pape HC, Williamson A (1991) Actions of norepinephrine in the cerebral cortex and thalamus: implications for function of the central noradrenergic system. Prog Brain Res 88:293-305.

Miles R, Toth K, Gulyas AI, Hajos N, Freund TF (1996) Differences between somatic and dendritic inhibition in the hippocampus. Neuron 16:815-823.

Mitchison G (1991) Neuronal branching patterns and the economy of cortical wiring. Proceedings 245:151-158.

Muller MM, Gruber T, Keil A (2000) Modulation of induced gamma band activity in the human EEG by attention and visual information processing. Int J Psychophysiol 38:283-299.

Munk MH, Roelfsema PR, Konig P, Engel AK, Singer W (1996) Role of reticular activation in the modulation of intracortical synchronization. Science 272:271-274.

Nicoll RA (1988) The coupling of neurotransmitter receptors to ion channels in the brain. Science 241:545-551.

Niessing J, Ebisch B, Schmidt KE, Niessing M, Singer W, Galuske RA (2005) Hemodynamic signals correlate tightly with synchronized gamma oscillations. Science 309:948-951.

Niven JE, Anderson JC, Laughlin SB (2007) Fly photoreceptors demonstrate energy-information trade-offs in neural coding. PLoS biology 5:e116.

Nowak LG, Azouz R, Sanchez-Vives MV, Gray CM, McCormick DA (2003) Electrophysiological classes of cat primary visual cortical neurons in vivo as revealed by quantitative analyses. J Neurophysiol 89:1541-1566.

Okawa H, Sampath AP, Laughlin SB, Fain GL (2008) ATP consumption by mammalian rod photoreceptors in darkness and in light. Curr Biol 18:1917-1921.

Oliva AA, Jr., Jiang M, Lam T, Smith KL, Swann JW (2000) Novel hippocampal interneuronal subtypes identified using transgenic mice that express green fluorescent protein in GABAergic interneurons. J Neurosci 20:3354-3368.

Olshausen BA, Field DJ (2005) How close are we to understanding v1? Neural Comput 17:1665-1699.

Olufsen MS, Whittington MA, Camperi M, Kopell N (2003) New roles for the gamma rhythm: population tuning and preprocessing for the Beta rhythm. J Comput Neurosci 14:33-54.

Papp E, Leinekugel X, Henze DA, Lee J, Buzsaki G (2001) The apical shaft of CA1 pyramidal cells is under GABAergic interneuronal control. Neuroscience 102:715-721.

Pare D, Gaudreau H (1996) Projection cells and interneurons of the lateral and basolateral amygdala: distinct firing patterns and differential relation to theta and delta rhythms in conscious cats. J Neurosci 16:3334-3350.

Pare D, Shink E, Gaudreau H, Destexhe A, Lang EJ (1998) Impact of spontaneous synaptic activity on the resting properties of cat neocortical pyramidal neurons In vivo. J Neurophysiol 79:1450-1460.

Pedarzani P, Krause M, Haug T, Storm JF, Stuhmer W (1998) Modulation of the Ca2+-activated K+ current sIAHP by a phosphatase-kinase balance under basal conditions in rat CA1 pyramidal neurons. J Neurophysiol 79:3252-3256.

Popov V, Medvedev NI, Davies HA, Stewart MG (2005) Mitochondria form a filamentous reticular network in hippocampal dendrites but are present as discrete bodies in axons: a three-dimensional ultrastructural study. J Comp Neurol 492:50-65.

Pouille F, Scanziani M (2001) Enforcement of temporal fidelity in pyramidal cells by somatic feed-forward inhibition. Science 293:1159-1163.

Prescott SA, Sejnowski TJ (2008) Spike-rate coding and spike-time coding are affected oppositely by different adaptation mechanisms. J Neurosci 28:13649-13661.

Raichle ME (2006) Neuroscience. The brain's dark energy. Science 314:1249-1250.

Raichle ME, Mintun MA (2006) Brain work and brain imaging. Annu Rev Neurosci 29:449-476.

Ray S, Niebur E, Hsiao SS, Sinai A, Crone NE (2008) High-frequency gamma activity (80-150Hz) is increased in human cortex during selective attention. Clin Neurophysiol 119:116-133.

Rodriguez R, Kallenbach U, Singer W, Munk MH (2004) Short- and long-term effects of cholinergic modulation on gamma oscillations and response synchronization in the visual cortex. J Neurosci 24:10369-10378.

Roopun AK, Lebeau FE, Ramell J, Cunningham MO, Traub RD, Whittington MA Cholinergic neuromodulation controls directed temporal communication in neocortex in vitro. Front Neural Circuits 4:8.

Sah P, Faber ES (2002) Channels underlying neuronal calcium-activated potassium currents. Prog Neurobiol 66:345-353.

Salinas E, Sejnowski TJ (2000) Impact of correlated synaptic input on output firing rate and variability in simple neuronal models. J Neurosci 20:6193-6209.

Salinas E, Sejnowski TJ (2001) Correlated neuronal activity and the flow of neural information. Nat Rev Neurosci 2:539-550.

Sarter M, Hasselmo ME, Bruno JP, Givens B (2005) Unraveling the attentional functions of cortical cholinergic inputs: interactions between signal-driven and cognitive modulation of signal detection. Brain Res Brain Res Rev 48:98-111.

Schadow J, Lenz D, Dettler N, Frund I, Herrmann CS (2009a) Early gamma-band responses reflect anticipatory top-down modulation in the auditory cortex. Neuroimage 47:651-658.

Schadow J, Lenz D, Thaerig S, Busch NA, Frund I, Herrmann CS (2007a) Stimulus intensity affects early sensory processing: sound intensity modulates auditory evoked gamma-band activity in human EEG. Int J Psychophysiol 65:152-161.

Schadow J, Lenz D, Thaerig S, Busch NA, Frund I, Rieger JW, Herrmann CS (2007b) Stimulus intensity affects early sensory processing: visual contrast modulates evoked gamma-band activity in human EEG. Int J Psychophysiol 66:28-36.

Schadow J, Dettler N, Paramei GV, Lenz D, Frund I, Sabel BA, Herrmann CS (2009b) Impairments of Gestalt perception in the intact hemifield of hemianopic patients are reflected in gamma-band EEG activity. Neuropsychologia 47:556-568.

Schreiber S, Fellous JM, Tiesinga P, Sejnowski TJ (2004) Influence of ionic conductances on spike timing reliability of cortical neurons for suprathreshold rhythmic inputs. J Neurophysiol 91:194-205.

Schulz DJ, Goaillard JM, Marder E (2006) Variable channel expression in identified single and electrically coupled neurons in different animals. Nat Neurosci 9:356-362.

Schulz DJ, Temporal S, Barry DM, Garcia ML (2008) Mechanisms of voltage-gated ion channel regulation: from gene expression to localization. Cellular and Molecular Life Sciences 65:2215-2231.

Sejnowski TJ, Paulsen O (2006) Network oscillations: emerging computational principles. J Neurosci 26:1673-1676.

Shu Y, Hasenstaub A, McCormick DA (2003) Turning on and off recurrent balanced cortical activity. Nature 423:288-293.

Shulman RG, Rothman DL, Behar KL, Hyder F (2004) Energetic basis of brain activity: implications for neuroimaging. Trends Neurosci 27:489-495.

Sohal VS, Zhang F, Yizhar O, Deisseroth K (2009) Parvalbumin neurons and gamma rhythms enhance cortical circuit performance. Nature 459:698-702.

Sokoloff L (1999) Energetics of functional activation in neural tissues. Neurochem Res 24:321-329.

Spencer KM, Nestor PG, Niznikiewicz MA, Salisbury DF, Shenton ME, McCarley RW (2003) Abnormal neural synchrony in schizophrenia. J Neurosci 23:7407-7411.

Steriade M, Amzica F, Contreras D (1996) Synchronization of fast (30-40 Hz) spontaneous cortical rhythms during brain activation. J Neurosci 16:392-417.

Steriade M, Timofeev I, Grenier F (2001) Natural waking and sleep states: a view from inside neocortical neurons. J Neurophysiol 85:1969-1985.

Sugino K, Hempel CM, Miller MN, Hattox AM, Shapiro P, Wu C, Huang ZJ, Nelson SB (2006) Molecular taxonomy of major neuronal classes in the adult mouse forebrain. Nat Neurosci 9:99-107.

Swensen AM, Bean BP (2005) Robustness of burst firing in dissociated purkinje neurons with acute or long-term reductions in sodium conductance. J Neurosci 25:3509-3520.

Szabadics J, Lorincz A, Tamas G (2001) Beta and gamma frequency synchronization by dendritic gabaergic synapses and gap junctions in a network of cortical interneurons. J Neurosci 21:5824-5831.

Tallon-Baudry C, Bertrand O, Delpuech C, Permier J (1997) Oscillatory gamma-band (30-70 Hz) activity induced by a visual search task in humans. J Neurosci 17:722-734.

Tamas G, Buhl EH, Lorincz A, Somogyi P (2000) Proximally targeted GABAergic synapses and gap junctions synchronize cortical interneurons. Nat Neurosci 3:366-371.

Tamas G, Szabadics J, Lorincz A, Somogyi P (2004) Input and frequency-specific entrainment of postsynaptic firing by IPSPs of perisomatic or dendritic origin. Eur J Neurosci 20:2681-2690.

Taylor K, Mandon S, Freiwald WA, Kreiter AK (2005) Coherent oscillatory activity in monkey area v4 predicts successful allocation of attention. Cereb Cortex 15:1424-1437.

Tiesinga PH, Toups JV (2005) The possible role of spike patterns in cortical information processing. J Comput Neurosci 18:275-286.

Tiesinga PH, Fellous JM, Salinas E, Jose JV, Sejnowski TJ (2004) Inhibitory synchrony as a mechanism for attentional gain modulation. J Physiol Paris 98:296-314.

Tiitinen H, Sinkkonen J, Reinikainen K, Alho K, Lavikainen J, Naatanen R (1993) Selective attention enhances the auditory 40-Hz transient response in humans. Nature 364:59-60.

Toida K, Kosaka K, Heizmann CW, Kosaka T (1996) Electron microscopic serial-sectioning/reconstruction study of parvalbumin-containing neurons in the external plexiform layer of the rat olfactory bulb. Neuroscience 72:449-466.

Touboul J, Brette R (2008) Dynamics and bifurcations of the adaptive exponential integrate-and-fire model. Biol Cybern 99:319-334.

Traub RD, Pais I, Bibbig A, LeBeau FE, Buhl EH, Hormuzdi SG, Monyer H, Whittington MA (2003) Contrasting roles of axonal (pyramidal cell) and dendritic (interneuron) electrical coupling in the generation of neuronal network oscillations. Proc Natl Acad Sci U S A 100:1370-1374.

Tukker JJ, Fuentealba P, Hartwich K, Somogyi P, Klausberger T (2007) Cell type-specific tuning of hippocampal interneuron firing during gamma oscillations in vivo. J Neurosci 27:8184-8189.

Uhlhaas PJ, Singer W Abnormal neural oscillations and synchrony in schizophrenia. Nat Rev Neurosci 11:100-113.

Vida I, Bartos M, Jonas P (2006) Shunting inhibition improves robustness of gamma oscillations in hippocampal interneuron networks by homogenizing firing rates. Neuron 49:107-117.

Vinck M, Lima B, Womelsdorf T, Oostenveld R, Singer W, Neuenschwander S, Fries P Gamma-phase shifting in awake monkey visual cortex. J Neurosci 30:1250-1257.

Viswanathan A, Freeman RD (2007) Neurometabolic coupling in cerebral cortex reflects synaptic more than spiking activity. Nat Neurosci 10:1308-1312.

Vogalis F, Harvey JR, Neylon CB, Furness JB (2002) Regulation of K+ channels underlying the slow afterhyperpolarization in enteric afterhyperpolarization-generating myenteric neurons: role of calcium and phosphorylation. Clin Exp Pharmacol Physiol 29:935-943.

von Stein A, Chiang C, Konig P (2000) Top-down processing mediated by interareal synchronization. Proc Natl Acad Sci U S A 97:14748-14753.

Waagepetersen HS, Sonnewald U, Schousboe A (1999) The GABA paradox: multiple roles as metabolite, neurotransmitter, and neurodifferentiative agent. J Neurochem 73:1335-1342.

Wang Z, McCormick DA (1993) Control of firing mode of corticotectal and corticopontine layer V burst-generating neurons by norepinephrine, acetylcholine, and 1S,3R-ACPD. J Neurosci 13:2199-2216.

Washburn MS, Moises HC (1992) Electrophysiological and morphological properties of rat basolateral amygdaloid neurons in vitro. J Neurosci 12:4066-4079.

Weibel ER (2000) Symmorphosis : on form and function in shaping life. Cambridge, Mass.: Harvard University Press.

Whittington MA, Traub RD, Jefferys JG (1995) Synchronized oscillations in interneuron networks driven by metabotropic glutamate receptor activation. Nature 373:612-615.

Whittington MA, Faulkner HJ, Doheny HC, Traub RD (2000) Neuronal fast oscillations as a target site for psychoactive drugs. Pharmacol Ther 86:171-190.

Womelsdorf T, Fries P (2006) Neuronal coherence during selective attentional processing and sensory-motor integration. J Physiol Paris 100:182-193.

Womelsdorf T, Fries P, Mitra PP, Desimone R (2006) Gamma-band synchronization in visual cortex predicts speed of change detection. Nature 439:733-736.

Womelsdorf T, Schoffelen JM, Oostenveld R, Singer W, Desimone R, Engel AK, Fries P (2007) Modulation of neuronal interactions through neuronal synchronization. Science 316:1609-1612.

Wong-Riley MT (1989) Cytochrome oxidase: an endogenous metabolic marker for neuronal activity. Trends Neurosci 12:94-101.

Xu X, Callaway EM (2009) Laminar specificity of functional input to distinct types of inhibitory cortical neurons. J Neurosci 29:70-85.

Xu X, Roby KD, Callaway EM (2006) Mouse cortical inhibitory neuron type that coexpresses somatostatin and calretinin. J Comp Neurol 499:144-160.

Zaborszky L (2002) The modular organization of brain systems. Basal forebrain: the last frontier. Prog Brain Res 136:359-372.

Zaborszky L, Duque A (2000) Local synaptic connections of basal forebrain neurons. Behav Brain Res 115:143-158.

Zaehle T, Frund I, Schadow J, Tharig S, Schoenfeld MA, Herrmann CS (2009) Inter- and intra-individual covariations of hemodynamic and oscillatory gamma responses in the human cortex. Front Hum Neurosci 3:8.